PROBING THE 5*f* ELECTRONS: A RELATIVISTIC DFT STUDY OF AMERICIUM SURFACES

by

PRATIK PANKAJKUMAR DHOLABHAI

Presented to the Faculty of the Graduate School of

The University of Texas at Arlington in Partial Fulfillment

of the Requirements

for the Degree of

DOCTOR OF PHILOSOPHY

THE UNIVERSITY OF TEXAS AT ARLINGTON

August 2008

ACKNOWLEDGEMENTS

I would like to express my sincere gratitude and appreciation to my advisor, Dr. Asok Ray, for his support, patience, and encouragement throughout my graduate studies. I am grateful to him for the guidance he has provided all this years. I also would like to extend my thanks to my committee members Dr. Raymond Atta-Fynn, Dr. Nail Fazleev, Dr. Suresh C. Sharma and Dr. Qiming Zhang for there advice and opinions. I am thankful to the entire physics department for providing an excellent work environment and support. I am thankful to the U. S. Department of Energy and Welch foundation for there support. I would further like to thank the entire physics staff for there help in completing this work. It was my pleasure to work in the quantum theoretical research group and I am thankful to the group members Dr. F. Islam, Kazi, Somil, Souptik and Molly for there help and interesting suggestions. I would like to thank in particular Dr. R. Atta-Fynn for his assistance.

Last, but not least, I would like to thank my wife for her understanding and love during past few years. Her support and encouragement was in the end what made this dissertation possible. My parents receive my deepest gratitude and love for their dedication and the many years of support during my undergraduate studies that provided the foundation

of this work. Finally I would like to dedicate this work to my late brother Jigish Dholabhai.

July 18, 2008

ABSTRACT

PROBING THE 5*f* ELECTRONS: A RELATIVISTIC DFT STUDY OF AMERICIUM SURFACES

Pratik Pankajkumar Dholabhai, PhD.

The University of Texas at Arlington, 2008

Supervising Professor: Dr Asok. K. Ray

Surface chemistry and physics have been and continues to be very active fields of research because of the obvious scientific and technological implications and consequent importance of such research. One of the *many* motivations for this burgeoning effort has been the desire to understand surface corrosion, metallurgy and catalytic activity in order to address environmental concerns. In particular, such efforts are important for a group of strongly correlated and heavy fermion systems like the actinides, for which experimental work is relatively difficult to perform due to material problems and toxicity. These metals are among the most complex of the long-lived elements, and in their solid state, they display some of the most unusual behaviors of any series

in the periodic table, including very low melting temperatures, large anisotropic thermal expansion coefficients, very low symmetry crystal structures, and many solid-to-solid phase transitions. Radioactive and highly electropositive, the actinides are characterized by the gradual filling of the 5*f* electron shell with the degree of localization increasing with the atomic number Z along the last series of the periodic table and are divided into two subgroups. The first subgroup consisting of Th to Pu, where the atomic volumes decrease with increasing 5f electron population, generally consists of delocalized 5f electrons. The second subgroup starting from Am onwards, shows increasing atomic volume with increasing 5f electrons, with the 5f electrons being localized. The open shell of the 5*f* electrons determines the magnetic and solid state properties of the actinide elements and their compounds. However, these properties of the actinides, particularly the transuranium actinides, are *still not* clearly understood. This stems primarily from the inherent difficulty in understanding the behavior of the 5*f* electrons, whose spatial extent and tendency to interact with electrons on ligand sites gives rise to the chemically complex nature of the transuranium actinides. The actinides are also characterized by the increasing prominence of relativistic effects and their study can, in fact, give us an in depth understanding of the role of relativity throughout the periodic table.

Among the transuranium actinides, the unique electronic properties of the manmade Americium (Am) metal, which was first successfully synthesized and isolated at the wartime Metallurgical Laboratory, have received increased

interests, from both scientific and technological points of view. Am occupies a central position in the actinide series in our understanding of the behavior of the *5f* electrons. It is widely believed that the properties and the behavior of the *5f* electrons change dramatically starting from somewhere between Pu and Am. As a result, a large number of experimental and theoretical works have been done in recent years to gain insight into the structural and electronic properties of Am. In this work, atomic hydrogen and oxygen, molecular hydrogen and oxygen and water adsorptions on the (0001) surface of double hexagonal closed packed americium have been studied at both non-spin-orbit coupling (NSO) and spin-orbit coupling (SO) using generalized gradient approximation to density functional theory using the Perdew-Burke-Ernzerhof (PBE) formulation for the exchange-correlation functional. For atomic and molecular adsorptions, various chemisorption sites such as, top(t1), bridge(b2) and hcp(h3) have been investigated. Details of energetics of the chemisorption process, such as chemisorption energies, adatom/admolecule separation distances and inter molecular distances will be presented. Magnetic moments are also calculated for bare americium and the chemisorbed system. Adsorption of molecular hydrogen and oxygen and possible dissociative adsorption on americium surface will be presented. The adsorbate-substrate interactions have been analyzed in detail using the partial charges inside the muffin-tin spheres, difference charge density distributions, and the local density of states. The effects of adsorption on the Am 5*f* electron localization-delocalization

characteristics will be conversed. The role of 5*f* electrons in the bonding of americium with the adatom/admolecule will be discussed.

TABLE OF CONTENTS

LIST OF ILLUSTRATIONS

LIST OF TABLES

CHAPTER 1

INTRODUCTION

Surface chemistry and physics have been and continues to be very active fields of research because of the obvious scientific and technological implications and consequent importance of such research.[1] One of the *many* motivations for this burgeoning effort has been the desire to understand surface corrosion, metallurgy and catalytic activity in order to address environmental concerns. In particular, such efforts are important for a group of strongly correlated and heavy fermion systems like the actinides, for which experimental work is relatively difficult to perform due to material problems and toxicity. These metals are among the most complex of the long-lived elements, and in their solid state, they display some of the most unusual behaviors of any series in the periodic table, including very low melting temperatures, large anisotropic thermal expansion coefficients, very low symmetry crystal structures, and many solid-to-solid phase transitions. Radioactive and highly electropositive, the actinides are characterized by the gradual filling of the 5*f* electron shell with the degree of localization increasing with the atomic number *Z* along the last series of the periodic table and are divided into two subgroups. The first subgroup consisting of Th to Pu, where the atomic volumes decrease with increasing 5f electron population, generally consists of delocalized 5f electrons. The second

subgroup starting from Am onwards, shows increasing atomic volume with increasing 5f electrons, with the 5f electrons being localized. The open shell of the 5f electrons determines the magnetic and solid-state properties of the actinide elements and their compounds and understanding the quantum mechanics of the 5f electrons is the defining issue in the physics and chemistry of the actinide elements. However, these properties of the actinides, particularly the transuranium actinides, are *still not* clearly understood. This stems primarily from the inherent difficulty in understanding the behavior of the 5*f* electrons, whose spatial extent and tendency to interact with electrons on ligand sites gives rise to the chemically complex nature of the transuranium actinides. The actinides are also characterized by the increasing prominence of relativistic effects and their study can, in fact, give us an in depth understanding of the role of relativity throughout the periodic table. [2-12] The 5f orbitals have properties intermediate between those of localized 4f and delocalized 3d orbitals and as such, the actinides constitute the "missing link" between the d transition elements and the lanthanides.[7] Thus, a proper and accurate understanding of the actinides will help us understand the behavior of the lanthanides and transition metals as well. The similarity between light actinides (Th – Pu) and the *d*- transition elements is due to the fact that both of them are supposed to have delocalized *f* and *d* electrons, respectively.[13-15]

Among the actinides, the unique electronic properties of Americium (Am), which was first successfully synthesized and isolated at the wartime

Metallurgical Laboratory[13], have received increased interests recently, from both scientific and technological points of view. It has been noted that Am occupies a pivotal position in the actinide series with regard to the behavior of *5f* electrons.[15] Atomic volumes of the actinides as a function of atomic number have experimentally displayed a sharp increase between Pu and Am.[16] In contrast to this sharp increase, the atomic volumes of the actinides before Pu continuously decreases as a function of increasing atomic number from Ac until Np, which is analogous to d transition metals. These behaviors reveal that the properties of the *5f* electrons change dramatically starting from somewhere between Pu and Am. It has been suggested[17,18] that the *5f* electrons of the actinides before Am (until Pu) participate in bonding while the *5f* electrons of the actinides after Pu (starting from Am) become localized and non bonding. Both theoretical calculations[19] and the X-ray and high-resolution ultraviolet photoemission study[20] of the 5*f* electrons in Am have supported the localized picture for Am. Another notable feature is the high-pressure behavior of americium. As pressure increases, the crystal structures of americium display the following phase transitions[21]: double hexagonal close packed (Am I) → face-centered cubic (Am II) → face-centered orthorhombic (Am III) → primitive orthorhombic (Am IV). Although experimental data indicates that the phase transition from Am II to Am III is probably accompanied with the 5*f* electron delocalization[15,21] recent density-functional studies by Penicaud[22,23] regarding the high-pressure behavior of americium found that only the fourth phase (Am

IV) is delocalized and the *5f* electrons of the three previous americium phases are localized. The dynamical mean field theory calculations by Savrasov *et al.* [14] also indicate that the location of the Mott transition is near the Am III to Am IV boundary and that the f electrons start to participate in bonding in the highly pressurized Am IV structure. Using the full-potential linear muffin-tin orbital (FP-LMTO) method, Sõderlind *et al.* [24,25] calculated the total energies of fcc, bcc, bcm (α"), α–U(α'), α–Np, and α–Pu structures of Am as a function of volume. At 80 kbar, they calculated a transition from fcc Am to monoclinic Am and a volume collapse of 25%. They interpreted this as a Mott transition and the onset of a low symmetry crystal structure was induced by 5*f* electron delocalization in Am. A later study by Sõderlind and Landa [24,25] indicated that the Am I phase was stabilized by contributions from the d shell to the cohesion whereas all other phases follow from 5f electron bonding *i.e.* delocalization. Such controversies clearly indicate that further experimental and theoretical studies are needed to improve our understanding of americium and the associated *5f* electrons.

Another controversy surrounding Am is the question of magnetism. Experimental results, in general, indicate that Am is nonmagnetic. For example, Naegele *et al.,* [20] in their photoemission study of the localization of 5*f* electrons in Am, assumed the ground-state electron configuration to be $5f^6$ (nonmagnetic). Huray *et al.* [26] in their experimental studies of the magnetism of the heavy 5*f* elements also found Am to have zero effective magnetic moment

with an f^6 probable ion configuration. Both Gouder *et al.*[27] and Cox *et al.*[28], in their respective photoemission studies, found Am to have localized f states in a $5f^6$ configuration, consistent with the absence of magnetic order. On the other hand, theoretical studies on Am metal, mostly based on *ab initio* self-consistent density functional theory, in general, indicate the presence of magnetism. [22-25, 29,30,38-41] Using fully relativistic, full-potential linear-muffin-tin-orbital calculations, Eriksson and Wills[29] reported strong disagreements with experimental data. Using the same method as also canonical band theory, Soderlind and Landa[25] actually found the fcc phase to be stable by a small margin over dhcp but when *d* contribution is included, their energies were degenerate. They also found that the 5*f* electrons in Am almost entirely spin-polarize. Penicaud[22,23] modeled the localization of the 5*f* electrons by an anti-ferromagnetic (AFM) configuration found to have a lower energy than a ferromagnetic configuration. Using the full potential Dirac relativistic basis, spin-polarized linearized-augmented-plane-wave method, Kutepov and Kutepova[30] found also the AFM ordering to be favored for dhcp Am. The around-men-field LSDA+U (AMF-LSDA+U) correlated band theory has been applied by Shick *et al*.[31] to study the electronic and magnetic structure of fcc-Pu-Am alloys. For fcc Am, they performed AMF-LSDA+U calculations, varying the Coulomb U from 3 eV to 4 eV and keeping the inter-atomic exchange parameter J at 0.75 eV. The calculations yielded practically zero magnetic moment, with an equilibrium atomic volume of 186 $(a.u.)^3$ and a bulk modulus of 55.1 GPa with U = 4eV. Kotliar *et al.* [32,33,34] have

used dynamical-mean-field-theory (DMFT) approach to study strongly correlated systems, such as the actinides. Using a DMFT-based spectral density functional approach, they observed that the *f* electrons in Am at zero pressure exist in a $f^6\ ^7F_0$ configuration, with a U value of about 4.5 eV. Our calculations for fcc Am II, using the FP-LAPW method, yielded an AFM state, with an equilibrium atomic volume of 195.3 $(a.u.)^3$ and a bulk modulus of 28.1 GPa. The experimental equilibrium volume is 198.5 $(a.u.)^3$ and a bulk modulus of 29.4 GPa. On the other hand, results at the NSP-SO level produce an equilibrium atomic volume of 137.8 $(a.u.)^3$ and a bulk modulus of 63.8 GPa. Thus, a non-magnetic calculation produces an error of 31% in the atomic volume and 117% in the bulk modulus! Savrasov *et al.* [14] have found that a nonmagnetic GGA calculation failed catastrophically in reproducing the equilibrium volume of the soft phase of Am by about 50%. Clearly, there is strong disagreement here between theory and experiment as far as the question of magnetism is concerned. Given this wide spectrum of results on Am, we believe that a systematic and fully relativistic density functional study of Am surface chemistry and physics using the same level of theory could certainly lead to significant insights and knowledge about the actinides and at the very least, produce a qualitative and quantitative trend in our understanding of the light to heavy actinides and stimulate further work in actinides.

The electronic structure of americium, wherein six *f* electrons presumably form an inert core, decoupled from the *spd* electrons that control the physical

properties of the material, also contributes to the superconductivity in Am.[35,36] Recently, a study of the superconductivity in americium[37] as a function of pressure has showed that such studies may be an effective method to understand the unique *5f* electron properties of americium including the Mott transition, *i.e*., the evolution of the *5f* electrons from localized to the delocalized.

Another effective way to probe the actinides (including americium) *5f* electron properties and their roles in chemical bonding is the study of their surface properties. The unusual aspects of the bonding in bulk Am are apt to be enhanced at a surface or in a thin layer of Am adsorbed on a substrate, as a result of the reduced atomic coordination of a surface atom and the narrow bandwidth of surface states. Thus, Am surfaces and thin films may also provide valuable information about the bonding in Am. However, to the best of our knowledge, *very few* studies exist in the literature about the Am surface, especially surfaces of the double hexagonal close packed (dhcp) structure Am (Am I), which is the most common phase of Am under normal pressure.

CHAPTER 2

THEORY

2.1 Density functional theory

An efficient and accurate scheme for solving the many-electron problem of a crystal is the local spin density approximation (LSDA) within density functional theory. Therein the key quantities are the spin densities $\rho_\sigma(r)$ in terms of which the total energy is

$$E_{tot}(\rho_\uparrow, \rho_\downarrow) = \mathrm{T}_s(\rho_\uparrow, \rho_\downarrow) + E_{ee}(\rho_\uparrow, \rho_\downarrow) + E_{Ne}(\rho_\uparrow, \rho_\downarrow) + E_{xc}(\rho_\uparrow, \rho_\downarrow) + E_{NN}$$

with E_{NN} E_{NN} the repulsive Coulomb energy of the fixed nuclei and the electronic contributions, labeled conventionally as, respectively, the kinetic energy, the electron-electron repulsion, nuclear-electron attraction, and exchange-correlation energies.

LSDA comprises of two approximations, i), the assumption that E_{xc} E_{xc} can be written in terms of a local exchange-correlation energy density μ_{xc} μ_{xc} times the total (spin-up plus spin-down) electron density as

$$E_{xc} = \int \mu_{xc}(\rho_\uparrow, \rho_\downarrow) * [\rho_\uparrow, \rho_\downarrow] dr$$

and ii), the particular form chosen for that μ_{xc} μ_{xc}.

E_{tot} E_{tot} has a variational equivalent with the familiar Rayleigh-Ritz principle.

The most effective way known to minimize E_{tot} E_{tot} by means of the variational

principle is to introduce orbitals χ_{ik}^{σ} constrained to construct the spin densities as

$$\rho_{\sigma}(r) = \sum_{i,k} \rho_{ik}^{\sigma} \left| \chi_{ik}^{\sigma}(r) \right|^2$$

Here, the ρ_{ik}^{σ} are occupation numbers.

Then variation of Etot gives the Kohn-Sham equations (in Ry atomic units),

$$\left[-\nabla^2 + V_{Ne} + V_{ee} + V_{XC}^{\sigma} \right] \chi_{ik}^{\sigma}(r) = \in_{ik}^{\sigma} \chi_{ik}^{\sigma}(r)$$

which must be solved and thus constitute the primary computational task. This Kohn-Sham equations must be solved self-consistently in an iterative process, since finding the Kohn-Sham orbitals requires the knowledge of the potentials which themselves depend on the (spin-) density and thus on the orbitals again.

2.1.1 The LAPW Method

The linearized augmented plane wave (LAPW) method is among the most accurate methods for performing electronic structure calculations for crystals. It is based on the density functional theory for the treatment of exchange and correlation and uses e.g. the local spin density approximation (LSDA).

Like most “energy-band methods“, the LAPW method is a procedure for solving the Kohn-Sham equations for the ground state density, total energy, and (Kohn-Sham) eigenvalues (energy bands) of a many-electron system (here a crystal) by introducing a basis set which is especially adapted to the problem.

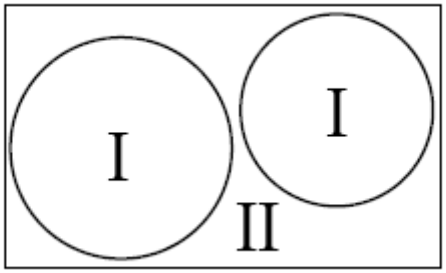

Figure 2.1: Partitioning of the unit cell into atomic spheres (I) and an interstitial region (II)

This adaptation is achieved by dividing the unit cell into (I) non-overlapping atomic spheres (centeredat the atomic sites) and (II) an interstitial region. In the two types of regions different basis sets are used:

1. (I) inside atomic sphere t, of radius Rt, a linear combination of radial functions times spherical harmonics $Y_{lm}(r)$ is used (we omit the index t when it is clear from the context)

$$\phi_{k_n} = \sum_{lm} \left[A_{lm,k_n} u_l(r, E_l) + B_{lm,k_n} \dot{u}_l(r, E_l) \right] Y_{lm}(\hat{r})$$

where $u_l(r, E_l)$ is the (at the origin) regular solution of the radial Schroedinger equation for energy E_l E_l and the spherical part of the potential inside sphere t; $u_l(r, E_l)$ is the energy derivative of u_l evaluated at the same energy E_l E_l. A linear combination of these two functions constitute the linearization of the radial function; the coefficients A_{lm} and B_{lm} are functions of kn determined by requiring that this basis function matches each plane wave (PW) the

corresponding basis function of the interstitial region; u_l and u_l are obtained by numerical integration of the radial Schroedinger equation on a radial mesh inside the sphere.

2. (II) in the interstitial region a plane wave expansion is used

$$\phi_{kn} = \frac{1}{\sqrt{\omega}} e^{ik_n \cdot r}$$

where $k_n = k + K_n; K_n$ are the reciprocal lattice vectors and k is the wave vector inside the first Brillouin zone. Each plane wave is augmented by an atomic-like function in every atomic sphere.

The solutions to the Kohn-Sham equations are expanded in this combined basis set of LAPW's according to the linear variation method

$$\psi_k = \sum_n c_n \phi_{k_n}$$

And the coefficients c_n c_n are determined by the Rayleigh-Ritz variational principle. The convergence of this basis set is controlled by a cutoff parameter $R_{mt} K_{\max}$ = 6 - 9, where R_{mt} R_{mt} is the smallest atomic sphere radius in the unit cell and $K_{\max}$ is the magnitude of the largest K vector in the equation above.

In order to improve upon the linearization (i.e. to increase the flexibility of the basis) and to make possible a consistent treatment of semicore and valence states in one energy window (to ensure orthogonality) additional (k_n independent) basis functions can be added. They are called "local orbitals (LO)"

and consist of a linear combination of two radial functions at two different energies:

$$\phi_{lm}^{LO} = \left[A_{lm} u_l(r, E_{1,l}) + B_{lm} \dot{u}_l(r, E_{1,l}) + C_{lm} u_l(r, E_{1,l})\right] Y_{lm}(\hat{r})$$

The coefficients A_{lm}, B_{lm} and C_{lm} are determined by the requirements that ϕ^{LO} should be normalized and has zero value and slope at the sphere boundary.

2.1.2 The APW + lo Method

It has been shown that the standard LAPW method with the additional constraint on the PWs of matching in value and slope to the solution inside the sphere is not the most efficient way to linearize Slater's APW method. It can be made much more efficient when one uses the standard APW basis, but of course with $u_l(r,E_l)$ $u_l(r, E_{1,})$ at a fixed energy E_l E_1 in order to keep the linear eigenvalue problem. One then adds a new local orbital (lo) to have enough variational flexibility in the radial basisfunctions:

$$\phi_{k_n} = \sum_{lm} \left[A_{lm,k_n} u_l(r, E_l)\right] Y_{lm}(\hat{r})$$

$$\phi_{lm}^{LO} = \left[A_{lm} u_l(r, E_{1,l}) + B_{lm} \dot{u}_l(r, E_{1,l})\right] Y_{lm}(\hat{r})$$

This new lo looks almost like the old "LAPW"-basis set, but here the A_{lm} and B_{lm} do not depend on k_n and are determined by the requirement that the lo is zero at the sphere boundary and normalized.

This new scheme converges practically to identical results as the LAPW method, but allows to reduce "$RK_{\max}$" by about one, leading to significantly smaller basis sets (up to 50 %) and thus the corresponding computational time is drastically reduced (up to an order of magnitude). In general one describes by APW+lo those orbitals which converge most slowly with the number of PWs or the atoms with a small sphere size, but the rest with ordinary LAPWs. One can also add a second LO at a different energy so that both, semicore and valence states, can be described simultaneously.

2.1.3 General Considerations

In its general form the LAPW (APW+lo) method expands the potential in the following form

$$V(r) = \begin{cases} \sum_{LM} V_{LM}(r) Y_{LM}(\hat{r}) & inside \quad sphere \\ \sum_{\mathrm{K}} V_{\mathrm{K}} e^{i\mathrm{K}\cdot r} & outside \quad sphere \end{cases}$$

and the charge densities analogously. Thus no shape approximations are made, a procedure frequently called a "full-potential"method. The "muffin-tin"approximation used in early band calculations corresponds to retaining only the l = 0 component in the first expression of the equation above and only the K = 0 component in the second. This (much older) procedure corresponds to taking the spherical average inside the spheres and the volume average in the interstitial region.

CHAPTER 3

ADSORPTION OF ATOMIC HYDROGEN AND OXYGEN ON (0001) SURFACE OF DOUBLE HEXAGONAL CLOSED PACKED AMERICIUM

In this chapter, first we give a brief outline about the computational details and the theory used for our calculations, followed by the discussion of our results on the atomic hydrogen and oxygen adsorption on (0001) surface of dhcp-Am. As in *some* of our previous works[38-44], all calculations have been performed within the generalized gradient approximation to density functional theory (GGA-DFT) with the Perdew-Burke-Ernzerhof (PBE) exchange-correlation functional.[45] The Kohn-Sham equations were solved using the full-potential linear augmented plane wave plus local basis (FP-LAPW+lo) method as implemented in the WIEN2k code.[46-48] This method makes no shape approximation to the potential or the electron density. Within the FP-LAPW+lo method, the unit cell is divided into non-overlapping muffin-tin spheres and an interstitial region. Inside the muffin-tin sphere of radius R_{MT}, the wave functions are expanded using radial functions (solutions to the radial Schrödinger equation) times spherical harmonics with angular momentum up to $l_{\max}^{wf}$ =10. Non-spherical contributions to the electron density and potential inside the muffin tin spheres were considered up to $l_{\max}^{pot}$ =6. APW+lo basis were used to describe *s, p, d,* and *f* (*l*=0, 1, 2, 3) states and LAPW basis were used for all

higher angular momentum states in the expansion of the wave function. Additional local orbitals (LO) were added to the 2*s* semi-core states of O and the 6*s*, 6*p* semi-core states of Am to improve their description. The radii of the muffin-tin spheres were R_{MT} (H) = R_{MT} (O)=1.2 Bohr and R_{MT}(Am) = 2.2 Bohr. The truncation of the modulus of the reciprocal lattice vector used for the expansion of the wave function in the interstitial region K_{MAX}, was set by $R_{MT}K_{MAX}$ = 8.5 for the clean slab and $R_{MT}K_{MAX}$ = 4.64 for the slab-with-adatom, where R_{MT} denotes the smallest muffin tin radius, that is, R_{MT} = 2.2 a.u. for the bare slab and R_{MT} = 1.2 a.u. for the slab-with-adatom.

In the WIEN2k code, core states are treated at the fully relativistic level. Semi-core and valence states are treated at either the scalar relativistic level, i.e., no spin-orbit coupling (NSOC) or at the fully relativistic level, i.e., spin-orbit coupling (SOC) included. Spin-orbit interactions for semi-core and valence states are incorporated via a second variational procedure using the scalar relativistic eigenstates as basis,[49] where all eigenstates with energies below the cutoff energy of 4.5 Ry were included, with the so-called $p_{1/2}$ extension,[50] which accounts for the finite character of the wave function at the nucleus for the $p_{1/2}$ state. We considered both the NSOC and SOC levels of theory to investigate spin-orbit coupling effects on chemisorption energies.

The dhcp-Am (0001) surface was modeled by a supercell consisting of a periodic 6-layer slab with a (2×2) surface unit cell and vacuum of 30 Bohr thickness. In accordance with our previous findings,[41,42] we have used an AFM

configuration for the slab which consists of alternating ferromagnetic layers of up-spin and down-spin atoms along the *c*-axis. The spin quantization axis for the magnetic SOC calculations was along the [001] direction. The relaxation of the surface was carried out in two steps: first, bulk dhcp Am was optimized followed by surface optimization. The atomic volume of bulk dhcp Am was expressed in terms a single lattice constant by constraining the ratio *c*/*a* to match experimental value. More precisely, the ratio *c*/*a* was set to 3.2 (experimental ratio) and the volume V was expressed in terms of only *a*. Then the total energy *E* (for an AFM configuration) was computed for several variations of *V*. The energy versus volume E-V fit via Murnaghan's equation of state[52] generated an equilibrium volume Vo = 208.6 $(a.u.)^3$ and B = 25.4 GPa. The equilibrium volume Vo corresponded to *a*=6.702 a.u. The experimental values are 198.4 $(a.u.)^3$ or 197.4 $(a.u.)^3$ and 29.7 GPa.[20,27,51] Integrations in the Brillouin zone (BZ) have been performed using the special k-points sampling method with the temperature broadening of the Fermi surface by the Fermi distribution, where a broadening parameter $K_B T$ = 0.005 Ry has been used. The temperature broadening scheme avoids the instability from level crossings in the vicinity of the Fermi surface in metallic systems and also reduces the number of k-points necessary to calculate the total energy of metallic systems .[55] For the present work, a 6×6×1 k-mesh density (18 k-points in the irreducible part of the BZ) was deemed to be sufficient. Self-consistency is achieved when the total energy variation from iteration to iteration is 0.01 mRy or better.

Using the optimized lattice constants, that is, a=6.702 a.u. and c = 3.2a, a 2x2 hexagonal surface unit cell (2 atoms along each lateral 2D direction yielding 4 Am atoms per surface unit cell) for (0001) orientation is constructed. Then the surface unit cell is used to build the slab with 6 atomic layers (with the proper layer stacking *ABABAB*....., taken into account) and 30 a.u. vacuum. Furthermore, the slab was built to have inversion symmetry for computational efficiency. The interlayer spacing between the surface unit cells in the slab above corresponded to the bulk spacing d_0= *c/4.* Next, the central layers are fixed at the bulk positions but the 2 outermost layers (this is the same from both sides of the central slabs because of inversion symmetry) are allowed to relax in order to lower the total energy. The relaxation was performed by minimizing the total energy by varying d_{12}, the separation between the central and subsurface layers and d_{23}, the separation distance between the subsurface and surface layers (variations of -4%, -2%, 0%, 2%, 4% measured in terms of the bulk interlayer spacing d_0 for d_{12} and d_{23} resulting in a 5x5 grid for the energy computation). The relaxations obtained were $\Delta d_{12}/d_0$ = 0% and $\Delta d_{23}/d_0$ = 2%, where d_0 is the bulk interlayer separation, with the reduction in the total energy of the slab being 2.19 mRy. The small relaxations and reduction in the total energy indicate the fair stability of the surface. To study adsorption on the *relaxed* Am surface, the adatom, corresponding to a surface coverage of Θ = 1/4 ML, was allowed to approach

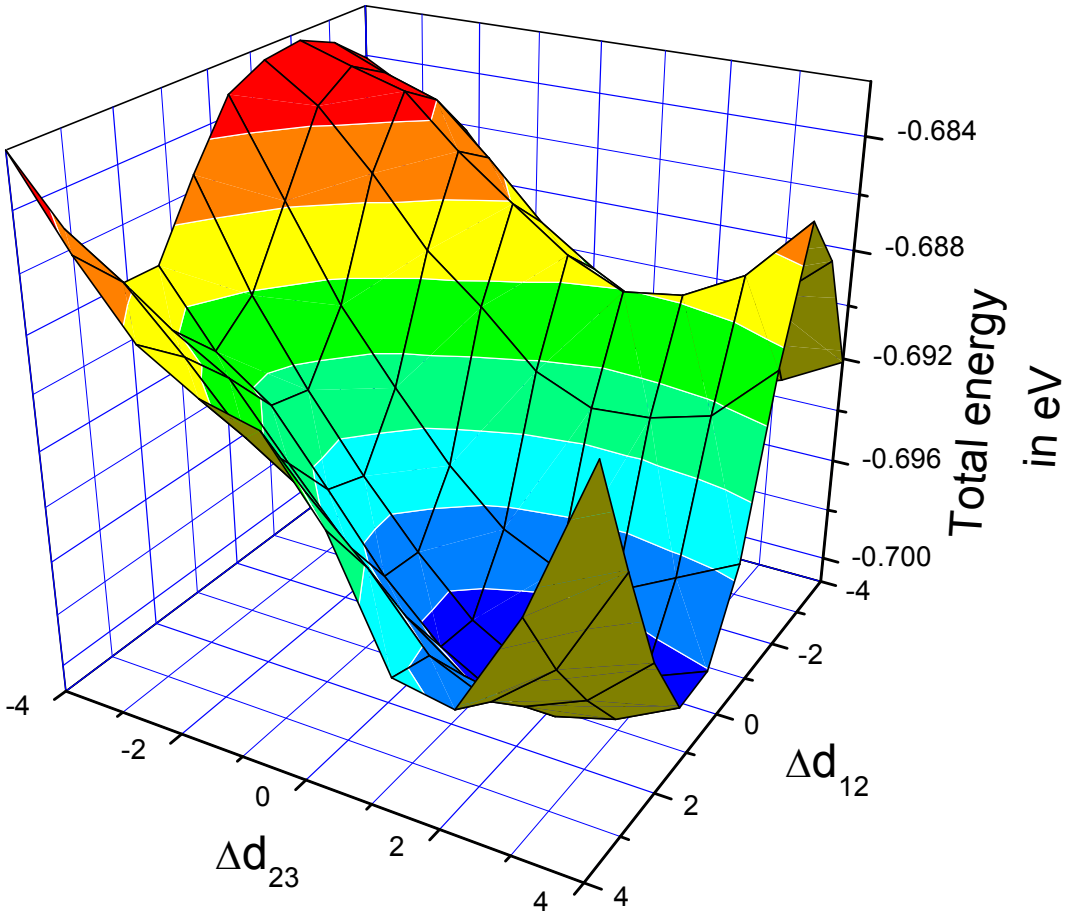

Figure 3.1 Relaxation of (0001) surface of dhcp-Am. Δd_{12} is the percent relaxation of the subsurface layer and Δd_{23} is the percent relaxation of the surface layer. Total energy is shifted by a constant factor.

the surface from both sides to preserve inversion symmetry. Three high symmetry adsorption sites were considered (see FIG. 2): (i) one-fold top site (adatom is directly on top of an Am atom) (ii) two-fold bridge site (adatom is placed in the middle of two nearest neighbor Am atoms); and (iii) three-fold hollow hcp site (adatom "sees" an Am atom located on the layer directly below the surface layer). The chemisorption energy E_C is optimized with respect to the height R of the adatom above the bare relaxed surface. No *further* surface relaxations and/or reconstructions were taken account for both physical (any further relaxations is expected to be quite small) and computational reasons We believe though that further relaxations and/or reconstructions during adsorption, *if any,* will *not* significantly alter the results reported here both qualitatively *and* quantitatively. This is discussed further below. The chemisorption energy E_C is given by:

$E_C(R) =$ 1/2[E(Am) + 2E(X) –E(Am+X)],

where E(Am) is the total energy of the bare Am slab, E(X) is the total energy of the isolated adatom, and E(Am+X) is the total energy are the slab-with-adatom. A positive value of E_C implies chemisorption and a negative value implies otherwise. To calculate the total energy of the adatom, the isolated atom was simulated in a large box of side 25 Bohr and at the Γ k-point, with all other computational parameters remaining the same. Also, our recent studies on adsorption on the δ-Pu surface indicated that spin-orbit coupling has negligible effect on the adsorption geometry but the binding was slightly stronger with the

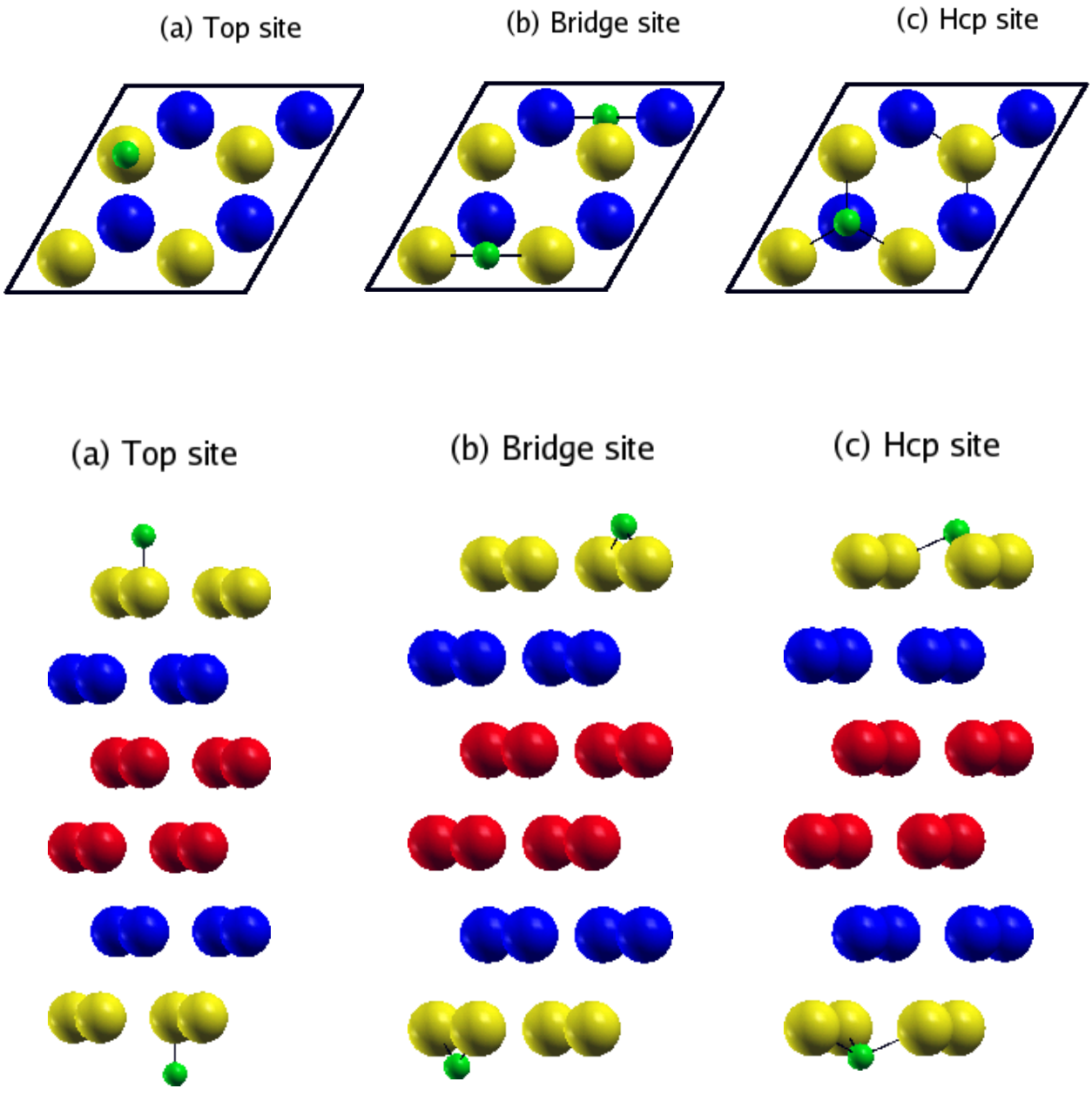

Figure 3.2 Top and side view illustrations of the three high-symmetry adsorption sites for the six-layer dhcp-Am(0001) slab with a 0.25 ML adlayer coverage: (a) one-fold top site; (b) two-fold bridge site; (c) three-fold hcp site. Atoms are colored to distinguish between the layers. Surface, subsurface, and central layers are colored gold, blue, and red, respectively. Adatom is colored green.

chemisorption energies increasing by 0.05 to 0.3 eV. Though we have not verified this explicitly for the dhcp Am (0001) surface, we expect the same trend to hold here. Hence in the current calculations, the geometry was optimized at the NSOC level and the final geometry was used for the SOC calculation to study the effects of spin-orbit coupling on the adsorption energies.

Table 1 lists the adsorption energies and associated geometrical information of the H and O atoms adsorbed on the (0001) surface of dhcp-Am. The differences between the NSOC and SOC chemisorption energies at each adsorption site, given by $\Delta E_C = E_C(SOC) - E_C(NSOC)$, are also listed. For H adsorption, the trend in the chemisorption energies at the NSOC level of theory is the same as the SOC case. The most stable site is the hollow hcp site (3.136 eV for the NSOC case, 3.217 eV for SOC case), closely followed by the bridge adsorption site (2.965 eV for NSOC case, 3.014 eV for the SOC case), with the least favorable site being the top site (2.272 eV for the NSOC case, 2.377 eV in the SOC case). The vertical height R of the H atom above the surface layer clearly show that at the least stable top site, the adatom is furthest away from the surface (2.122 Å) followed by the next stable bridge site (1.429 Å), with the vertical height of the adatom from the surface layer being the lowest at the most stable hollow hcp site (1.196 Å). Hence, increasing stability at both the NSOC and SOC levels of theory implies decreasing vertical distance of the H adatom from the surface layer. Also increasing stability implies increasing adatom coordination number at both theoretical levels, that is, the H adatom prefers to

Table 3.1 Chemisorption Energies E_c, Distance of the Adatom from the Surface Layer R, the Distance of the Adatom from the Nearest Neighbor Am Atom $D_{Am\text{-}adatom}$ at Both the NSOC and SOC Levels of Theory. $\Delta E_C = E_C(SOC) - E_C(NSOC)$ is the Difference Between the Chemisorption Energies at each Adsorption Site.

Adatom	Site	E_C (eV) (NSO)	E_C (eV) (SO)	R (Å)	$D_{Am\text{-}adatom}$ (Å)	ΔE_C (eV)
Hydrogen	Top	2.272	2.377	2.122	2.122	0.105
	Bridge	2.965	3.014	1.429	2.277	0.049
	Hcp	3.136	3.217	1.196	2.371	0.081
Oxygen	Top	6.388	6.599	1.911	1.911	0.211
	Bridge	8.204	8.368	1.164	2.121	0.164
	Hcp	8.109 (8.139)	8.347 (8.315)	0.878	2.228	0.238 (0.176)

bind at the maximally coordinated three-fold hollow hcp site. The Am-H bond lengths listed in Table I also indicate a relationship with the adatom coordination numbers, with the one-fold coordinated top site having the shortest bond and the three-fold hollow hcp site having the longest bond. All chemisorption energies indicate that binding is slightly stronger with the inclusion SOC compared the NSOC case. The SOC-NSOC chemisorption energy differences ΔE_C are listed in Table I; ΔE_C is maximum at the least stable top site (0.105 eV) closely followed by the next stable hollow hcp adsorption site (0.081 eV), with the intermediately stable bridge adsorption site having an SOC-NSOC ΔE_C = 0.049 eV.

For O adsorption, the trend in the chemisorption energies for the NSOC case is also the same as that in the SOC case. The most stable site is the bridge site (8.204 eV for the NSOC case, 8.368 eV for SOC case). This is closely followed by the hollow hcp site (8.109 eV for NSOC case, 8.347 eV for the SOC case), with the least favorable site being the top site (6.388 eV for the NSOC case, 6.599 eV in the SOC case). As a comparison, for NSOC calculations for O adsorption on the δ – Pu (111) surface, the hollow hcp adsorption site was found to be the most stable site for O with chemisorption energy of 8.025 eV. For SOC calculations, the hollow fcc adsorption site was found to be the most stable site with a chemisorption energy of 8.2 eV respectively. The optimized distance of the O adatom from the Pu surface was found to be 1.25 Å. The vertical height R of the O atom above the Am surface

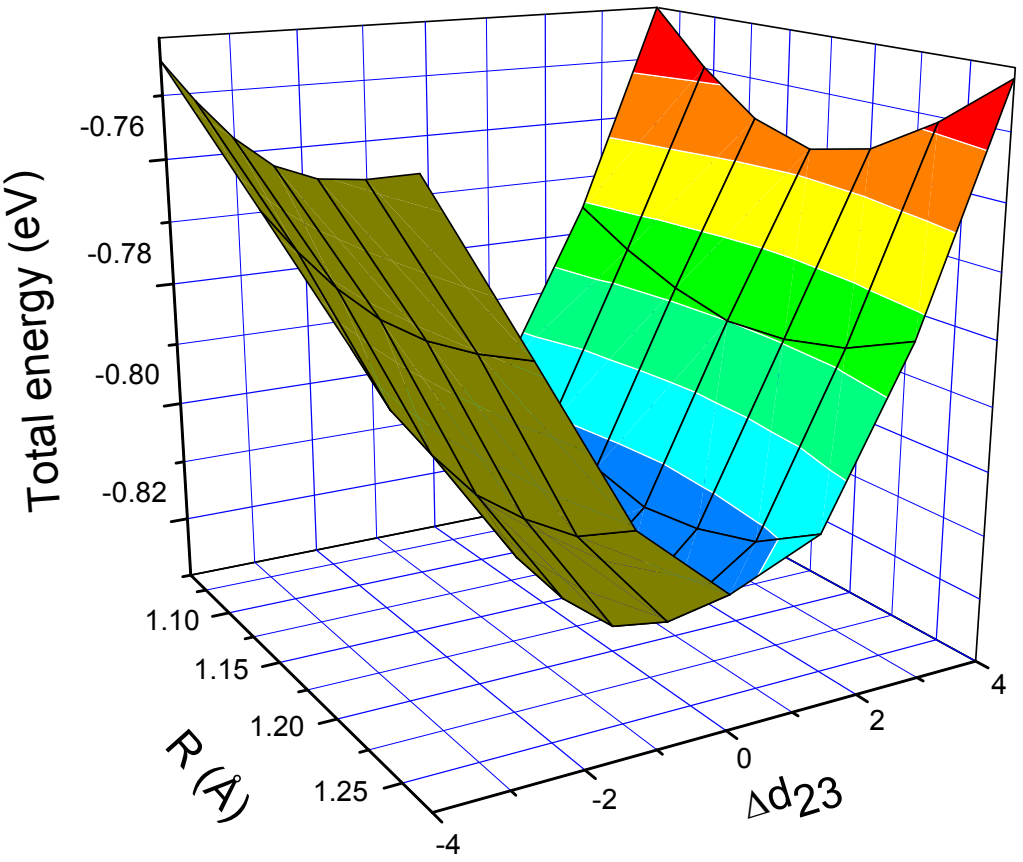

Figure 3.3 Simultaneous relaxation of adatom and the surface layer of (0001) surface of dhcp-Am at the two-fold bridge adsorption site. Δd_{23} is the percent relaxation of the surface layer and R (Å) is the distance of the adatom from the surface. Total energy is shifted by a constant factor.

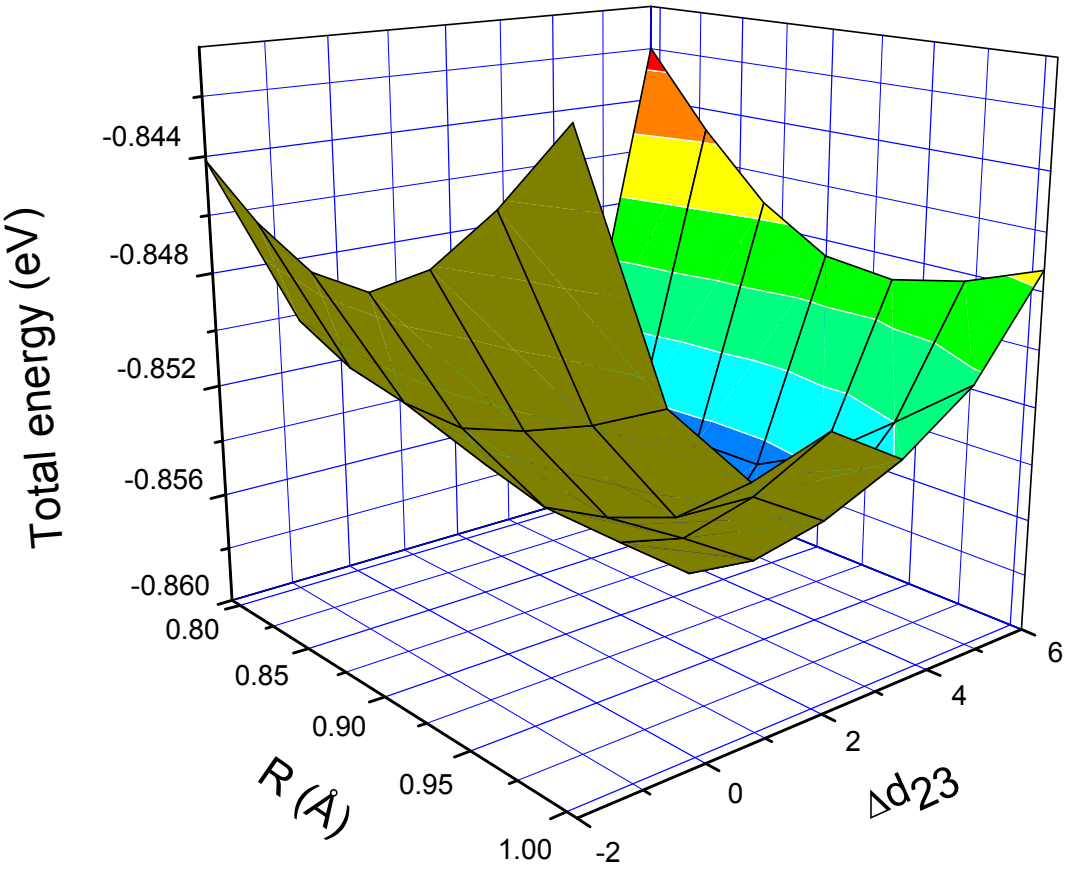

Figure 3.4 Simultaneous relaxation of adatom and the surface layer of (0001) surface of dhcp-Am at the three-fold hcp adsorption site. Δd_{23} is the percent relaxation of the surface layer and R (Å) is the distance of the adatom from the surface.

layer clearly show that for the least stable top site, the adatom is furthest away from the surface (1.911 Å), followed by the most stable bridge site (1.164 Å), with smallest distance corresponding to the intermediately stable hollow hcp site (0.878 Å). Here, unlike the case for H, increasing stability at both the NSOC and SOC levels of theory does not necessarily imply decreasing vertical distance of the O adatom from the surface layer, since the distance at the most stable bridge site is greater than the distance at the next stable hollow hcp site. Furthermore, the most preferred bridge adsorption site does not have the maximum coordination. However, chemisorption energies in the SOC case are more stable than the NSOC case; ΔE_C is maximum at the hcp hollow site (0.238 eV) closely followed by the least stable top adsorption site (0.211 eV), with the most stable bridge adsorption site having an SOC-NSOC ΔE_C = 0.164 eV. Also, it is worth noting that the Am-H bond lengths are longer than Am-O bond lengths for each adsorption site as expected.

As stated earlier, we expect the adsorbate-induced relaxations to have very little effect on the geometry and chemisorption energies. We tested this for the oxygen adatom, which is more reactive than hydrogen, by allowing it and the Am surface layer to relax simultaneously. The tests were performed explicitly for the hollow hcp and bridge sites as they have nearly degenerate chemisorption energies. Upon relaxation, the interlayer separation between the surface and subsurface layers, $\Delta d_{23}/d_0$, was 0% for the bridge site and 4% for the hollow hcp site, (Figs 3 and 4) with the vertical distance of O from the

surface remaining unchanged. Thus for the bridge site, there was no change is the chemisorption energy reported in Table 1. However, for the hollow hcp site, the relaxation stabilizes the NSOC chemisorption energy in Table 1 by 0.030 eV and the SOC chemisorption energy by -0.032 eV, with the bridge site still being most stable (the relaxed energies are shown in brackets in Table 1). It therefore can be concluded that relaxation of the slab during chemisorption is insignificant and does not change the preferential ordering of the sites.

In table 2, the adsorbate-induced work function changes with respect to the clean metal surface, given by $\Delta\Phi = \Phi^{adatom/Am} - \Phi^{Am}$, are listed for the NSOC and SOC levels of theory for each adsorbate and each adsorption site. We observe that for the hydrogen adatom at each theoretical level high chemisorption energies generally correspond to low work function shifts. In fact, the changes in the work functions are largest at the least preferred top site and lowest at the most preferred hcp hollow site. This is not true for oxygen adsorption though, where the most preferred bridge site has a higher change in the work function compared to the hcp hollow site. In both cases however, the magnitude of the work function shifts is related to the adsorption site coordination; the lower coordinated top site shows the largest shift and the higher coordinated hollow hcp site shows the lowest shift. The adsorbate-induced work function shifts can be understood in terms of the surface dipoles arising due to the displacement of electron density from the substrate towards the adsorbates since the electronegativities of the adsorbates are larger than

Table 3.2 Change in Work Function $\Delta\Phi = \Phi^{adatom/Am} - \Phi^{Am}$ (in eV) for Both the NSOC and SOC Levels of Theory. Φ^{Am} = 2.906 eV and 2.989 eV respectively at the NSOC and SOC Theoretical Level.

Theory	Site	Hydrogen	Oxygen
NSOC	Top	1.149	1.343
	Bridge	0.321	0.499
	Hcp	0.156	0.388
SOC	Top	1.138	1.339
	Bridge	0.319	0.477
	Hcp	0.151	0.314

that of Am. The surface dipole moment μ (in Debye) and the work function shift ΔΦ (in eV) are linearly related by the Helmholtz equation ΔΦ =12ΠΘμ/A, where A is the area in $Å^2$ per (1×1) surface unit cell and Θ is the adsorbate coverage in monolayers. From the Helmholtz equation, we see that for each adsorbed adatom, μ is largest at the top site and smallest at the hcp hollow site.

In table 3, the magnitude and alignment of the site projected spin magnetic moments for each Am atom on the *surface* atomic layer is reported for the clean metal surface and the chemisorbed systems. Here we report the moments for the SOC calculations. NSOC moments follow a similar qualitative trend and are not reported here. Also, when the chemisorbed system was compared to the bare slab, the moments for subsurface and central layers reduced by a very small amount of 0 to 0.02 μ_B and were therefore not reported. For each adsorption site, the spin moment of the closest neighbor surface layer Am atoms with which the adatom primarily interacts is indicated in bold fonts in the table 3. For the top sites, we see reductions of 0.14 μ_B and 0.62 μ_B in the spin moment of the Am atom for H and O chemisorptions respectively, while the moments of the remaining three Am atoms remain basically unaltered when compared to the clean surface. This naturally leads to a reduction in the net spin magnetic moment per Am atom. For the bridge sites, we see reductions of 0.08 μ_B and 0.27 μ_B in the spin moments of each of the two surface Am atoms for H and O chemisorptions respectively, while very small or no change in the moments of the other two Am atoms occurs when

Table 3.3 μ (μ_B) are the Site Projected Spin Magnetic Moment for each Am Atom for the Surface Layer of the Bare Slab, Hydrogen Adsorbed System and Oxygen Adsorbed System. Spin Moments are Quoted for SOC Calculations.

	Site	μ (μ_B)		Site	μ (μ_B)
Bare Slab		5.81, 5.81 5.81, 5.81			
Hydrogen	Top	5.67, 5.80 5.80, 5.80	Oxygen	Top	5.19, 5.81 5.81, 5.81
	Bridge	5.73, 5.73 5.80, 5.80		Bridge	5.54, 5.54 5.81, 5.81
	Hcp	5.75, 5.75 5.75, 5.79		Hcp	5.65, 5.65 5.65, 5.81

compared to the clean slab. For the hollow hcp sites, reductions of 0.06 μ_B and 0.16 μ_B in the spin moments for each of the three Am atoms can be observed for H and O respectively, with little or no changes in the moment of the fourth Am atom. Therefore the reduction in the net moment stems primarily from the reduction in the spin moments of the surface Am atoms interacting with the adatoms. We note also that the moments in the interstitial region decreased after chemisorption in all cases. The quench in the magnetic moments can be directly attributed to the charge transfer from Am to the adatoms during chemisorption. .

Due to the nature of the APW+lo basis, the electronic charges inside the muffin-tin spheres can be decomposed into contributions from the different angular momentum channels. We refer to these charges as partial charges. By comparing the partial charges Q_B of the Am layers and adatoms before adsorption to the corresponding partial charges Q_A after adsorption, we can get an idea of the nature of the interaction between the adsorbate and substrate. Thus we have reported Q_A and Q_B for each adatom and the Am atoms at each adsorption site in tables 4 and 5. In each table, we have also reported the differential partial charge of a given state *l* corresponding to a given atom, which is given by $\Delta Q(l) = Q_A - Q_B$. $\Delta Q(l) > 0$ indicates charge gain inside the muffin tin sphere while $\Delta Q < 0$ indicates otherwise. Upon examining ΔQ for the Am atoms on the central and subsurface layers, we observed no significant changes. Hence the partial charges will be discussed only for the surface layer.

Table 3.4 Partial Charges Inside Muffin Tin Spheres Before Adsorption (Q_B), After Adsorption (Q_A), and Difference in Partial Charges $\Delta Q = Q_A - Q_B$ at the Various Adsorption Sites for Hydrogen at the SOC Level of Theory.

Site	Atom/Layer	Partial charges in muffin-tin						$\Delta Q = Q_A - Q_B$		
		Before adsorption Q_B			After adsorption Q_A					
		H *s*	Am *d*	Am *f*	H *s*	Am *d*	Am *f*	H *s*	Am *d*	Am *f*
Top	Hydrogen	0.41			0.57			0.16		
	Am surface		0.27	5.85		0.26	5.87		-0.01	0.02
	layer		0.27	5.85		0.26	5.87		-0.01	0.02
			0.27	5.85		0.31	5.76		0.04	-0.09
			0.27	5.85		0.26	5.87		-0.01	0.02
Bridge	Hydrogen	0.41			0.59			0.18		
	Am surface		0.27	5.85		0.28	5.82		0.01	-0.03
	layer		0.27	5.85		0.28	5.82		0.01	-0.03
			0.27	5.85		0.26	5.86		-0.01	0.01
			0.27	5.85		0.26	5.86		-0.01	0.01
Hcp	Hydrogen	0.41			0.59			0.18		
	Am surface		0.27	5.85		0.28	5.83		0.01	-0.02
	layer		0.27	5.85		0.28	5.83		0.01	-0.02
			0.27	5.85		0.27	5.85		0.00	0.00
			0.27	5.85		0.28	5.83		0.01	-0.02

Table 3.5 Partial Charges Inside Muffin Tin Spheres Before Adsorption (Q_B), After Adsorption (Q_A), and Difference in Partial Charges $\Delta Q = Q_A - Q_B$ at the Various Adsorption Sites for Oxygen at the SOC Level of Theory.

Site	Atom/Layer	Partial charges in muffin-tin						$\Delta Q = Q_A - Q_B$		
		Before adsorption Q_B			After adsorption Q_A					
		O *p*	Am *d*	Am *f*	O *p*	Am *d*	Am *f*	O *p*	Am *d*	Am *f*
Top	Oxygen	2.17			2.38			0.21		
	Am surface layer		0.27	5.85		0.25	5.88		-0.02	0.03
			0.27	5.85		0.25	5.88		-0.02	0.03
			0.27	5.85		0.48	5.59		0.21	-0.26
			0.27	5.85		0.25	5.88		-0.02	0.03
Bridge	Oxygen	2.17			2.42			0.25		
	Am surface layer		0.27	5.85		0.33	5.73		0.06	-0.12
			0.27	5.85		0.33	5.74		0.06	-0.11
			0.27	5.85		0.25	5.88		-0.02	0.03
			0.27	5.85		0.25	5.88		-0.02	0.03
Hcp	Oxygen	2.17			2.44			0.27		
	Am surface layer		0.27	5.85		0.29	5.79		0.02	-0.06
			0.27	5.85		0.29	5.79		0.02	-0.06
			0.27	5.85		0.27	5.86		0.00	0.01
			0.27	5.85		0.29	5.79		0.02	-0.06

In table 4, Q_A, Q_B, and $\Delta Q(l)$ for H adsorbed at the top, bridge, and hcp sites respectively on the dhcp-Am(0001) surface are reported. For the one-fold top site, $\Delta Q(1s) = 0.16$ for H, $\Delta Q(6d) = 0.04$ and $\Delta Q(5f) = -0.09$ for the Am atom, implying significant Am(6*d*)-Am(5*f*)-H(1*s*) hybridizations. For the two-fold bridge site, $\Delta Q(1s) = 0.18$ for H, $\Delta Q(6d) = 0.01$ and $\Delta Q(5f) = -0.03$ for each of the two Am atoms, suggesting the participation of some of the Am 5*f* electrons in chemical bonding with H. For the three-fold hollow hcp site, ΔQ (1*s*) = 0.18 for H, $\Delta Q(6d) = 0.01$ and $\Delta Q(5f) = -0.02$ for each of the three Am atoms, which again suggest some contribution of the Am 5*f* electrons to Am-H bonding. In table 5, Q_A, Q_B, and $\Delta Q(l)$ for O adsorbed at the top, bridge, and hcp sites respectively on the dhcp-Am(0001) surface are reported. For the top site, ΔQ (2*p*) = 0.27 for O, $\Delta Q(6d) = 0.21$ and $\Delta Q(5f) = -0.24$ for the Am atom, which like the case for H, implies significant Am(6*d*)-Am(5*f*)-O(2*p*) interactions. For the bridge site, ΔQ (2*p*) = 0.25 for O, $\Delta Q(6d) = 0.06$ and $\Delta Q(5f) = -0.11$ per each of the two Am atoms, suggesting the participation of some the Am 5*f* electrons in Am-O bonding. For the hollow hcp site, $\Delta Q(2p) = 0.27$ for O, $\Delta Q(6d) = 0.02$ and $\Delta Q(5f) = -0.06$ per each of the three Am atoms, which again suggest some contribution of the Am 5*f* electrons to Am-O chemical bonding. Overall, the partial charge analyses tend to suggest that some of the Am 5*f* electrons participate in chemical bonding. We wish to stress that the partial charges are confined inside the muffin tin spheres and do not give any information of the interactions between the atoms in the interstitial region. Information which

includes the electronic charges in interstitial region can be obtained from the difference charge density distributions.

To investigate the nature of the bonds that have been formed between the adatoms and the Am atoms on the surface, we computed the difference charge density distribution. We define the difference charge density Δn(r) as follows:

$$\Delta n(r) = n(X+Am) - n(Am) - n(X),$$

where n(X+Am) is the total electron charge density of the Am slab-with-X adatom, n(Am) is the total charge density of the bare Am slab, and n(X) is the total charge density of the adatom. In computing n(X) and n(Am), the adatom X and Am atoms are kept fixed at exactly the same positions as they were in the chemisorbed systems. All charge densities reported here were computed in the plane passing through the adatom and two surface Am atoms using the Xcrysden utility.[60] For the 1-fold coordinated top site, the plane passes through the adatom, the Am atom interacting with the adatom, and a neighboring Am atom. For the 2-fold coordinated bridge site, the plane passes through the adatom and the two Am atoms interacting with the adatom. For the 3-fold coordinated hollow hcp site, the plane passes through the adatom and the two of three Am atoms interacting with the adatom. In figure 5, the difference charge densities distribution for H and O adsorptions are shown for each site. For the top site, we clearly see charge accumulation around each adatom and significant charge loss around the Am atom bonded to the adatom

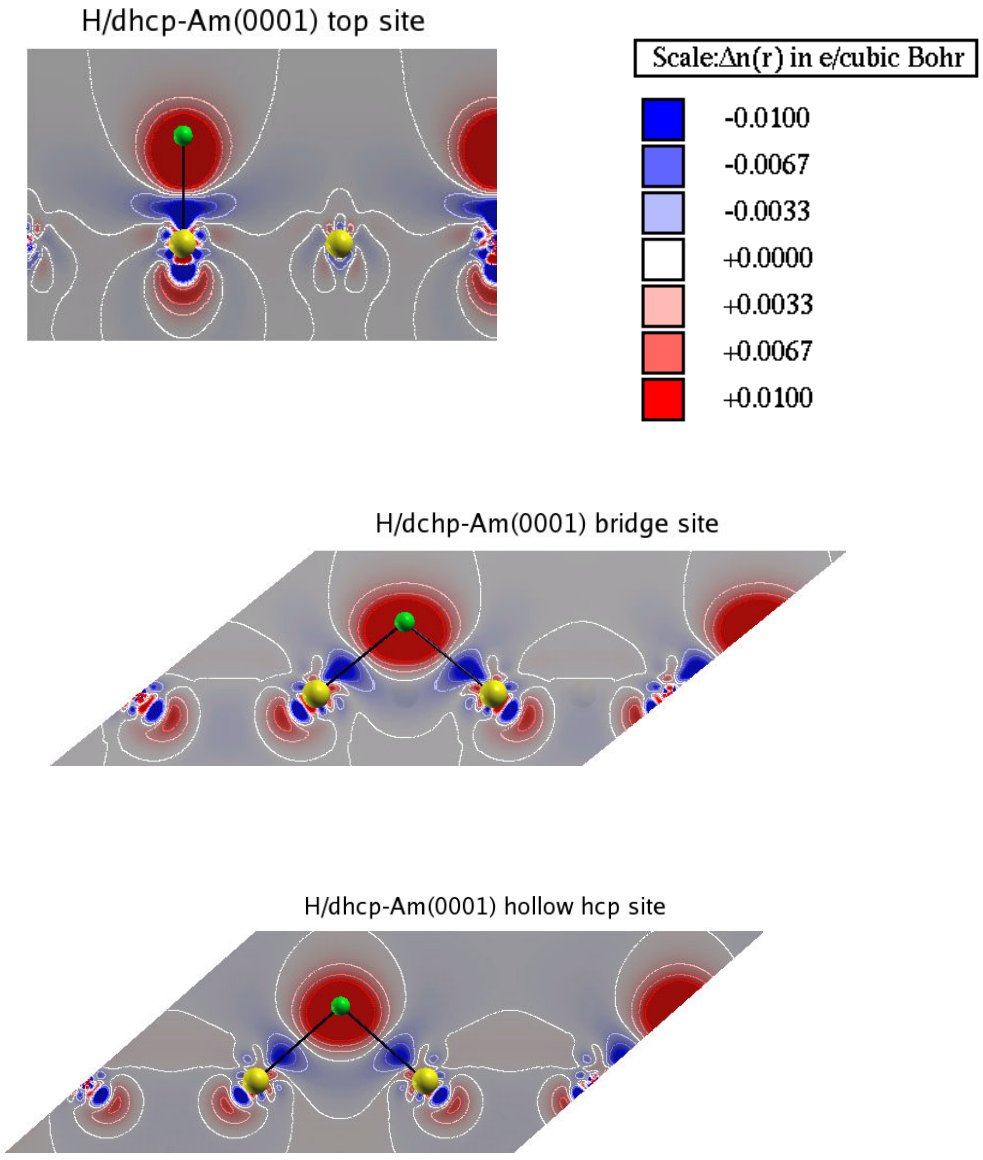

Figure 3.5. Difference charge density distributions Δn(r) for H chemisorbed on the dhcp-Am(0001) surface. Charge densities were computed in a plane passing through the adatom and two neighboring Am atoms. The scale used is shown at the bottom. Red (positive) denotes regions of charge accumulation and blue (negative) denotes regions of charge loss. Adatoms are colored green and Am atoms are colored gold.

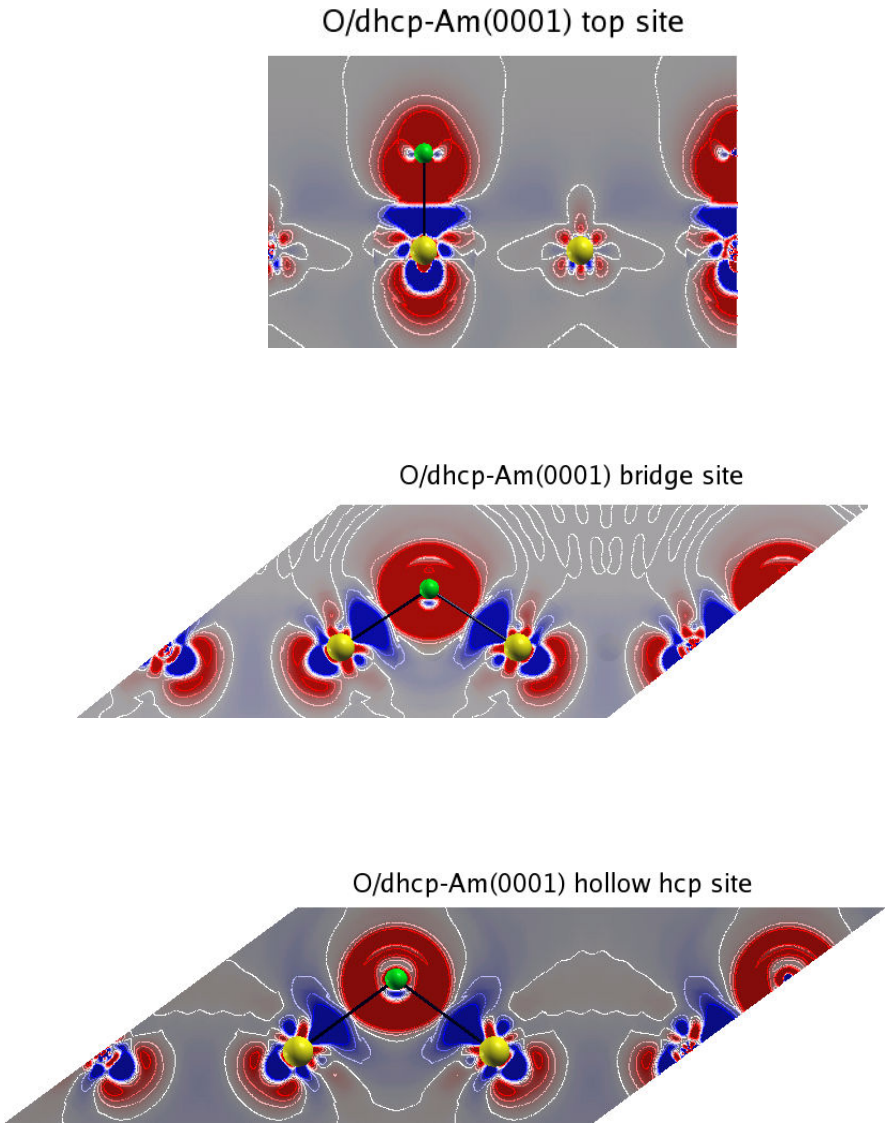

Figure 3.6. Difference charge density distributions Δn(r) for O chemisorbed on the dhcp-Am(0001) surface. Charge densities were computed in a plane passing through the adatom and two neighboring Am atoms. The scale used is shown at the bottom. Red (positive) denotes regions of charge accumulation and blue (negative) denotes regions of charge loss. Adatoms are colored green and Am atoms are colored gold.adatoms,

implying that the bond has a strong ionic character, which is expected as the adatoms are more electronegative than Am. Also the charge loss around Am is larger for O chemisorption since O is more electronegative than H. For the bridge and hollow hcp sites, the Am-adatom bonds are again largely ionic in character as significant charge accumulation around the adatoms can be observed. The difference charge density plots are fairly consistent with the differential partial charges reported in tables 4-5.

The local density of states, which is obtained by decomposing the total density of the single particle Kohn-Sham eigenstates into contributions from each angular momentum channel *l* of the constituent atoms inside the muffin tin sphere have also been examined. Here, we have reported the LDOS for only the SOC computation as the DOS for NSOC calculations yields a similar qualitative description. In figure 6, the Gaussian-broadened (with a width of 0.045 eV) *f* and *d* LDOS curves for each of the layers of the bare dhcp Am (0001) metal slab are shown. Clearly, we see well-defined peaks in the 5*f* electron LDOS in the vicinity of the Fermi level, which have also been observed for bulk dhcp-Am(0001), and is a clear signature of 5*f* electron localization. Also, the $5f_{5/2}$ electron localization is more pronounced for the surface and subsurface layers than the central layer. However, the $5f_{5/2}$ peak centered on a binding energy of 1 eV below the Fermi level instead of the 2.8 eV observed in X-ray and ultraviolet photoemission spectra experiments.[14,19]

In figure 7, we show the LDOS plots for the H adatom and the surface Am atoms before and after chemisorption. As there are four nonequivalent sites on the surface, we depict the LDOS for only the Am atom(s) directly bonded to the adatom in order to assess the changes in DOS upon chemisorption. At the top site, we note some modification in the Am 5*f* DOS just below the Fermi level in comparison to the 5*f* DOS before adsorption which implies that the some 5*f* electrons participate in chemical bonding. We also observe significant Am (6*d*)-H (1*s*) hybridizations with a small admixture of Am (6*f*) states, implying that the Am contribution to bonding is dominated by the 6*d* electrons. The LDOS distributions for the bridge and hcp hollow sites show a slight reduction in the 5*f* DOS below the Fermi level, with the H 1*s* bonding state pushed to lower binding energies, which naturally suggests stronger binding as observed in the chemisorption energies. Except for the slight reduction in the 5*f* DOS below the Fermi level, it is fair to say that the localization of the 5*f* bands are primarily retained after chemisorption.

In figure 8, the LDOS plots for O chemisorptions are shown. For the top site, we see a significant character of the 5*f* and 6*d* bands of Am in the O 2*p* bands. This indicates significant Am (6*d*)-Am (5*f*)-O(2*p*) hybridizations in the -4 eV to -2 eV energy range, which is in fair agreement with the partial charge analysis. The hybridizations lead to modifications in the 5*f* DOS below the Fermi level at the top sites. For the bridge and hcp sites, hybridizations is dominated by Am(6*d*)-O(2*p*) and only slight modifications in the 5*f* bands below the Fermi

level is observed. The overlap of O 2*p* bands with the Am 5*f* bands decreases and O 2*p* bands are pushed to lower energies which is reflected in the strong binding energies. Just like H adsorption, the sharp and peaky nature of the 5*f* bands are retained in general after chemisorption as no significant broadening of the bands is observed.

In summary, we have used the generalized gradient approximation to density functional theory with the full potential LAPW+lo method to study chemisorption of H and O atoms on the (0001) surface of dhcp Am at two theoretical levels; one with no spin-orbit coupling (NSOC) and the other with spin-orbit coupling (SOC). For H adsorption, the hollow hcp site was the most preferred site, while the bridge adsorption was the most preferred site in O adsorption. The inclusion of spin-orbit coupling lowers the chemisorption energies by 0.049-0.238 eV. Work functions increased in all cases compared to the clean Am surface, with the largest shift corresponding to the least coordinated top site and lowest shifts corresponding to the maximally coordinated hollow hcp sites. Upon adsorption, the net spin magnetic moment of the chemisorbed system decreases in each case compared to the bare surface. Difference charge density distributions clearly show that bonds between the surface Am atoms and the adatoms at each site is largely ionic in character. A study of the local density of states for O showed Am (6*d*)-Am (5*f*)-adatom(2*p*) hybridizations at the top site electrons upon chemisorption, while at the bridge and hollow hcp sites the interactions are dominated by Am(6*d*)-

adatom(2*p*). In the general, the 5*f* electron localization behavior of the Am atoms is primarily retained after chemisorption.

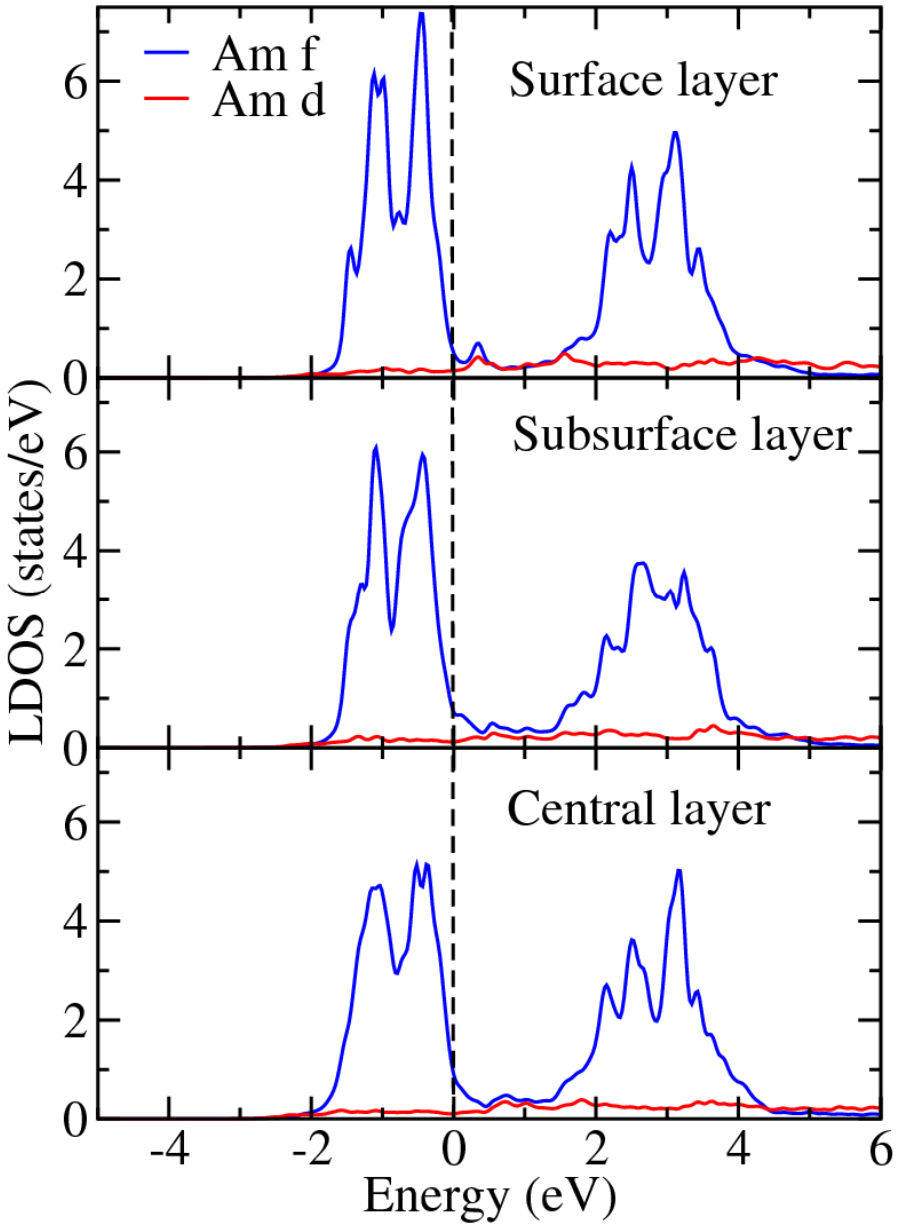

Figure 3.7 *d* and *f* LDOS curves inside the muffin-tins for each layer of the bare dhcp-Am(0001) slab. Vertical line through E=0 is the Fermi level. LDOS correspond to calculations with SOC.

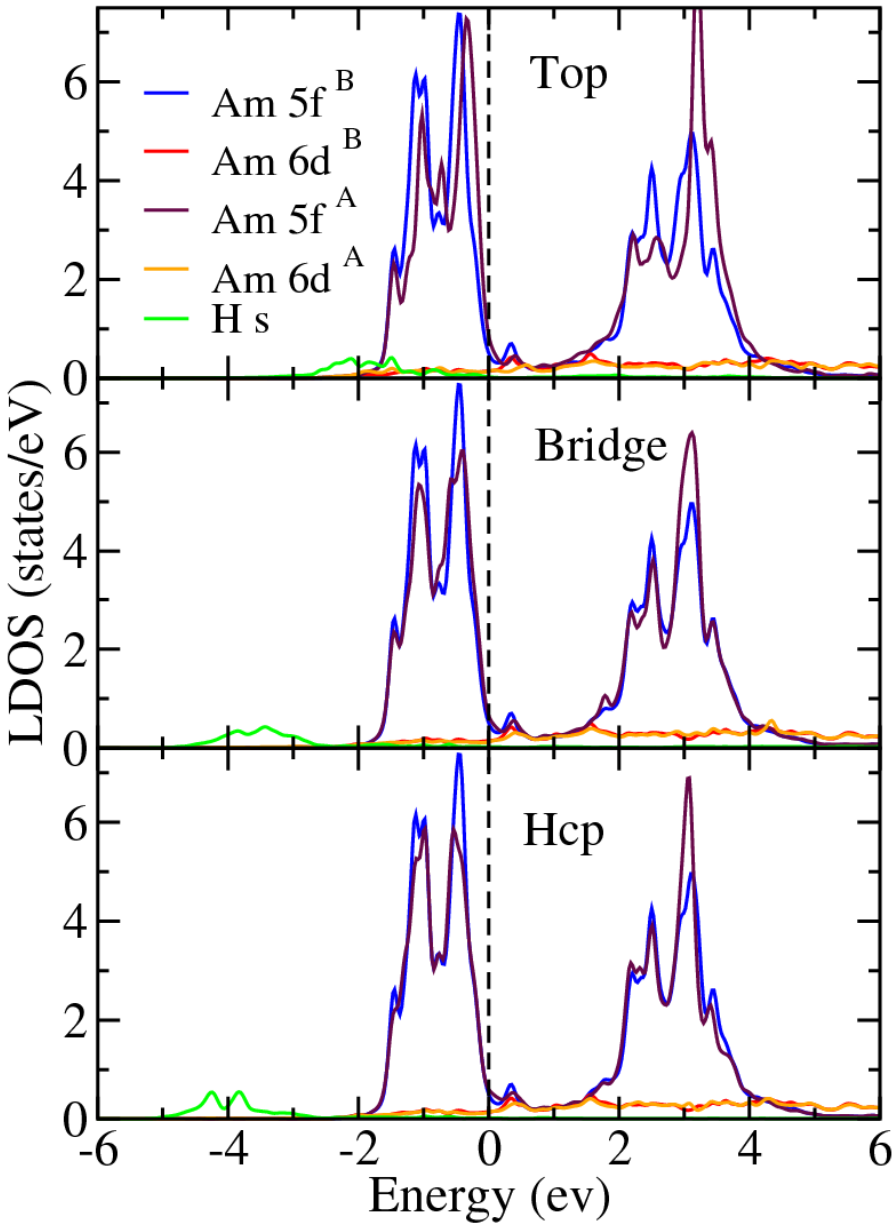

Figure 3.8 *d* and *f* LDOS curves inside the muffin-tins for the Am atoms on the surface layer and *s* LDOS curves for H adatom. Vertical line through E=0 is the Fermi level. LDOS correspond to calculations with SOC. Superscripts *B* and *A* refer to Am *d* and *f* surface layer LDOS before (top panel in FIG. 3) and after adsorption, respectively.

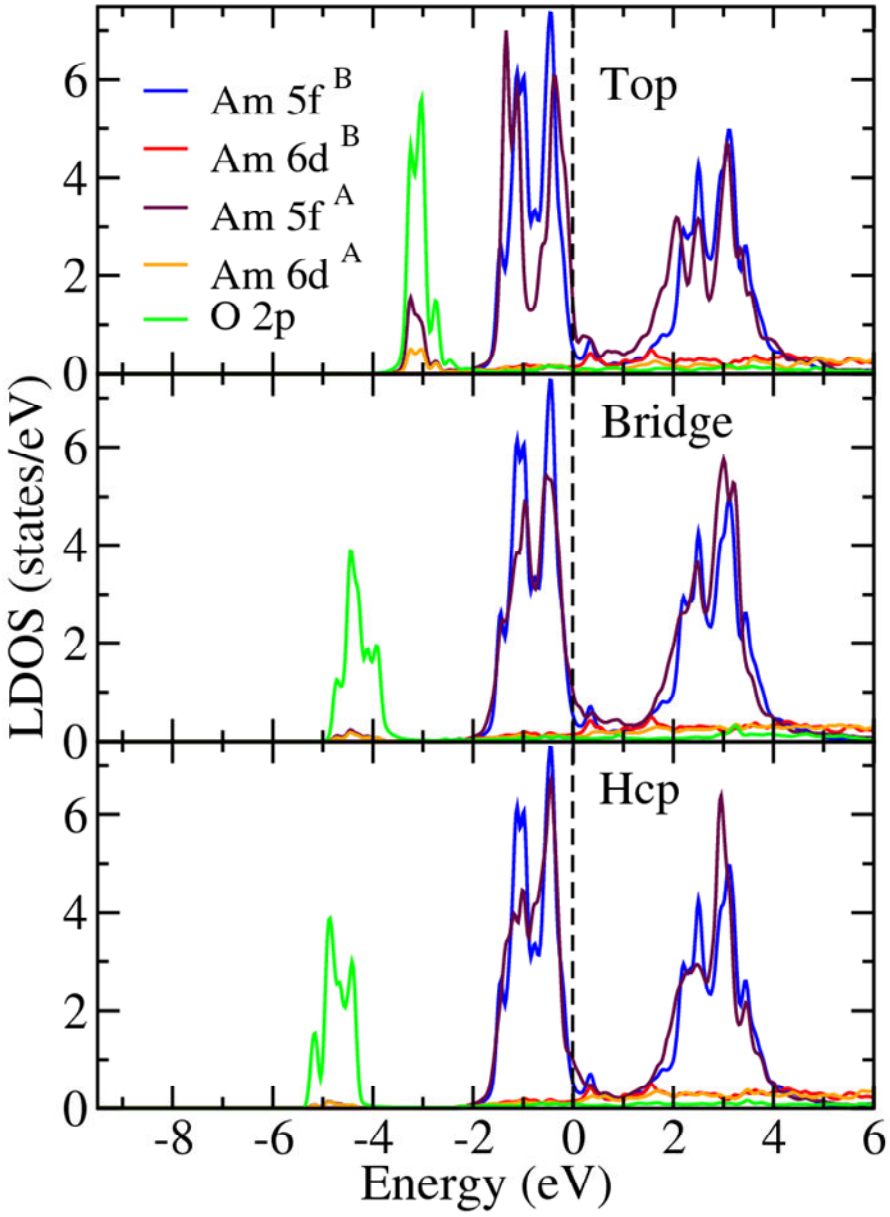

Figure 3.9 *d* and *f* LDOS curves inside the muffin-tins for the Am atoms on the surface layer and *p* LDOS curves for O adatom. Vertical line through E=0 is the Fermi level. LDOS correspond to calculations with SOC. Superscripts *B* and *A* refer to Am *d* and *f* surface layer LDOS before (top panel in FIG. 3) and after adsorption, respectively.

CHAPTER 4

ADSORPTION OF MOLECULAR HYDROGEN AND OXYGEN ON (0001) SURFACE OF DOUBLE HEXAGONAL CLOSED PACKED AMERICIUM

4.1 Molecular Adsorption of H_2 Molecule on (0001) Surface of dhcp-Am

Similar to the previous calculations for the atomic hydrogen and oxygen adsorption on dhcp-Am, all calculations have been performed within the generalized gradient approximation to density functional theory [46-48] using the Perdew-Burke-Ernzerhof (PBE) formulation for the exchange-correlation functional.[45] The Kohn-Sham equations were solved using the full-potential linear augmented plane wave plus local basis (FP-LAPW+lo) method as implemented in the WIEN2k code.[48] Here we would like to mention the differences in different parameters compared to the atomic case. The radii of the muffin tin spheres were R_{MT}(H) = 0.65 Bohr and R_{MT}(Am) = 2.2 Bohr. The truncation of the modulus of the reciprocal lattice vector used for the expansion of the wave function in the interstitial region K_{MAX}, was set to $R_{MT}K_{MAX}$ = 8.5 for the clean slab and $R_{MT}\times K_{MAX}$ = 2.51 for the slab-with-molecule, where R_{MT} denotes the smallest muffin tin radius, that is, R_{MT} = 2.2 Bohrs for the bare slab and R_{MT} = 0.65 Bohrs for the slab-with-molecule (this ensures that K_{MAX} is the same each case). Three high symmetry adsorption sites were considered: (i) one-fold top site t1 (admolecule is directly on top of a Am atom) (ii) two-fold bridge site b2 (admolecule is placed in the middle of two nearest neighbor Am

atoms); and (iii) three-fold hollow hcp site h3 (admolecule sees a Am atom located on the layer directly below the surface layer). For each of these three adsorption sites, three approaches of the H_2 molecule towards to the surface were considered: (a) approach vertical to the surface (Vert approach); (b) approach parallel to a lattice vector (Hor1 approach); (c) approach perpendicular to a lattice vector (Hor2 approach). It is obvious that for both the horizontal approaches the atoms of the hydrogen molecule are at the same distance from the americium surface, whereas for the vertical approach one hydrogen atom is closer to the surface than the other. With these choices of the surface and the ad-molecule, the hydrogen-hydrogen interaction between cell repetitions is not expected to be significant.

For geometry optimizations, the distances of the hydrogen atoms from the surface (R_d) and the distance between the hydrogen atoms (R_o) were simultaneously optimized. The adsorption energy E_C is given by:

$$E_C(R_d, R_o) = 1/2\ [E(Am) + 2E(H_2) - E(Am+H_2)],$$

where E(Am) is the total energy of the bare Am slab, $E(H_2)$ is the total energy of the hydrogen molecule at the theoretically optimized bond length of 0.757Å, and $E(Am+H_2)$ is the total energy of the slab-with-molecule. Thus a positive value of E_C implies adsorption and a negative value implies otherwise. To calculate the total energy of the ad-molecule, the molecule was fully relaxed in a large box of side 30 Bohr and at the Γ k-point, with all other computational

(a) Bare (0001) surface of dhcp-Am (side view)

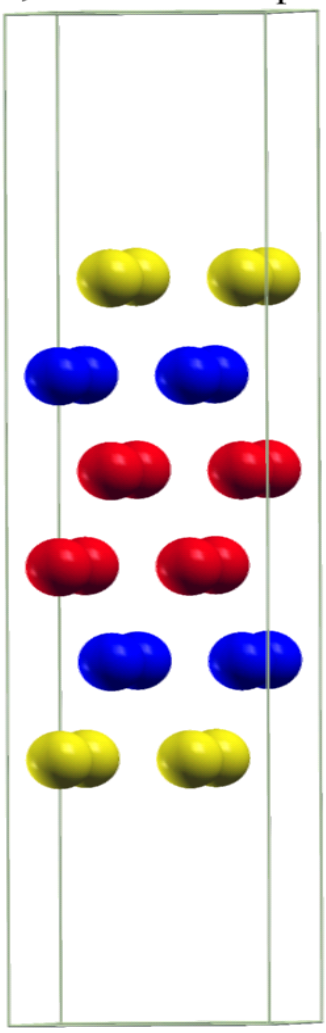

(b) Bare (0001) surface of dhcp-Am (top view)

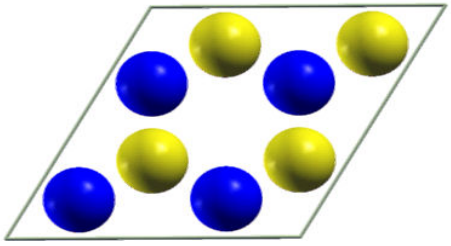

Figure 4.1 Side view and top view illustrations of six layers of bare (0001) surface of dhcp-Am.

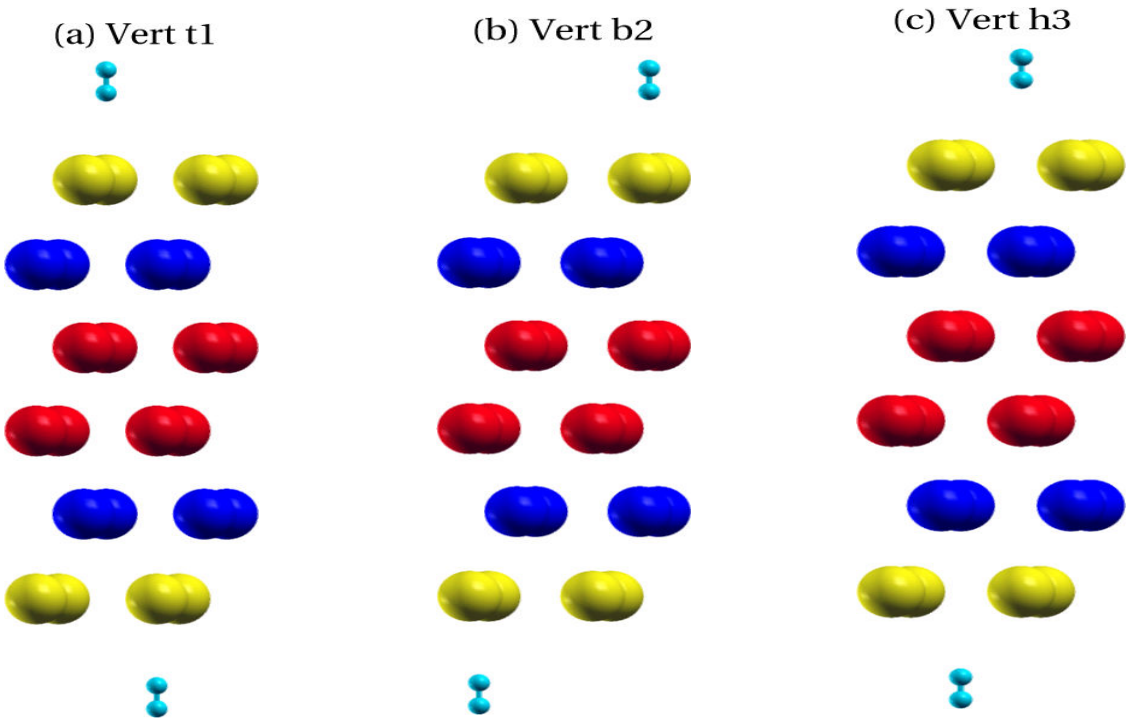

Figure 4.2 Side view of H_2 molecular adsorption on the Am surface at three different adsorption sites for the Vert approach: (a) one-fold top site t1; (b) two-fold bridge site b2; (c) three-fold hollow site h3

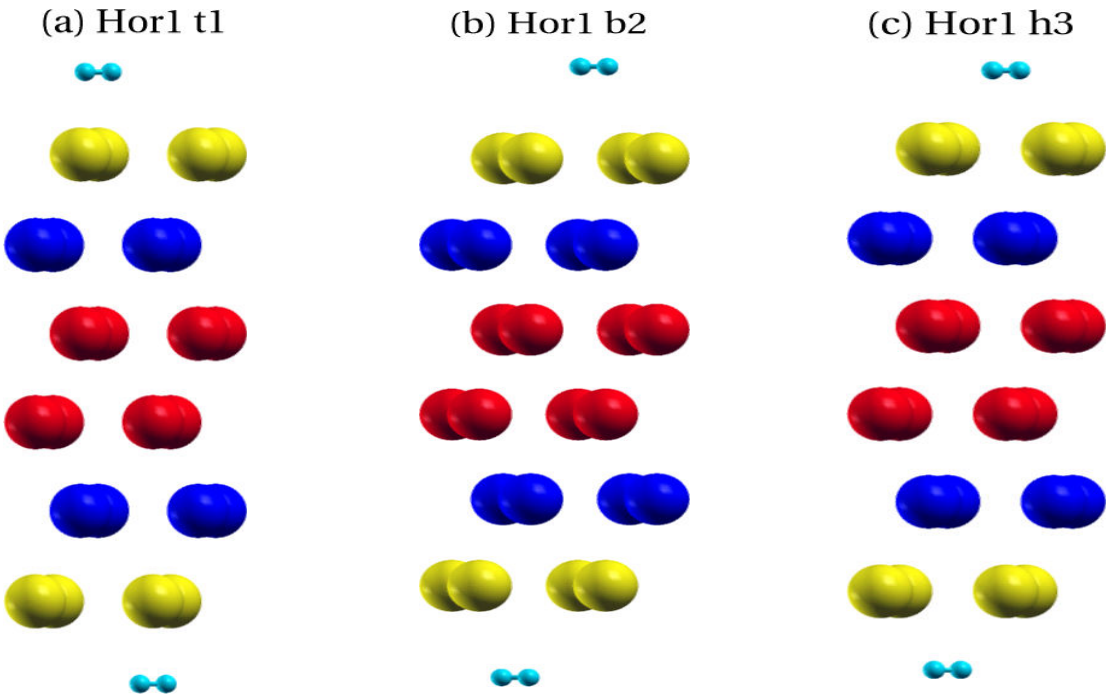

Figure 4.3 Side view of H_2 molecular adsorption on the Am surface at three different adsorption sites for the Hor1 approach: (a) one-fold top site t1; (b) two-fold bridge site b2; (c) three-fold hollow site h3

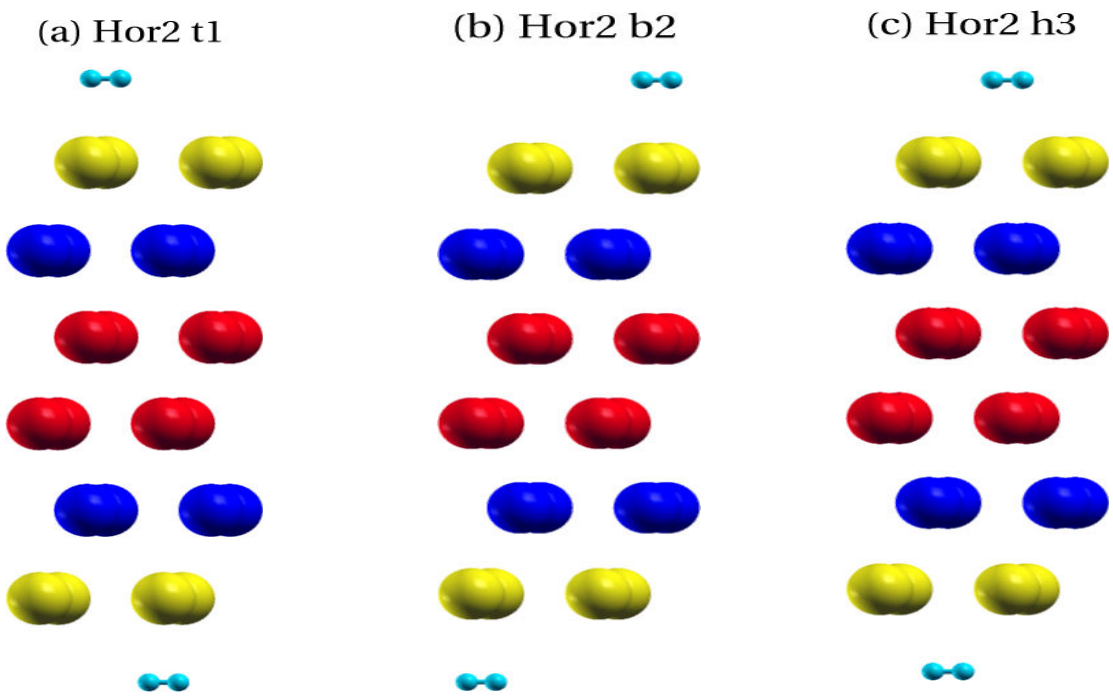

Figure 4.4 Side view of H_2 molecular adsorption on the Am surface at three different adsorption sites for the Hor2 approach: (a) one-fold top site t1; (b) two-fold bridge site b2; (c) three-fold hollow site h3

parameters remaining the same. We wish to note here that no additional relaxations were taken into account primarily because of the all electron nature of the calculations and the consequent extreme computational effort required. Also, from our recent findings[42], the difference in adsorption energies between the system where the adatom and the surface layer of the Am slab were relaxed simultaneously and the system where only the adatom was relaxed with the Am slab being fixed, was found to be of the order of 0.03 eV with no change in site preferences as far as adsorption was concerned. Thus we expect that surface relaxation effects during adsorption will not be significant in our molecular adsorption study also and will not alter our results qualitatively, if not quantitatively. Also, our recent studies on adsorption on the δ-Pu surface[43,56] indicated that spin-orbit coupling has negligible effect on adsorption geometry but the binding was slightly stronger with the adsorption energies increasing by 0.05 to 0.3 eV. Though we have not verified this explicitly for the dhcp Am (0001) surface, we expect the same trend to hold true here. Hence in the current calculations, the geometry was optimized at the NSOC level and the final geometry was used for the SOC calculation to study the effects of spin-orbit coupling on the adsorption energies.

The optimized adsorption parameters and energies for the hydrogen molecule adsorbed on the (0001) surface of dhcp-Am are provided in Table 1. The differences between the NSOC and SOC adsorption energies at each adsorption site, given by $\Delta E_c = E_c(SOC) - E_c(NSOC)$, are also quoted. We first

Table 4.1 Chemisorption Energies E_c at Both NSOC and SOC Levels of Theory, R_d, the Distances of the Hydrogen Molecule from the Americium Surface and R_O, the H – H distances, $D_{Am\text{-}admolecule}$., the Distance of the Adatom from the Nearest Neighbor Am Atom. $\Delta E_c = E_c(SOC) - E_c(NSOC)$ is the Difference Between the Chemisorption Energies at each Adsorption Site.

H_2 Approach	Site	E_C (eV) (NSO)	E_C (eV) (SO)	R_d(Å)	R_O(Å)	$D_{Am\text{-}admolecule}$ (Å)	ΔE_C (eV)
Vert	Top	0.0192	0.0119	3.176	0.788	3.176	-0.0073
	Bridge	0.0343	0.0211	3.069	0.779	3.544	-0.0132
	Hcp	0.0352	0.0215	2.964	0.756	3.602	-0.0137
Hor1	Top	0.0955	0.0962	2.646	0.789	2.675	0.0007
	Bridge	0.0204	0.0186	3.598	0.757	3.859	-0.0018
	Hcp	0.0147	0.0226	3.493	0.758	3.897	0.0079
Hor2	Top	0.0997	0.1022	2.645	0.789	2.675	0.0025
	Bridge	0.0285	0.0248	3.069	0.761	3.564	-0.0037
	Hcp	0.0112	0.0104	3.184	0.783	3.579	-0.0008

discuss the Vert approach, where the hydrogen molecule approaches the surface at the three different adsorption sites in the vertical molecular orientation. Figure 1 has the optimized H_2 chemisorbed geometries of the americium surface for the Vert approach at the three different adsorption sites. As listed in table 1 for the Vert approach, the distances from the americium surface (R_d) are 3.176 Å, 3.069 Å, and 2.964 Å for the three adsorption sites t1, b2 and h3, respectively. The equilibrium H – H bond lengths (R_O) are stretched up to 0.788 Å and 0.779 Å from the theoretically optimized bond length of 0.757 Å for the t1 and b2 adsorption sites respectively, whereas for the h3 site the molecule compresses negligibly to 0.756 Å. The most stable site is the three-fold hollow h3 site (0.0352 eV for the NSOC case, 0.0215 eV for SOC case), followed by the two-fold b2 site (0.0343 eV for the NSOC case, 0.0211 eV for SOC case), with the least favorable site being the one-fold t1 (0.0192 eV for the NSOC case, 0.0119 eV for SOC case). The distance between the americium surface and H_2 molecule clearly show that at the least stable t1 site, the admolecule is furthest away from the surface (3.176 Å) followed by the next stable b2 site (3.069 Å), with the distance being the smallest (2.964 Å) for the most stable h3 site. Hence, increasing stability at both the NSOC and SOC levels of theory implies decreasing vertical distance of the H_2 molecule from the surface layer. Also increasing stability implies increasing admolecule coordination number at both theoretical levels, that is, the H_2 molecule prefers to bind at the maximally coordinated three-fold hollow h3 site. The H – H bond

lengths for the Vert approach at the three adsorption sites shows that at none of the adsorption site does the H_2 molecule tend to dissociate. All adsorption energies for the Vert approach indicate that binding becomes weaker with the inclusion of SOC compared to the NSOC case.

Next we discuss adsorption corresponding to the Hor1 approach, where the H_2 molecular orientation is parallel to a lattice vector. In this case, the atoms of the hydrogen molecule are at the same distance from the americium surface and R_d is measured from the center of mass of the H_2 molecule to the surface. Figure 2 shows the optimized H_2 chemisorbed geometries on the americium surface for the Hor1 approach at the three different adsorption sites. It is known [57,58,59] that the probability of dissociation of gas molecules on metal surfaces is higher when the molecules are oriented horizontally/parallel with respect to the surface as compared to the case where the molecules are oriented vertically/perpendicularly. This was not found to be true for our Am-H_2 system, as in none of the cases (for Hor1 and Hor2 approaches), the hydrogen molecule dissociated. As listed in table I for the Hor1 approach, the distances of the H_2 molecule from the americium surface (R_d) are 2.646 Å, 3.598 Å, and 3.493 Å for the adsorption sites t1, b2 and h3 respectively. The equilibrium H – H bond lengths (R_O) are stretched up to 0.789 Å and 0.758 Å from the theoretically optimized bond length of 0.757 Å for t1 and h3 adsorption sites respectively, whereas for b2 adsorption site the molecule stays at the theoretically optimized bond length. The most stable site is the one-fold t1 site

(0.0955 eV for the NSOC case, 0.0962 eV for SOC case), followed by the two-fold b2 site (0.0204 eV for the NSOC case, 0.0186 eV for SOC case), with the least favorable site being the three-fold hollow h3 (0.0147 eV for the NSOC case, 0.0226 eV for SOC case). As can be seen, the inclusion of spin orbit coupling reverses the priority of binding as at the NSOC level of theory the b2 site is more preferred compared to h3 site, while at the SOC level of theory the h3 site is more favorable compared to b2 site. Dissimilar to the trend for the Vert approach, increasing stability at both the NSOC and SOC levels of theory does not imply decreasing vertical distance of the H_2 molecule from the surface layer. The adsorption energies for the Hor1 approach indicate that binding is slightly stronger with the inclusion of SOC compared to the NSOC case for the t1 and h3 adsorption sites, whereas it is weaker for the b2 adsorption site.

For the Hor2 approach, where the H_2 molecular approach is horizontal but perpendicular to a lattice vector, the adsorption process is molecular. The final adsorption configurations are shown in fig. 3. Again R_d is measured from the center of mass of the molecule to the surface. As listed in table I, the distances from the americium surface (R_d) are 2.645 Å, 3.069 Å, and 3.184 Å for the t1, b2 and h3, and the equilibrium H – H bond lengths (R_O) are stretched to 0.789 Å, 0.761 Å and 0.783 Å for the three adsorption sites t1, b2 and h3, respectively. The most stable site is the one-fold t1 site (0.0997 eV for the NSOC case, 0.1022 eV for SOC case), followed by the two-fold b2 site (0.0285 eV for the NSOC case, 0.0248 eV for SOC case), with the least favorable site

being the three-fold hollow h3 (0.0112 eV for the NSOC case, 0.0104 eV for SOC case). Analogous to the trend for the Vert approach, increasing stability at both the NSOC and SOC levels of theory implies decreasing vertical distance of the H_2 molecule from the surface layer. The adsorption energies for the Hor2 approach indicate that binding is slightly stronger with the inclusion of SOC compared to the NSOC case for the t1 adsorption site, whereas the binding is weaker for the b2 and h3 adsorption sites after the inclusion of SOC.

In table 2, the adsorbate-induced work function changes with respect to the clean metal surface, given by $\Delta\Phi = \Phi^{admolecule/Am} - \Phi^{Am}$, are listed at the NSOC and SOC levels of theory for each adsorbate and each adsorption site. The adsorbate-induced work function shifts can be understood in terms of the surface dipoles arising due to the displacement of electron density from the substrate towards the adsorbates since the electronegativity of H is much larger than that of Am. The surface dipole moment μ (in Debye) and the work function shift ΔΦ (in eV) are linearly related by the Helmholtz equation $\Delta\Phi = 12\Pi\Theta\mu/A$, where A is the area in $Å^2$ per (1×1) surface unit cell and Θ is the adsorbate coverage in monolayers. The work functions for the slab with the admolecule decreases compared to the work function for the bare slab, and hence the work function shifts are negative for all the cases studied. This is a distinctive aspect for this calculation, as one expects the work function to increase upon adsorption due to charge transfer from the substrate to the adsorbate. This was the case in our previous calculations for the adsorption of atomic hydrogen,

Table 4.2 Change in Work Function $\Delta\Phi = \Phi^{admolecule/Am} - \Phi^{Am}$ (in eV) for Both the NSOC and SOC Levels of Theory, where Φ^{Am} is Work Function of the Bare Surface and $\Phi^{admolecule/Am}$ is the Work Function of the Surface with Admolecule. Φ^{Am} = 2.906 eV and 2.989 eV respectively at the NSOC and SOC Theoretical levels.

H_2 Approach	Site	ΔΦ (eV) NSOC	ΔΦ (eV) SOC
Vert	t1	-0.037	-0.048
	b2	-0.054	-0.017
	h3	-0.073	-0.057
Hor1	t1	-0.015	-0.003
	b2	-0.262	-0.026
	h3	-0.035	-0.025
Hor2	t1	-0.012	-0.006
	b2	-0.223	-0.025
	h3	-0.053	-0.023

oxygen and molecular oxygen on the same americium metal slab. But in the current case there is no charge transfer from the americium atoms to the H_2 molecule, which can be seen in our partial charge analysis in tables 4-6. To explain the decrease in work function after adsorption, we have also studied in detail the difference charge density distribution which we will discuss below.

In table 3, the magnitudes and alignments of the site projected spin magnetic moments for each Am atom on the *surface* atomic layer are reported for the clean and adsorbate-covered surfaces. Minor changes in the moments after adsorptions occurred on only the surface layer; no significant changes were observed on the subsurface and central layers. Also, the spin moments reported correspond to the SOC calculations. NSOC moments follow a similar qualitative trend and are not reported here. For the Vert approach, we see reductions of 0.01 μ_B in the spin magnetic moment for each of the four surface layer Am atoms for the adsorption site t1, b2 and h3. For the Hor1 approach, we see spin magnetic moment reductions of 0.03 μ_B for one of the Am atom and 0.01 μ_B for the three Am atoms for the t1 adsorption site, 0.01 μ_B for each of the four surface layer Am atoms for the adsorption sites b2 and h3. Finally for the Hor2 approach, similar the results for Hor1 approach, we see spin magnetic moment reductions of 0.03 μ_B for one of the Am atom and 0.01 μ_B for the three Am atoms for the t1 adsorption site, 0.01 μ_B for each of the four surface layer

Table 4.3 The Site Projected Spin Magnetic Moments for the Am Atoms at the Surface Layer of the Bare Slab and the Chemisorbed Systems. Spin Moments are Quoted for SOC Calculations.

	Site	μ (μ_B)		Site	μ (μ_B)		Site	μ (μ_B)
Bare Slab		5.81, 5.81 5.81, 5.81						
	t1	5.80, 5.80 5.80, 5.80		t1	5.78, 5.80 5.80, 5.80		T1	5.78, 5.80 5.80, 5.80
Vert	b2	5.80, 5.80 5.80, 5.80	Hor1	b2	5.80, 5.80 5.80, 5.80	Hor2	B2	5.80, 5.80 5.80, 5.80
	h3	5.80, 5.80 5.80, 5.80		h3→	5.80, 5.80 5.80, 5.80		H3	5.80, 5.80 5.80, 5.80

Am atoms for the adsorption sites b2 and h3. In all cases, the moments in the interstitial region also decreased by a small magnitude after adsorption.

The nature of the APW+lo basis allows us to decompose the electronic charges inside the muffin-tin spheres into contributions from different angular momentum channels. These charges are referred to as partial charges. Comparing the partial charges Q_B of the Am layers and the adsorbates before adsorption to the corresponding partial charges Q_A after adsorption gives us an idea of the nature of the interaction between the adsorbates and substrate. These are reported in Tables 4-6. For Am, only the *surface layer atoms* were considered as no significant changes were observed on the subsurface and central layers. In each table, we have also reported the differential partial charge of the different angular momentum state *l* corresponding to a given atom given by $\Delta Q(l) = Q_A - Q_B$. $\Delta Q(l) > 0$ indicates charge gain inside the muffin tin sphere while $\Delta Q < 0$ indicates otherwise. ΔQ (*l*) may be loosely interpreted as a measure of charge transfer. In table 4, Q_A, Q_B, and ΔQ (*l*) for H_2 molecule with Vert approach adsorbed at the t1, b2, and h3 adsorption sites respectively on the dhcp-Am (0001) surface are reported. For the one-fold t1 site, ΔQ (1*s*) = -0.01 *e* for the two H atoms, ΔQ (6*d*) = 0.00 and ΔQ(5*f*) = 0.01 *e* for the four Am atoms. For the two-fold b2 site, ΔQ (1*s*) = -0.01 *e* for the two H atoms, ΔQ(6*d*) = 0.00 *e* for the four Am atoms, ΔQ(5*f*) = 0.01 *e* for two Am atoms and ΔQ(5*f*) = 0.01 *e* for the other two Am atoms. For the three-fold hollow h3 site, ΔQ (1*s*) =

Table 4.4 Partial Charges Inside the Muffin Tin Spheres Before Adsorption (Q_B), After Adsorption (Q_A), and Difference in Partial Charges $\Delta Q = Q_A - Q_B$ at the t1, b2 and h3 Sites for the Vert Approach for Hydrogen Molecule. Only the Am *Surface Layer Atoms* were Considered.

Vert approach	Partial charges in muffin-tin						$\Delta Q = Q_A - Q_B$		
	Before adsorption Q_B			After adsorption Q_A					
	H *s*	Am *d*	Am *f*	H *s*	Am *d*	Am *f*	H *s*	Am *d*	Am *f*
t1	0.20			0.19			-0.01		
	0.20			0.19			-0.01		
		0.27	5.85		0.27	5.86		0.00	0.01
		0.27	5.85		0.27	5.86		0.00	0.01
		0.27	5.85		0.27	5.86		0.00	0.01
		0.27	5.85		0.27	5.86		0.00	0.01
b2	0.20			0.19			-0.01		
	0.20			0.19			-0.01		
		0.27	5.85		0.27	5.86		0.00	0.01
		0.27	5.85		0.27	5.86		0.00	0.01
		0.27	5.85		0.27	5.85		0.00	0.00
		0.27	5.85		0.27	5.85		0.00	0.00
h3	0.20			0.20			0.00		
	0.20			0.20			0.00		
		0.27	5.85		0.27	5.86		0.00	0.01
		0.27	5.85		0.27	5.86		0.00	0.01
		0.27	5.85		0.27	5.86		0.00	0.01
		0.27	5.85		0.27	5.86		0.00	0.01

Table 4.5 Partial Charges Inside Muffin Tin Spheres Before Adsorption (Q_B), After Adsorption (Q_A), and Difference in Partial Charges $\Delta Q = Q_A - Q_B$ at the t1, b2 and h3 Sites for the Hor1 Approach for Hydrogen Molecule. Only the Am *Surface Layer Atoms* were Considered.

Hor1 approach	Partial charges in muffin-tin						$\Delta Q = Q_A - Q_B$		
	Before adsorption Q_B			After adsorption Q_A					
	H *s*	Am *d*	Am *f*	H *s*	Am *d*	Am *f*	H *s*	Am *d*	Am *f*
t1	0.20			0.19			-0.01		
	0.20			0.19			-0.01		
		0.27	5.85		0.27	5.85		0.00	0.00
		0.27	5.85		0.27	5.85		0.00	0.00
		0.27	5.85		0.29	5.83		0.02	-0.02
		0.27	5.85		0.27	5.85		0.00	0.00
b2	0.20			0.20			0.00		
	0.20			0.20			0.00		
		0.27	5.85		0.27	5.86		0.00	0.01
		0.27	5.85		0.27	5.85		0.00	0.00
		0.27	5.85		0.27	5.85		0.00	0.00
		0.27	5.85		0.27	5.85		0.00	0.00
h3	0.20			0.20			0.00		
	0.20			0.20			0.00		
		0.27	5.85		0.27	5.85		0.00	0.00
		0.27	5.85		0.27	5.87		0.00	0.02
		0.27	5.85		0.27	5.85		0.00	0.00
		0.27	5.85		0.27	5.85		0.00	0.00

Table 4.6 Partial Charges Inside Muffin Tin Spheres Before Adsorption (Q_B), After Adsorption (Q_A), and Difference in Partial Charges $\Delta Q = Q_A - Q_B$ at the t1, b2 and h3 Sites for the Hor2 Approach for Hydrogen Molecule. Only the Am *Surface Layer Atoms* were Considered.

Hor2 approach	Partial charges in muffin-tin						$\Delta Q = Q_A - Q_B$		
	Before adsorption Q_B			After adsorption Q_A					
	H *s*	Am *d*	Am *f*	H *s*	Am *d*	Am *f*	H *s*	Am *d*	Am *f*
t1	0.20			0.19			-0.01		
	0.20			0.19			-0.01		
		0.27	5.85		0.27	5.85		0.00	0.00
		0.27	5.85		0.29	5.83		0.02	-0.02
		0.27	5.85		0.27	5.85		0.00	0.00
		0.27	5.85		0.27	5.85		0.00	0.00
b2	0.20			0.20			0.00		
	0.20			0.20			0.00		
		0.27	5.85		0.27	5.85		0.00	0.00
		0.27	5.85		0.27	5.85		0.00	0.00
		0.27	5.85		0.27	5.85		0.00	0.00
		0.27	5.85		0.27	5.85		0.00	0.00
h3	0.20			0.19			-0.01		
	0.20			0.19			-0.01		
		0.27	5.85		0.27	5.85		0.00	0.00
		0.27	5.85		0.27	5.85		0.00	0.00
		0.27	5.85		0.27	5.85		0.00	0.00
		0.27	5.85		0.27	5.85		0.00	0.00

0.00 *e* for the two H atoms, ΔQ(6*d*) = 0.00 *e* and ΔQ(5*f*) = -0.01 *e* for each of the four Am atoms.

In table 5, Q_A, Q_B, and ΔQ (*l*) for the Hor1 approach corresponding to the t1, b2 and h3 adsorption sites are shown. For the one-fold t1 site, ΔQ (1*s*) = -0.01 *e* for the two H atoms, ΔQ(6*d*) = 0.00 for three Am atoms, ΔQ(6*d*) = 0.02 for the other Am atom, ΔQ(5*f*) = 0.00 *e* for the three Am atoms and ΔQ(5*f*) = -0.02 for the other Am atom. For the two-fold b2 site, ΔQ(1*s*) = 0.00 *e* for the two H atoms, ΔQ(6*d*) = 0.00 *e* for the four Am atoms, ΔQ(5*f*) = 0.01 *e* for three Am atoms and ΔQ(5*f*) = 0.01 *e* for the other Am atom. For the three-fold hollow h3 site, ΔQ (1*s*) = 0.00 *e* for the two H atoms, ΔQ(6*d*) = 0.00 *e* for the four Am atoms, ΔQ(5*f*) = 0.00 *e* for three Am atoms and ΔQ(5*f*) = 0.02 *e* for the other Am atom. In table 6, Q_A, Q_B, and ΔQ (*l*) for the Hor2 approach corresponding to the t1, b2 and h3 adsorption sites are shown. For the one-fold t1 site, ΔQ (1*s*) = -0.01 *e* for the two H atoms, ΔQ(6*d*) = 0.00 for three Am atoms, ΔQ(6*d*) = 0.02 for the other Am atom, ΔQ(5*f*) = 0.00 *e* for the three Am atoms and ΔQ(5*f*) = -0.02 for the other Am atom. For the two-fold b2 site, ΔQ(1*s*) = 0.00 *e* for the two H atoms, ΔQ(6*d*) = 0.00 *e* for the four Am atoms, ΔQ(5*f*) = 0.01 *e* for the four Am atoms. For the three-fold hollow h3 site, ΔQ (1*s*) = -0.01 *e* for the two H atoms, ΔQ (6*d*) = 0.00 *e* for the four Am atoms, ΔQ(5*f*) = 0.00 *e* for the four Am atoms. These numbers involving all three approaches for all three respective adsorption sites suggest that there are no noteworthy Am(6*d*)-Am(5*f*)-H(1*s*) interactions present in the system. Also none of the Am 5f electrons play a role

in bonding as the hydrogen molecule tends to stay rather far away from the americium surface for all cases considered. We wish to stress that the partial charges are confined inside the muffin tin spheres and do not give any information of the interactions between the atoms in the interstitial region. Information which includes the electronic charges in interstitial region can be obtained from the difference charge density distributions.

The nature of the bonds between the adsorbate and the Am atoms on the surface have been investigated by computing the difference charge density Δn(r) defined as follows:

$$\Delta n(r) = n(H_2 + Am) - n(Am) - n(H_2),$$

where $n(H_2+Am)$ is the total electron charge density of the Am slab with H_2 admolecule, n(Am) is the total charge density of the bare Am slab, and $n(H_2)$ is the total charge density of the admolecule. In computing $n(H_2)$ and n(Am), the admolecule H_2 and Am atoms are kept fixed at exactly the same positions as they were in the chemisorbed systems. All charge densities reported here were computed in the plane passing through the admolecule and one or two surface Am atoms using the Xcrysden utility.[60] We have reported the difference charge density plots for the most favorable adsorption site for each of the approaches, Vert, Hor1 and Hor2 in fig 4. For the Vert approach, h3 was the most favorable adsorption site and Δn was computed in the plane passing through the two H atoms and the two Am atoms directly below the H atom facing the surface, but the H atoms are not bonded to the surface Am atoms as the distance from the

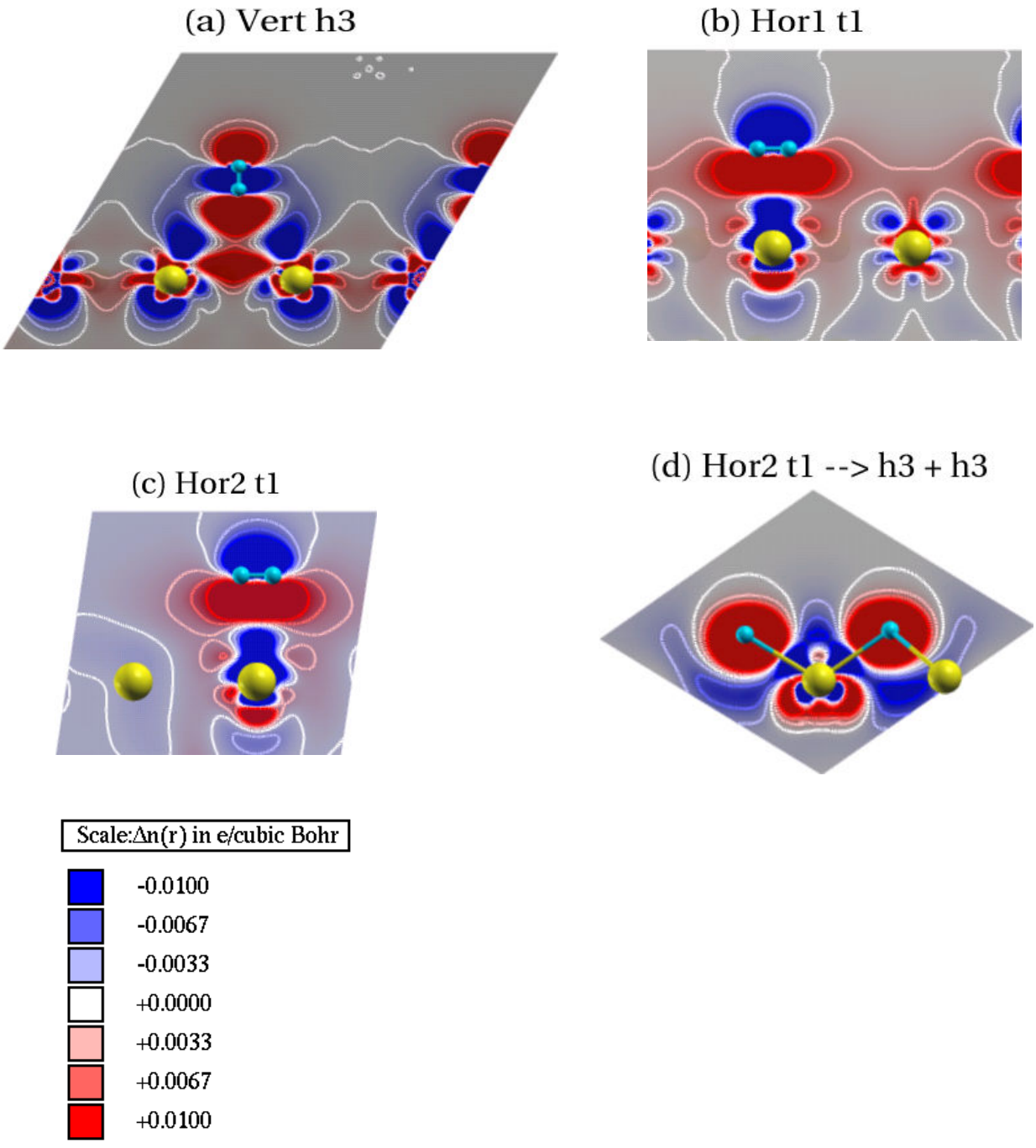

Figure 4.5 Difference charge density distributions Δn(r) for H_2 chemisorbed on the dhcp-Am(0001) surface at the most stable configurations corresponding to the Vert, Hor1 and Hor2 approaches. The scale used is shown at the bottom. Red (positive) denotes regions of charge accumulation and blue (negative) denotes regions of charge loss. H_2 molecule is colored blue and Am atoms are colored gold.

surface is 2.964 Á. For the Hor1 approach, the most stable configuration for the t1 adsorption site is depicted. In this case Δn was computed in the plane passing through the two H atoms and nearest neighbor Am atom. Similarly for the Hor2 approach, Δn for the most stable configuration for the t1 adsorption site is shown. Again the plane passes through the two H atoms and neighboring Am atoms. In fig. 4(a) for the Vert approach for the h3 adsorption site, we clearly see that the hydrogen molecule is polarized and there is no charge sharing between the surface Am atoms and the hydrogen molecule. This in turn makes the interaction very weak which results in physisorption of hydrogen molecule. In a way the hydrogen molecule adheres to the surface through Van der Waals (weak intermolecular) interactions. From our previous results, after the adsorption of atomic hydrogen we observed significant charge transfer from the surface Am atoms to the hydrogen atom which resulted in an increase in the adsorption energy and ionic bonding. But due to the fact that in the current case the adsorbate is a hydrogen molecule, it does not require any external charge to stabilize the system and achieves a configuration which is stable on its own. For the Hor1 approach, fig 4(b) t1 is the most favorable adsorption site. Similar to the previous case, we clearly see that the hydrogen molecule is polarized and there is no charge sharing between the surface Am atoms and the hydrogen molecule. Again the interaction is weak. For the Hor2 approach, fig4(c) t1 is again the most favorable adsorption site and it is almost degenerate to the Hor1 case. In this case we see the same charge redistribution behavior

as the Hor1 case and it is evident from the two difference charge density plots that the two cases are more or less similar energetically and geometrically except the different direction of approach. The difference charge density plots are fairly consistent with the negative changes in the work function as well as the differential partial charges reported in tables 4-6. We observed that the work functions decreased in all the cases after adsorption compared to the bare slab. In many cases this behavior can be explained by the charge transfer from the adsorbate to the substrate. There are cases when the work function changes can not be attributed to charge transfer.[62] In our case this is not visible though and the main reason behind this anomaly is the electron depletion at the vacuum region above the hydrogen atoms [63] which can be seen in the difference charge density plots. The blue semicircles above the hydrogen molecule near the vacuum shows that there is some charge depletion above the hydrogen molecule. To compare this to the case where the H_2 molecule dissociates and two H atoms sit at two different three-fold h3 adsorption site and the adsorption from thereon becomes atomic; we also plotted the difference charge distribution for the dissociated species (fig 4d). It can be seen in this plot that the two hydrogen atoms gain substantial amount of charge from the surface layer americium atoms. Hence, the work function shifts for this case turns out to be positive. The calculated work function shift after adsorption for this case is 0.198 eV and 0.237 eV at the NSOC and SOC levels of theory, respectively. This is in contrast with the molecular adsorption scenario.

We also computed the local density of states (LDOS), obtained by decomposing the total density of the single particle Kohn-Sham eigenstates into contributions from each angular momentum channel *l* of the constituent atoms inside the muffin tin spheres. Here, we have reported the LDOS for only the SOC computation, the LDOS for NSOC calculations yielding a similar qualitative description. In fig. 5, the Gaussian-broadened (with a width of 0.05 eV) *f* and *d* LDOS curves for each of the layers of the bare dhcp Am (0001) metal slab are shown. Clearly, we see well-defined peaks in the 5*f* electron LDOS in the vicinity of the Fermi level, which have also been observed for bulk dhcp-Am(0001), and is a clear signature of 5*f* electron localization. Also, the $5f_{5/2}$ electron localization is more pronounced for the surface and subsurface layers than the central layer. However, the $5f_{5/2}$ peak centered on a binding energy of 1 eV below the Fermi level instead of the 2.8 eV observed in X-ray and ultraviolet photoemission spectra experiments .[20,27] In fig. 6, we show the LDOS plots for the H_2 molecule and the surface Am atoms after adsorption for the most favorable case for each of the three approaches, namely Vert, Hor1 and Hor2. The LDOS for the all other adsorption sites among different approaches show the same qualitative and quantitative pictures and hence are not shown here. As there are four nonequivalent sites on the surface, we depict the LDOS for only the Am atom(s) which are direct nearest neighbors to the H_2

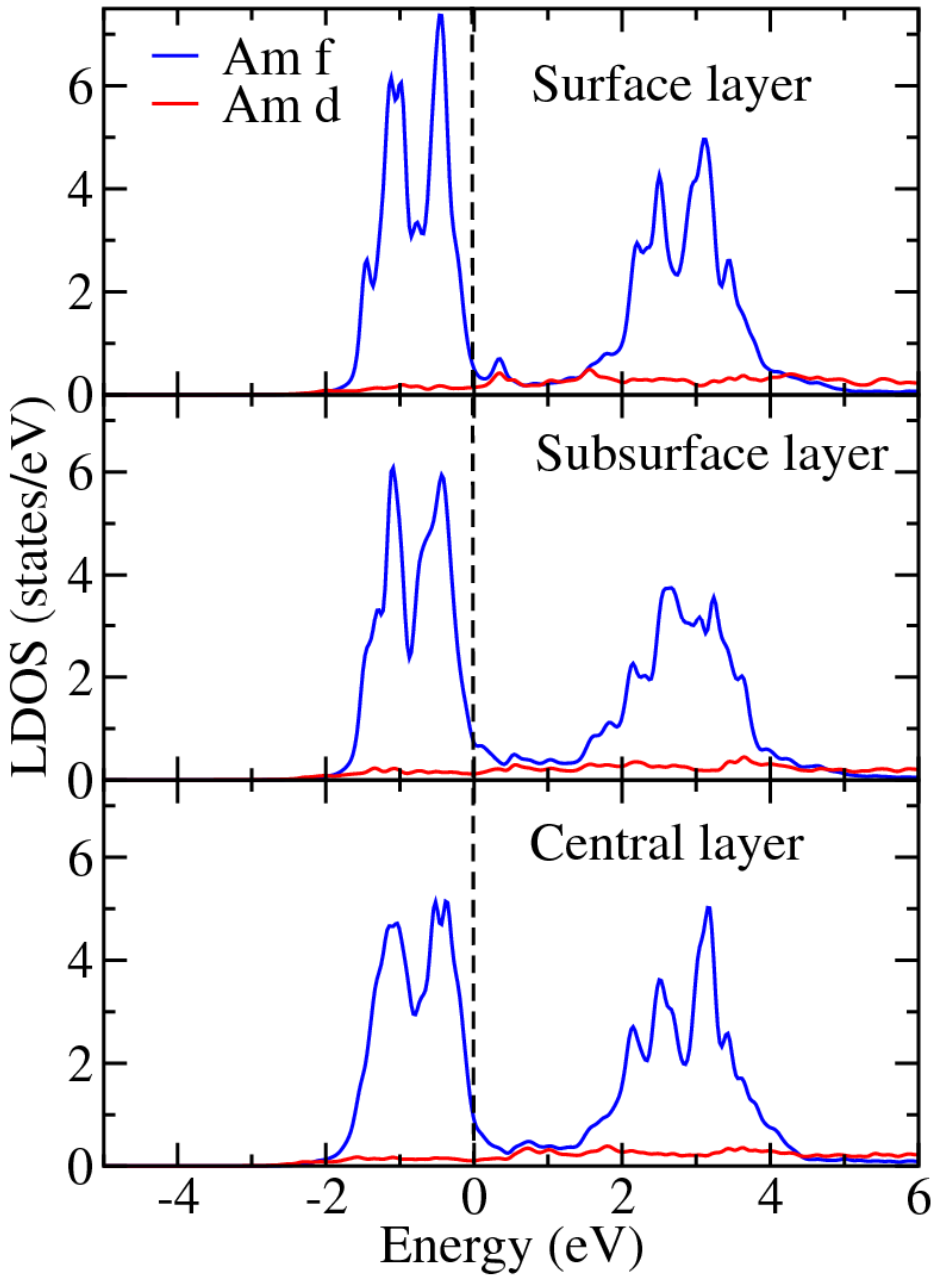

Figure 4.6 6*d* and 5*f* LDOS curves inside the muffin-tins for each layer of the bare dhcp-Am(0001) slab. Vertical line through E=0 is the Fermi level. LDOS correspond to calculations with SOC.

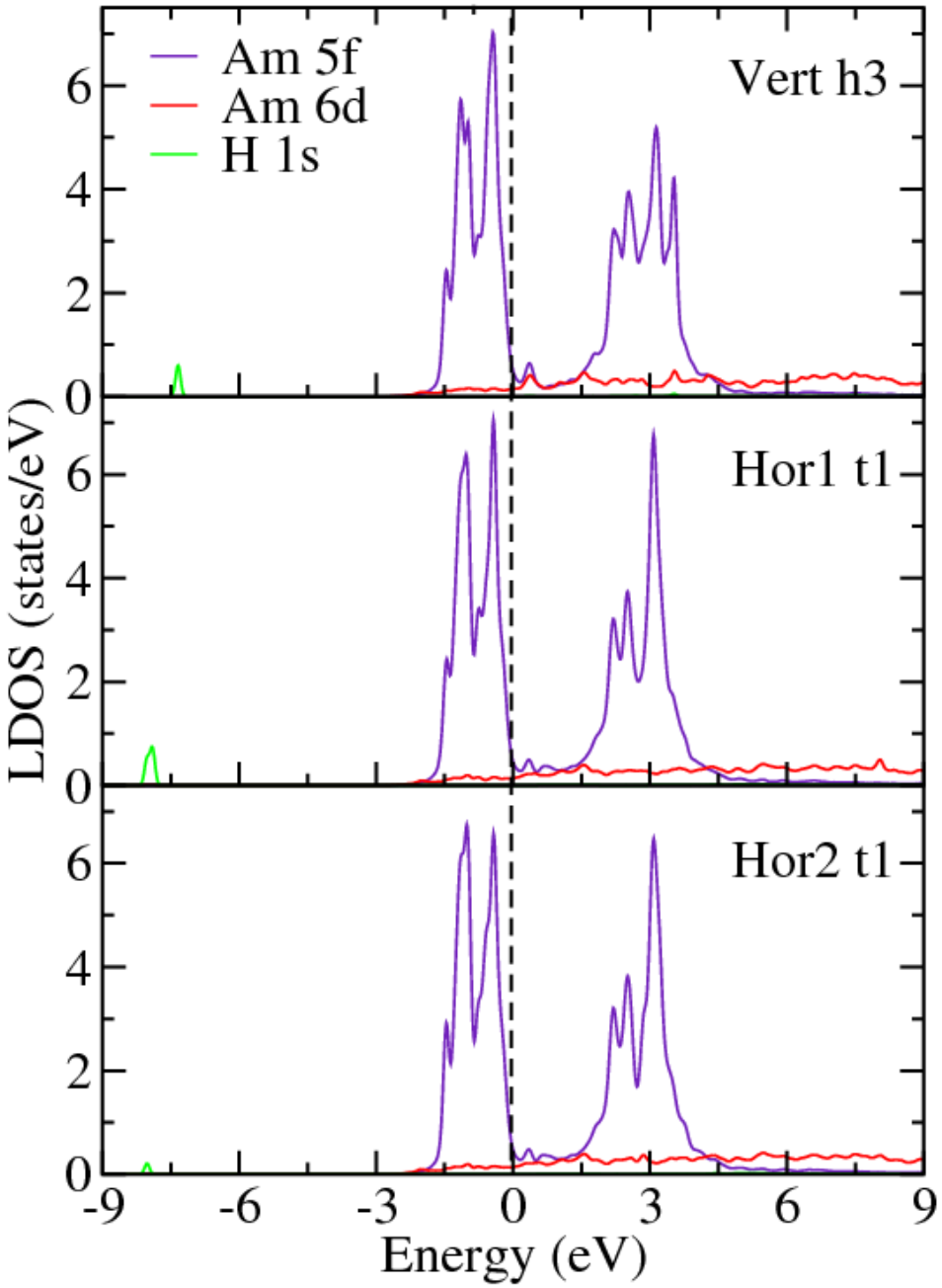

Figure 4.7 6*d* and 5*f* LDOS curves inside the muffin-tins for the Am atoms on the surface layer and 1*s* LDOS curves for H_2 admolecule for the Vert, Hor1 and Hor2 approaches for the adsorption site t1. Vertical line through E=0 is the Fermi level. LDOS correspond to calculations with SOC.

molecule in order to assess the changes in DOS upon adsorption. For the Vert approach, (fig 6) at the adsorption site h3, we note slight reduction in the Am 5*f* DOS and insignificant reduction in the 5f peak around at 0.5 eV just below the Fermi level in comparison to the 5*f* DOS of the bare surface. No Am(5*f*)-Am(6*d*)-H(1*s*) hybridizations were observed and as such 5f electrons do not really participate in the chemical bonding. The LDOS distributions for the most favorable cases among the Hor1 and Hor2 approaches are also shown. For both the t1 adsorption sites, similar to the conclusions drawn for the Vert case, no Am(5*f*)-Am(6*d*)-H(1*s*) hybridizations was observed. The hydrogen peak for the Hor1 and Hor2 approaches t1 site shows a small shift compared to the Vert approach for the h3 site. Overall none of the sites show significant modifications in the 5*f* DOS below the Fermi level in comparison to the surface layer LDOS of the bare slab. Also the localization behavior for the Am 5*f* states for all the Vert, Hor1, and Hor2 approaches is primarily retained after adsorption.

To understand the dissociation process of the hydrogen molecule on the (0001) surface of dhcp-Am, we studied the reaction barrier by constraint minimization of the total energy along a chosen reaction coordinate. We have calculated the reaction barrier for only the most favorable adsorption site t1 for the Hor2 approach. One reason behind the reaction barrier calculation for the most favorable adsorption site is that the probability of hydrogen molecule adsorption at this site is higher and dissociation of the molecule is feasible provided enough energy is supplied to overcome the dissociation barrier. As for

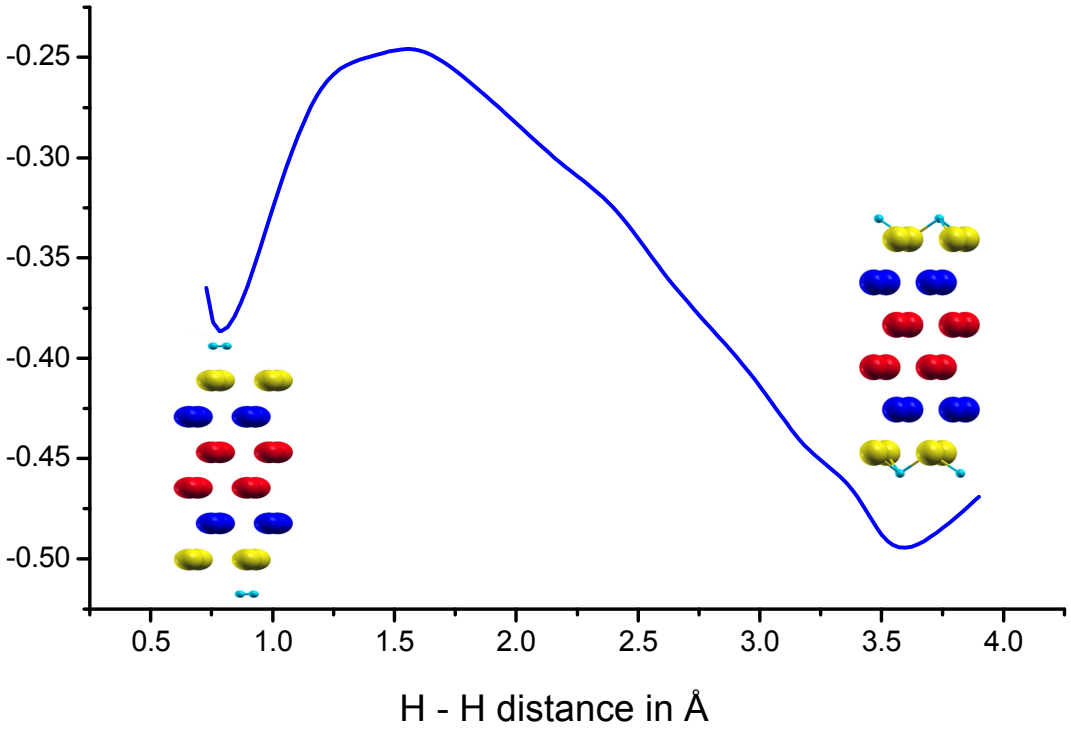

Figure 4.8 Reaction barrier for the Hor2 approach. The total energy is shifted by a constant factor.

the reaction coordinate, we have chosen the H – H distances starting at the optimized bond length for the hydrogen molecule. For the reaction barrier calculation H_2 was placed above the americium surface with the H – H distance held constant at a given value, and the distance between the H_2 molecule and the surface being optimized to yield the total energy of the system. Figure 7 shows the optimized energy curve with respect to different H – H distances. The total energies are plotted with an extra negative sign to have minima at higher adsorption energy point. In fig. 7 the first minima of the curve shows the molecular adsorption of hydrogen near the optimized H_2 bond length of 0.789 Å. The second minima occurs at an H – H distance of 3.547 Å, where each hydrogen atom sits nearly on two three-fold h3 adsorption sites with an adsorption energy of 0.8298 eV. The curve has maxima at a H – H distance of 1.6 Å, and between the two minima's of the curve, there exists an energy hill of 0.142 eV. This energy is defined as the activation energy to be supplied at 0 K to the H_2 molecule for the dissociation process to proceed. In a way, after dissociation, the adsorption is primarily atomic in nature. Also, this is consistent with our previous finding for the adsorption of atomic hydrogen where the three-fold hcp site was found to be most favorable and in the current work the hydrogen molecule dissociates to two three-fold h3 adsorption sites giving the most stable configuration.

In summary, we have used the generalized gradient approximation to density functional theory with the full potential LAPW+lo method to study

adsorption of hydrogen molecule on the (0001) surface of dhcp Am at two theoretical levels; one with no spin-orbit coupling (NSOC) and the other with spin-orbit coupling (SOC). Weak molecular adsorptions were observed for the cases studied. For H_2 adsorption, the one-fold t1 site with Hor2 approach was found to be the most favorable. The inclusion of spin-orbit coupling did not lower the adsorption energies for all the cases. Work functions decreased in all cases compared to the clean Am surface. Upon adsorption, the net spin magnetic moment of the chemisorbed system decreased slightly in each case compared to the bare surface. The partial charge analyses illustrate that none of the Am 5*f* electrons participate in chemical bonding. The hydrogen molecule tends to stay far away from the americium surface giving rise to physisorption. Difference charge density distributions clearly show that the interaction between the surface Am atoms and the hydrogen molecule at each site is governed by weak Van der Waals interactions and the hydrogen molecule becomes polarized. A study of the local density of states showed no Am (6*d*)-Am (5*f*)-H(1*s*) hybridizations after adsorption. Overall, the localized behavior of Am 5*f* below the Fermi Level is primarily retained after adsorption. Reaction barrier calculations for the dissociation of hydrogen molecule at the t1 adsorption site for the Hor2 approach show the presence of an energy barrier, indicating that activation energy is required to dissociate the hydrogen molecule upon adsorption on (0001) surface of dhcp-Am.

4.2 Molecular Adsorption of O_2 Molecule on (0001) Surface of dhcp-Am

For O_2 adsorption, the radii of the muffin tin spheres were $R_{MT}(O)$ = 1.1 Bohr and $R_{MT}(Am)$ = 2.2 Bohr. The truncation of the modulus of the reciprocal lattice vector used for the expansion of the wave function in the interstitial region K_{MAX}, was set to $R_{MT}K_{MAX}$ = 8.5 for the clean slab and $R_{MT}\times K_{MAX}$ = 4.25 for the slab-with-molecule, where R_{MT} denotes the smallest muffin tin radius, that is, R_{MT} = 2.2 Bohrs for the bare slab and R_{MT} = 1.1 Bohrs for the slab-with-molecule (this ensures that K_{MAX} is the same each case). To study adsorption on the *relaxed* Am surface, the oxygen molecule, corresponding to a surface coverage of Θ = 1/4 of a monolayer (ML), was allowed to approach the surface from both sides to preserve inversion symmetry. Three high symmetry adsorption sites were considered: (i) one-fold top site t1 (admolecule is directly on top of a Am atom) (ii) two-fold bridge site b2 (admolecule is placed in the middle of two nearest neighbor Am atoms); and (iii) three-fold hollow hcp site h3 (admolecule sees a Am atom located on the layer directly below the surface layer). For each of these three adsorption sites, three approaches of the O_2 molecule towards to the surface were considered: (a) approach vertical to the surface (Vert approach); (b) approach parallel to a lattice vector (Hor1 approach); (c) approach perpendicular to a lattice vector (Hor2 approach). It is obvious that for both the horizontal approaches the atoms of the oxygen molecule are at the same distance from the americium surface, whereas for the vertical approach one oxygen atom is closer to the surface than

the other. With these choices of the surface and the ad-molecule, the oxygen-oxygen interaction between cell repetitions is not expected to be significant.

For geometry optimizations, the distances of the oxygen atoms from the surface (R_d) and the distance between the oxygen atoms (R_o) were simultaneously optimized. The chemisorption energy E_C is given by:

$$E_C(R_d, R_o) = 1/2\ [E(Am) + 2E(O_2) - E(Am+O_2)],$$

where E(Am) is the total energy of the bare Am slab, $E(O_2)$ is the total energy of the oxygen molecule at the optimized bond length of 1.217Å, and $E(Am+O_2)$ is the total energy of the slab-with-molecule. Thus a positive value of E_C implies chemisorption and a negative value implies otherwise. To calculate the total energy of the ad-molecule, the molecule was fully relaxed in a large box of side 30 Bohr and at the Γ k-point, with all other computational parameters remaining the same. We wish to note here that no additional relaxations were taken into account primarily because of the all electron nature of the calculations and the consequent extreme computational effort required. Also, from our recent findings[42], the difference in chemisorption energies between the system where the adatom and the surface layer of the Am slab were relaxed simultaneously and the system where only the adatom was relaxed with the Am slab being fixed, was found to be of the order of 0.03 eV with no change in site preferences as far as chemisorption was concerned. Thus we expect that surface relaxation effects during adsorption will not be significant in our

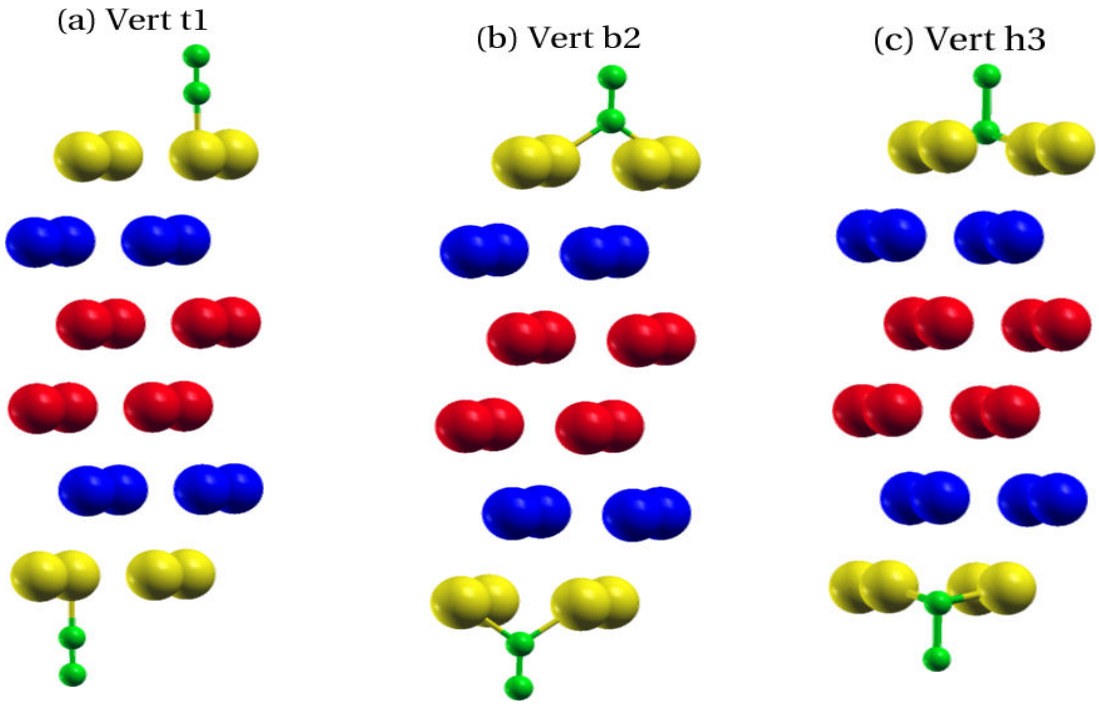

Figure 4.9 Side view of O_2 molecular adsorption on the Am surface at three different adsorption sites for the Vert approach: (a) one-fold top site t1; (b) two-fold bridge site b2; (c) three-fold hollow site h3.

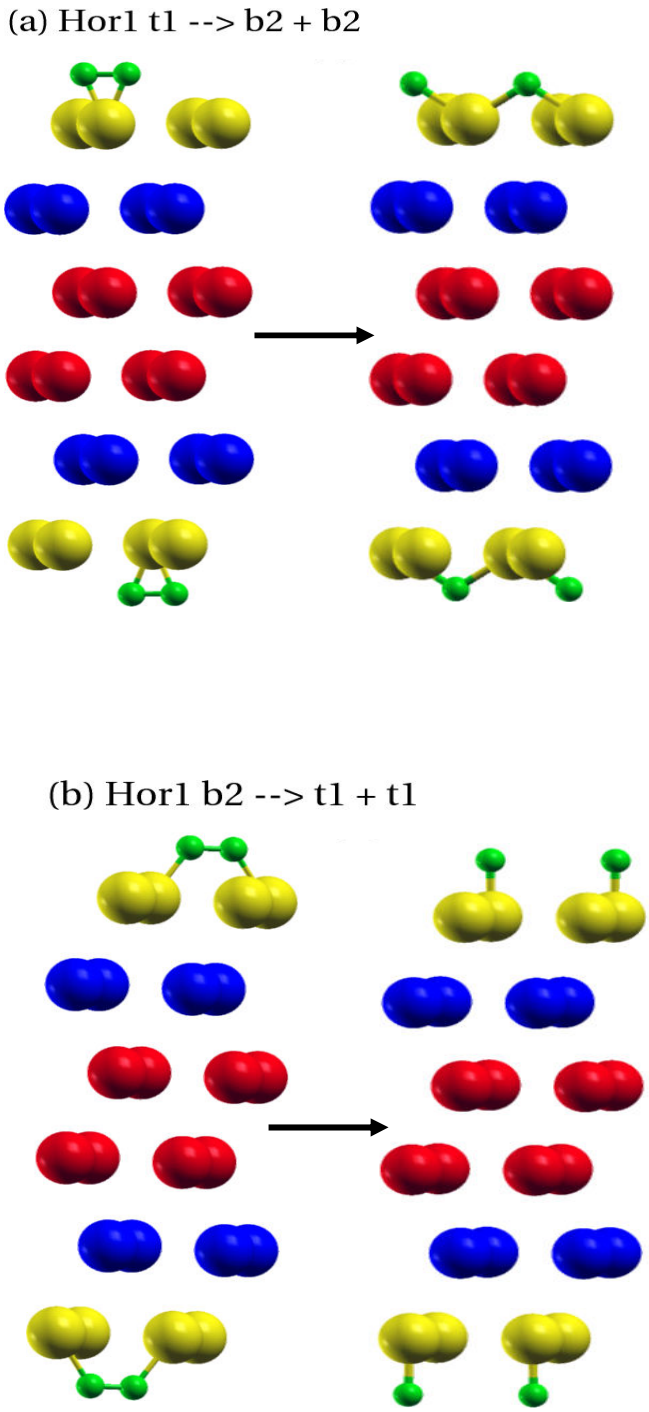

Figure 4.10 Side view illustrations for the dissociation of O_2 molecule on the Am surface for the Hor1 approach: (a) initial site t1, final sites b2+b2; (b) initial site b2, final sites t1+t1.

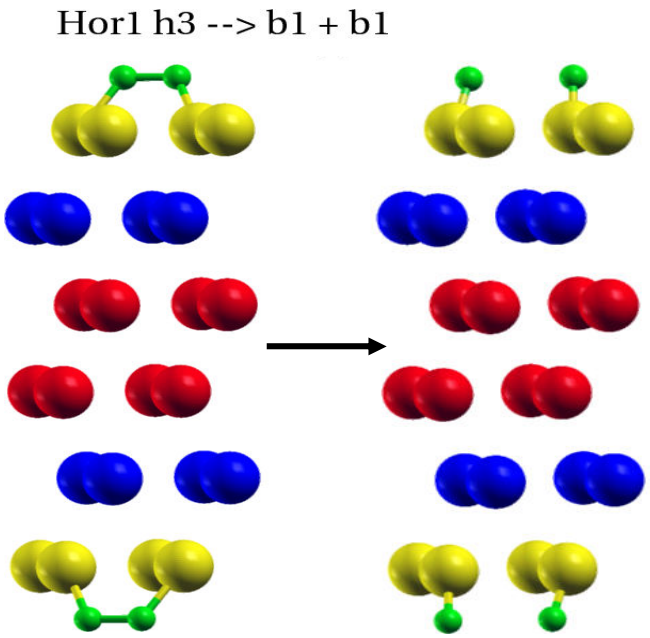

Figure 4.11 Side view illustrations for the dissociation of O_2 molecule on the Am surface for the Hor1 approach: initial site h3, final sites b1+b1.

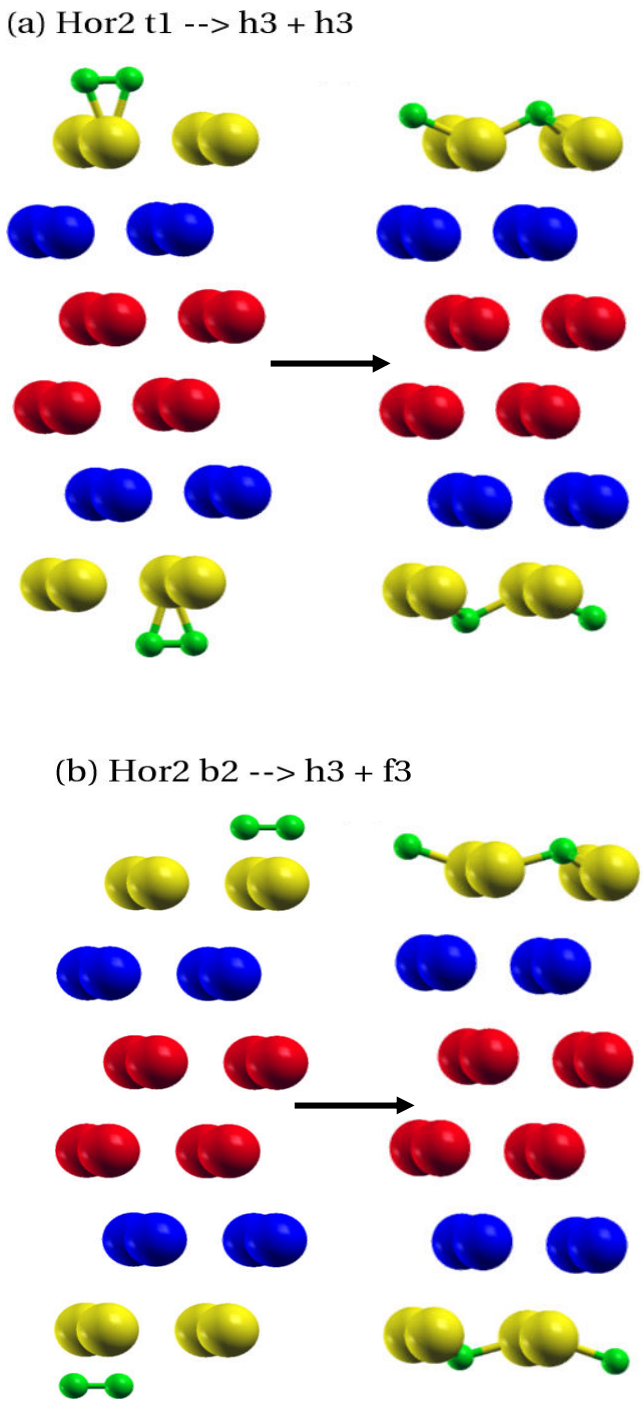

Figure 4.12 Side view illustrations for the dissociation of O_2 molecule on the Am surface for the Hor2 approach: (a) initial site t1, final sites h3+b3; (b) initial site b2, final sites h3+f3.

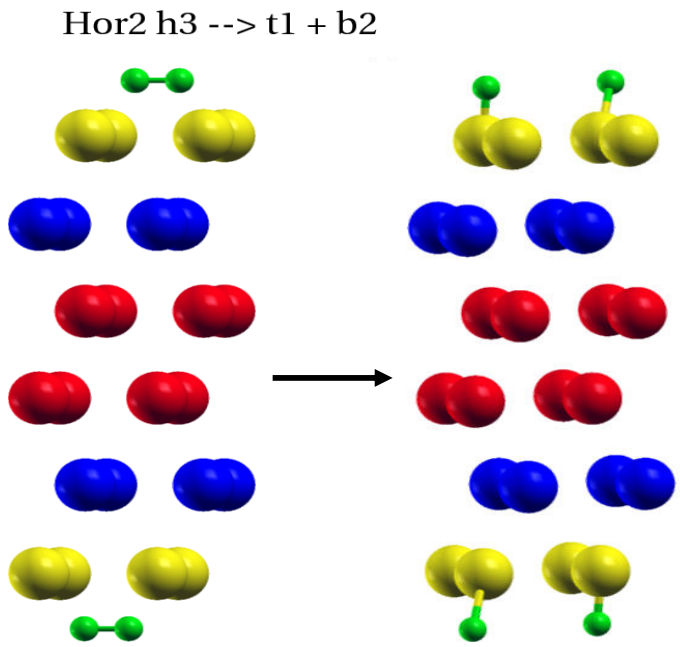

Figure 4.13 Side view illustrations for the dissociation of O_2 molecule on the Am surface for the Hor2 approach: initial site h3, final sites t1+b2.

molecular adsorption study also and will not alter our results qualitatively, if not quantitatively.

Table 1 enlists the adsorption energies and associated geometrical parameters of the oxygen molecule adsorbed on the (0001) surface of dhcp-Am. The differences between the NSOC and SOC chemisorption energies at each adsorption site, given by $\Delta E_c = E_c(SOC) - E_c(NSOC)$, are also listed. We first discuss the Vert approach, where the oxygen molecule approaches the surface at the three different adsorption sites in the vertical molecular orientation. Figure 3 has the optimized O_2 chemisorbed geometries of the americium surface for the Vert approach at the three different adsorption sites. As listed in table 1 for the Vert approach, the distances from the americium surface (R_d) are 2.117 Å, 1.323 Å, and 0.529 Å and the equilibrium O – O bond lengths (R_O) are 1.267 Å, 1.418 Å and 1.821 Å for the three adsorption sites t1, b2 and h3, respectively. The most stable site is the three-fold hollow h3 site (3.315 eV for the NSOC case, 3.668 eV for SOC case), followed by the two-fold b2 site (2.638 eV for the NSOC case, 2.811 eV for SOC case), with the least favorable site being the one-fold t1 (1.979 eV for the NSOC case, 2.068 eV for SOC case). The distance between the americium surface and O_2 molecule clearly show that at the least stable t1 site, the admolecule is furthest away from the surface (2.117 Å) followed by the next stable b2 site (1.323 Å), with the distance being the smallest (0.529 Å) for the most stable h3 site. Hence, increasing stability at both the NSOC and SOC levels of theory implies

Table 4.7 E_c is the Chemisorption Energy, R_d is the Perpendicular Distance of the Oxygen Molecule from the Surface, R_O is the O – O Separation and D is Am-O Nearest Neighbor Distance. The Difference Between the SOC and NSOC Chemisorption Energies is Given by $\Delta E_c = E_c(SOC) - E_c(NSOC)$. For the Dissociative Configurations Corresponding to the Hor1 and Hor2 Approach, the Site Labeling A→ B+C Refers to an Initial Adsorption Site A and Final Dissociation Adsorption Sites B and C.

O_2 Approach	Site	E_C (eV) (NSOC)	E_C (eV) (SOC)	R_d(Å)	R_O(Å)	D (Å)	ΔE_C (eV)
	t1	1.979	2.068	2.117	1.267	2.117	0.089
Vert	b2	2.638	2.811	1.323	1.418	2.213	0.173
	h3	3.315	3.668	0.529	1.821	2.115	0.353
	t1→ b2+b2	8.681	9.191	1.165	3.517	2.109	0.510
Hor1	b2→ t1+t1	5.472	5.861	1.905	3.620	1.905	0.389
	h3→ b1+ b1	6.564	7.057	1.587	3.118	1.901	0.493
	t1→ h3+h3	9.395	9.886	0.953	3.731	2.094	0.491
Hor2	b2→ h3+f3	8.972	9.456	0.636	2.183	2.079	0.484
	h3→ t1+ b2	5.615	6.084	1.589	2.569	1.762	0.469

decreasing vertical distance of the O_2 molecule from the surface layer. Also increasing stability implies increasing admolecule coordination number at both theoretical levels, that is, the O_2 molecule prefers to bind at the maximally coordinated three-fold hollow h3 site. The O – O bond lengths for the Vert approach at the three adsorption sites shows that at none of the adsorption site does the O_2 molecule tend to dissociate Even though the O_2 molecule is stretched maximally at the most favorable h3 site (1.821 Å), it cannot be considered as dissociated species. All chemisorption energies for the Vert approach indicate that binding is slightly stronger with the inclusion of SOC compared to the NSOC case. The SOC-NSOC chemisorption energy differences ΔE_c are also listed in Table 1; ΔE_c is minimum at the least stable t1 site (0.089 eV) closely followed by the next stable b2 adsorption site (0.173 eV), with the most stable h3 adsorption site having an SOC-NSOC ΔE_c = 0.353 eV.

Next we discuss adsorption corresponding to the Hor1 approach, where the O_2 molecular orientation is parallel to a lattice vector. In this case, the atoms of the oxygen molecule are at the same distance from the americium surface and R_d is measured from the center of mass of the O_2 molecule to the surface. Figure 4 shows the optimized O_2 chemisorbed geometries on the americium surface for the Hor1 approach at the three different adsorption sites. It is known [39, 40, 41] that the probability of dissociation of gas molecules on metal surfaces is higher when the molecules are oriented horizontally/parallel with respect to the surface as compared to the case where the molecules are oriented vertically.

This was also found to be true for our Am-O_2 system, where the molecule completely dissociates for the Hor1 approach as clearly shown in figure 4. Each subfigure is labeled A → B + C, where A is the initial adsorption site (the center of mass of the O_2 was initially placed at this site) and B and C are the final adsorption sites (each atom of the dissociated molecule sits at this site). Throughout this manuscript, we will use this notation to describe all dissociated configurations. The three dissociated configurations corresponding to the three initial adsorption sites t1, b2 and h3 are: (a) t1 → b2 + b2; (b) b2 → t1 + t1; (c) h3 → b1 + b1, respectively. In figure 4(c), the site b1 in transition h3 → b1 + b1, is the bridge site derived from the bond between an atom on the surface layer and an atom on the sub-surface layer and as such is one-fold coordinated whereas the site b2 is a bridge site between two surface layer atoms, making it two-fold coordinated. As listed in table I for the Hor1 approach, the distances of each O atom from the americium surface R_d are 1.165 Å, 1.905 Å, and 1.587 Å and the O – O separations R_O are 3.517 Å, 3.620 Å and 3.118 Å for the dissociated processes t1 → b2 + b2, b2 → t1 + t1 and h3 → b1 + b1, respectively. Regarding the chemisorption energies, the most stable configuration is the t1 → b2 + b2 dissociation (8.681 eV for the NSOC case, 9.191 eV for SOC case), followed by the h3 → b1 + b1 dissociation (6.564 eV for the NSOC case, 7.057 eV for SOC case), with the least favorable site being b2 → t1 + t1 (5.472 eV for the NSOC case, 5.861 eV for SOC case). Similar to the trend for the Vert approach, increasing stability at both the NSOC and SOC

levels of theory implies decreasing vertical distance of the O_2 molecule from the surface layer. Analogous to case of Vert approach, the chemisorption energies for the Hor1 approach indicate that binding is slightly stronger with the inclusion of SOC compared to the NSOC case. The SOC-NSOC chemisorption energy differences ΔE_c are also listed in Table 1; ΔE_c is minimum at the least stable b2 → t1 + t1 dissociation (0.389 eV) closely followed by the next stable h3 → b1 + b1 dissociation (0.493 eV), with the most stable t1 → b2 + b2 dissociation having the largest difference of ΔE_c = 0.510 eV.

For the Hor2 approach, where the O_2 molecular approach is horizontal but perpendicular to a lattice vector, the adsorption process is dissociative. The final adsorption configurations are shown in fig. 5. Again R_d is measured from the center of mass of the molecule to the surface. As labeled in fig. 5, the following dissociative configurations were observed: (a) t1 → h3 + h3; (b) b2 → h3 + f3; (c) h3 → t1 + b2. It should be noted that in fig. 5(b) the site f3 corresponds to the three-fold hollow fcc site. The f3 site was not considered as an initial adsorption site since our previous calculations[30,42] have clearly indicated that chemisorption energies at the h3 and f3 sites are nearly degenerate and the geometry (specifically the distance from the surface) are almost identical. This is mainly due to the fact that the h3 and f3 sites have the same local environment (both are three-fold coordinated) except that their relative positions on the surface are different. Thus one hollow site h3 was deemed sufficient for this work. Also, we note that a proper inclusion of the f3

site requires nine layers with 36 Am atoms and an all electron calculation would be computationally prohibitive without generating physically meaningful results. As listed in Table I, the distances from the americium surface R_d are 0.953 Å, 0.636 Å, and 1.589 Å and the O – O bond lengths (R_O) are 3.731 Å, 2.183 Å and 2.569 Å for the three dissociation processes t1 → h3 + h3, b2 → h3 + f3, and h3 → t1 + b2 respectively. The most energetically stable configuration corresponded to the t1 → h3 + h3 dissociation (9.395 eV for the NSOC case, 9.886 eV for SOC case), followed by the dissociation b2 → h3 + f3 (8.972 eV for the NSOC case, 9.456 eV for SOC case), with the least energetically favorable configuration being the dissociation h3 → t1 + b2 (5.615 eV for the NSOC case, 6.084 eV for SOC case). For the most favorable configuration for Hor2 approach, t1 → h3 + h3, which is also the most favorable configuration among all the three approaches, we also studied the reaction pathway for the dissociation of oxygen molecule to the most stable hollow sites and no existence of any energy barrier was found. Unlike the trends for the Vert and Hor1 approach, increasing stability at both the NSOC and SOC levels of theory does not necessarily imply decreasing vertical distance of the O_2 molecule from the surface layer. However, as observed for the Vert and Hor1 approach, the chemisorption energies for the Hor2 approach indicate that binding is slightly stronger with the inclusion of SOC compared to the NSOC case. The SOC-NSOC chemisorption energy differences ΔE_c are also listed in Table 1; ΔE_c is minimum at the least stable h3 → t1 + b2 configuration (0.469 eV) closely

followed by the next stable b2 → h3 + f3 configuration (0.484 eV), with the most stable t1 → h3 + h3 configuration having an SOC-NSOC ΔE_c = 0.491 eV.

In Table 2, the adsorbate-induced work function changes with respect to the clean metal surface, given by $\Delta\Phi = \Phi^{admolecule/Am} - \Phi^{Am}$, are listed at the NSOC and SOC levels of theory for each adsorbate and each adsorption site. For Vert approach high chemisorption energies generally correspond to high work function shifts. In fact, the changes in the work functions are largest at the most preferred h3 site and lowest at the least preferred adsorption site t1. This though is not true for the Hor1 and Hor2 approaches. For Hor1 and Hor2 approaches, we find that dissociative configurations with high chemisorption energies generally correspond to low work function shifts. For Hor1 approach, the changes in the work functions are largest at the least preferred b2→ t1+t1 configuration and lowest at the most stable t1→ b2+b2 configuration. For Hor2 approach, the change in the work functions is similar to the Hor1 approach, with the largest corresponding to the least preferred h3→ t1+ b2 configuration and lowest change corresponding to the most preferred t1 → h3 + h3 configuration. The adsorbate-induced work function shifts can be understood in terms of the surface dipoles arising due to the displacement of electron density from the substrate towards the adsorbates since the electronegativity of O is much larger than that of Am. The surface dipole moment μ (in Debye) and the work function shift ΔΦ (in eV) are linearly related by the Helmholtz equation ΔΦ =12ΠΘμ/A,

Table 4.8 Change in Work Function $\Delta\Phi = \Phi^{admolecule/Am} - \Phi^{Am}$ (in eV) for Both the NSOC and SOC Levels of Theory, Where Φ^{Am} is Work Function of the Bare Surface and $\Phi^{admolecule/Am}$ is the Work Function of the Surface with Admolecule. Φ^{Am} = 2.906 eV and 2.989 eV respectively at the NSOC and SOC Theoretical Levels.

O_2 Approach	Site	ΔΦ (eV) NSOC	ΔΦ (eV) SOC
Vert	t1	1.951	1.945
	b2	1.983	1.952
	h3	2.053	2.027
Hor1	t1→ b2+b2	1.103	1.005
	b2→ t1+t1	3.086	3.009
	h3→ b1+ b1	2.336	2.211
Hor2	t1→ h3+h3	0.783	0.621
	b2→ h3+f3	0.884	0.719
	h3→ t1+ b2	2.294	2.187

where A is the area in $Å^2$ per (1×1) surface unit cell and Θ is the adsorbate coverage in monolayers. For each of the approaches, Vert, Hor1 and Hor2, and each adsorption configuration, the calculated work function shifts at the NSOC level of theory are found to be slightly larger than that at the SOC level of theory.

In Table 3, the magnitudes and alignments of the site projected spin magnetic moments for each Am atom on the *surface* atomic layer are reported for the clean and adsorbate-covered surfaces. Major changes in the moments after chemisorptions occurred on only the surface layer; no significant changes were observed on the subsurface and central layers. Also, the spin moments reported correspond to the SOC calculations. NSOC moments follow a similar qualitative trend and are not reported here. For each adsorption site, the spin moment of the closest neighbor surface layer Am atoms with which the admolecule primarily interacts is indicated in bold fonts in the Table 3. For the Vert approach, we see reductions of 0.28 μ_B for the adsorption site t1, 0.20 μ_B for each of the two atoms for the adsorption site b2 and 0.20 μ_B for each of the three atoms for the adsorption site h3 in the spin moment of the Am atom. The moments of the remaining Am atoms which are not bonded to the oxygen molecule remain basically unaltered when compared to the clean surface. For the Hor1 approach, we see spin magnetic moment reductions of 0.60 μ_B and 0.55 μ_B for the two Am atoms for the t1→b2+b2 dissociative configuration, 0.68 μ_B for each of the two Am atoms for the b2→ t1+t1 dissociative configuration,

Table 4.9 μ (μ_B) are the Site Projected Spin Magnetic Moments for the Am Atoms at the Surface Layer of the Bare Slab and the Chemisorbed Systems. Spin Moments are Quoted for SOC Calculations.

Site	μ (μ_B)	Site	μ (μ_B)	Site	μ (μ_B)
Vert	5.81, 5.81 5.81, 5.81	Hor1		Hor2	
t1	5.53, 5.80 5.80, 5.80	T1→b2+b2	5.21, 5.26 5.80, 5.80	t1→ h3+h3	5.22, 5.55 5.55, 5.82
b2	5.61, 5.61 5.80, 5.80	b2→ t1+t1	5.13, 5.13 5.80, 5.80	b2→ h3+f3	5.54, 5.55 5.50, 5.80
h3	5.61, 5.61 5.61, 5.80	H3→ b1+b1	5.19, 5.19 5.80, 5.80	h3→ t1+b2	4.99, 5.60 5.60, 5.80

and 0.62 μ_B for each of the two Am atoms for the h3→b1+b1 dissociative configuration. Similar to the Vert approach, we note that the spin moments of the remaining Am atoms which are not interacting with oxygen atoms remain basically unaltered when compared to moments of the bare surface. Finally for the Hor2 approach, we see spin magnetic moment reductions of 0.59 μ_B for one Am atom and 0.26 μ_B for two Am atoms for the t1→ h3+h3 dissociation; 0.27 μ_B, 0.26 μ_B and 0.31 μ_B for the three Am atoms for the b2→ h3+f3 dissociation, and 0.82 μ_B for one Am atom and 0.21 μ_B for two Am atoms for the h3→ t1+b2 dissociation. In all cases, the moments in the interstitial region also decreased after chemisorption. The quench in the Am magnetic moments after chemisorption is attributed to the transfer of charge from Am to O as predicted by the work function increase.

The nature of the APW+lo basis allows us to decompose the electronic charges inside the muffin-tin spheres into contributions from different angular momentum channels. These charges are referred to as partial charges. Comparing the partial charges Q_B of the Am layers and the adsorbates before adsorption to the corresponding partial charges Q_A after adsorption gives us an idea of the nature of the interaction between the adsorbates and substrate. These are reported in Tables 4-6. For Am, only the *surface layer atoms* were considered as no significant changes were observed on the subsurface and central layers. In each table, we have also reported the differential partial charge of the different angular momentum state *l* corresponding to a given atom

Table 4.10 Partial Charges Inside Muffin Tin Spheres Before Adsorption (Q_B), After Adsorption (Q_A), and Difference in Partial Charges $\Delta Q = Q_A - Q_B$ at the t1, b2 and h3 Sites for the Vert Approach for Oxygen Molecule at the SOC Level of Theory. Only the Am *Surface Layer Atoms* were Considered. The Surface Layer Am Atoms Interacting with O Atoms are Given in Bold Fonts.

Vert approach	Partial charges in muffin-tin						$\Delta Q = Q_A - Q_B$		
	Before adsorption Q_B			After adsorption Q_A					
	O *p*	Am *d*	Am *f*	O *p*	Am *d*	Am *f*	O *p*	Am *d*	Am *f*
t1	2.03			2.08			0.05		
	2.03			2.04			0.01		
		0.27	5.85		0.27	5.88		0.00	0.03
		0.27	5.85		0.27	5.88		0.00	0.03
		0.27	5.85		0.36	5.71		0.09	-0.14
		0.27	5.85		0.27	5.88		0.00	0.03
b2	2.03			1.99			-0.04		
	2.03			2.08			0.05		
		0.27	5.85		0.30	5.79		0.03	-0.06
		0.27	5.85		0.30	5.79		0.03	-0.06
		0.27	5.85		0.26	5.88		-0.01	0.03
		0.27	5.85		0.26	5.88		-0.01	0.03
h3	2.03			1.96			-0.07		
	2.03			2.11			0.08		
		0.27	5.85		0.31	5.78		0.04	-0.07
		0.27	5.85		0.31	5.78		0.04	-0.07
		0.27	5.85		0.31	5.78		0.04	-0.07
		0.27	5.85		0.26	5.87		-0.01	0.02

Table 4.11 Partial Charges Inside Muffin Tin Spheres Before Adsorption (Q_B), After Adsorption (Q_A), and Difference in Partial Charges $\Delta Q = Q_A - Q_B$ at the t1, b2 and h3 Sites for the Hor1 Approach for Oxygen Molecule at the SOC Level of Theory. Only the Am *Surface Layer Atoms* were Considered. The Surface Layer Am Atoms Interacting with O Atoms are Given in Bold Fonts.

Hor1 approach	Partial charges in muffin-tin						$\Delta Q = Q_A - Q_B$		
	Before adsorption Q_B			After adsorption Q_A					
	O *p*	Am *d*	Am *f*	O *p*	Am *d*	Am *f*	O *p*	Am *d*	Am *f*
t1→b2+b2	2.03			2.09			0.06		
	2.03			2.09			0.06		
		0.27	5.85		0.24	5.91		-0.03	0.06
		0.27	5.85		0.40	5.63		0.13	-0.22
		0.27	5.85		0.40	5.63		0.13	-0.22
		0.27	5.85		0.24	5.91		-0.03	0.06
b2→ t1+t1	2.03			2.05			0.02		
	2.03			2.05			0.02		
		0.27	5.85		0.50	5.56		0.23	-0.29
		0.27	5.85		0.50	5.56		0.23	-0.29
		0.27	5.85		0.24	5.90		-0.03	0.05
		0.27	5.85		0.24	5.90		-0.03	0.05
h3→b1+b1	2.03			2.07			0.04		
	2.03			2.07			0.04		
		0.27	5.85		0.48	5.62		0.21	-0.23
		0.27	5.85		0.48	5.62		0.21	-0.23
		0.27	5.85		0.24	5.88		-0.03	0.03
		0.27	5.85		0.24	5.88		-0.03	0.03

Table 4.12 Partial Charges Inside Muffin Tin Spheres Before Adsorption (Q_B), After Adsorption (Q_A), and Difference in Partial Charges $\Delta Q = Q_A - Q_B$ at the t1, b2 and h3 Sites for the Hor2 Approach for Oxygen Molecule at the SOC Level of Theory. Only the Am *Surface Layer Atoms* were Considered. The Surface Layer Am Atoms Interacting with O Atoms are Given in Bold Fonts.

Hor2 approach	Partial charges in muffin-tin						$\Delta Q = Q_A - Q_B$		
	Before adsorption Q_B			After adsorption Q_A					
	O *p*	Am *d*	Am *f*	O *p*	Am *d*	Am *f*	O *p*	Am *d*	Am *f*
t1→h3+h3	2.03			2.10			0.07		
	2.03			2.10			0.07		
		0.27	5.85		0.29	5.76		0.02	-0.09
		0.27	5.85		0.29	5.76		0.02	-0.09
		0.27	5.85		0.40	5.63		0.13	-0.22
		0.27	5.85		0.27	5.87		0.00	0.02
b2→ h3+f3	2.03			2.14			0.11		
	2.03			2.14			0.11		
		0.27	5.85		0.33	5.74		0.06	-0.11
		0.27	5.85		0.33	5.74		0.06	-0.11
		0.27	5.85		0.34	5.76		0.07	-0.09
		0.27	5.85		0.27	5.86		0.00	0.01
h3→ t1+b2	2.03			2.03			0.00		
	2.03			2.09			0.06		
		0.27	5.85		0.27	5.83		0.00	-0.02
		0.27	5.85		0.27	5.83		0.00	-0.02
		0.27	5.85		0.24	5.89		-0.03	0.04
		0.27	5.85		0.59	5.61		0.22	-0.24

given by $\Delta Q(l) = Q_A - Q_B$. $\Delta Q(l) > 0$ indicates charge gain inside the muffin tin sphere while $\Delta Q < 0$ indicates otherwise. ΔQ (l) may be loosely interpreted as a measure ofcharge transfer. In table 4, Q_A, Q_B, and ΔQ (l) for O_2 molecule with Vert approach adsorbed at the t1, b2, and h3 adsorption sites respectively on the dhcp-Am(0001) surface are reported. For the one-fold t1 site, ΔQ (2*p*) = 0.05 *e* and 0.01 *e* for the two O atoms, ΔQ(6*d*) = 0.09 and ΔQ(5*f*) = -0.14 *e* for the Am atom, implying Am(6*d*)-Am(5*f*)-O(2*p*) hybridizations. For the two-fold b2 site, ΔQ(2*p*) = -0.04 *e* and 0.05 *e* for the two O atoms, ΔQ(6*d*) = 0.03 *e* and ΔQ(5*f*) = -0.06 *e* for each of the two Am atoms, again suggesting the participation of some of the Am 5*f* electrons in chemical bonding with O. For the three-fold hollow h3 site, ΔQ (2*p*) = -0.07 *e* and 0.08 *e* for the two O atoms, ΔQ(6*d*) = 0.04 *e* and ΔQ(5*f*) = -0.07 *e* for each of the three Am atoms, which again suggest some contribution of the Am 5*f* electrons to Am-O bonding. In table 5, Q_A, Q_B, and ΔQ (l) for the Hor1 approach corresponding to the t1→ b2+b2, b2→ t1+t1, and h3→ b1+ b1 dissociations are shown. For the t1→ b2+b2 dissociation, ΔQ (2*p*) = 0.06 *e* for the two O atoms, ΔQ(6*d*) = 0.13 *e* and ΔQ(5*f*) = -0.22 *e* for each of the two Am atoms, which like the case for Vert approach, implies significant Am(6*d*)-Am(5*f*)-O(2*p*) interactions. For the b2→ t1+t1 dissociation, ΔQ (2*p*) = 0.02 *e* for the two O atoms, ΔQ (6*d*) = 0.23 *e* and ΔQ(5*f*) = -0.29 *e* for each of the two Am atoms, suggesting the participation of some the Am 5*f* electrons in Am-O bonding. For the h3→ b1+ b1 dissociation, ΔQ(2*p*) = 0.04 *e* for the two O atoms, ΔQ(6*d*) = 0.21 *e* and ΔQ(5*f*) = -0.23 *e* for

each of the two Am atoms, which again suggest some contribution of the Am 5*f* electrons to Am-O chemical bonding. In table 6, where the partial charges for the Hor2 approach are reported, we observe for the t1→h3+h3 dissociation that, ΔQ (2*p*) = 0.07 *e* for the two O atoms, ΔQ(6*d*) = 0.02 *e*, 0.02 *e* and 0.13 *e* and ΔQ(5*f*) = -0.09 *e*, -0.09 *e* and -0.22 *e* for each of the three Am atoms, which like the previous cases for Vert and Hor1 approaches, imply significant Am(6*d*)-Am(5*f*)-O(2*p*) interactions. For the b2→ h3+f3 dissociation, ΔQ (2*p*) = 0.11 *e* for the two O atoms, ΔQ(6*d*) = 0.06 *e*, 0.06 *e* and 0.07 *e* and ΔQ(5*f*) = -0.11 *e*, -0.11 *e* and -0.09 *e* for each of the three Am atoms while for the h3→ t1+b2 dissociation, ΔQ(2*p*) = 0.00 *e* and 0.06 *e* for the two O atoms, ΔQ(6*d*) = -0.03 *e* and 0.22 *e* and ΔQ(5*f*) = 0.04 *e* and -0.24 *e* for each of the two Am atoms. Overall, the partial charge analyses tend to suggest that *some* of the Am 5*f* electrons participate in chemical bonding. The question of whether all the *5f* electrons are localized or not cannot, of course, be proven from the present analysis. We wish to stress that the partial charges are confined inside the muffin tin spheres and do not give any information of the interactions between the atoms in the interstitial region. Information which includes the electronic charges in interstitial region can be obtained from the difference charge density distributions.

The nature of the bonds between the adsorbate and the Am atoms on the surface have been investigated by computing the difference charge density Δn(r) defined as follows:

$$\Delta n(r) = n(O_2 + Am) - n(Am) - n(O_2),$$

where $n(O_2+Am)$ is the total electron charge density of the Am slab with O_2 admolecule, n(Am) is the total charge density of the bare Am slab, and $n(O_2)$ is the total charge density of the admolecule. In computing $n(O_2)$ and n(Am), the admolecule O_2 and Am atoms are kept fixed at exactly the same positions as they were in the chemisorbed systems. All charge densities reported here were computed in the plane passing through the admolecule and one or two surface Am atoms using the Xcrysden utility .[60] We have reported the difference charge density plots for the most favorable chemisorption site for each of the approaches, Vert, Hor1 and Hor2 in fig 6. For the Vert approach, h3 was the most favorable adsorption site and Δn was computed in the plane passing through the two O atoms and the Am atom directly bonded to the O atom facing the surface. For the Hor1 approach, the most stable t1→b2+b2 dissociated configuration is depicted. In this case Δn was computed in the plane passing through the two dissociated O atoms and nearest neighbor Am atoms. Similarly for the Hor2 approach, Δn for the most stable t1→h3+h3 dissociated configuration is shown. Again the plane passes through the two dissociated O atoms and neighboring Am atoms. In fig. 6(a) we clearly see charge accumulation around the oxygen atom labeled O2 and a strong polarization towards the oxygen atom labeled O1. Also, significant charge loss around the Am atom bonded to the atom O2 implies that the Am-O bond has a strong ionic character, which is expected as the oxygen atom is more electronegative than

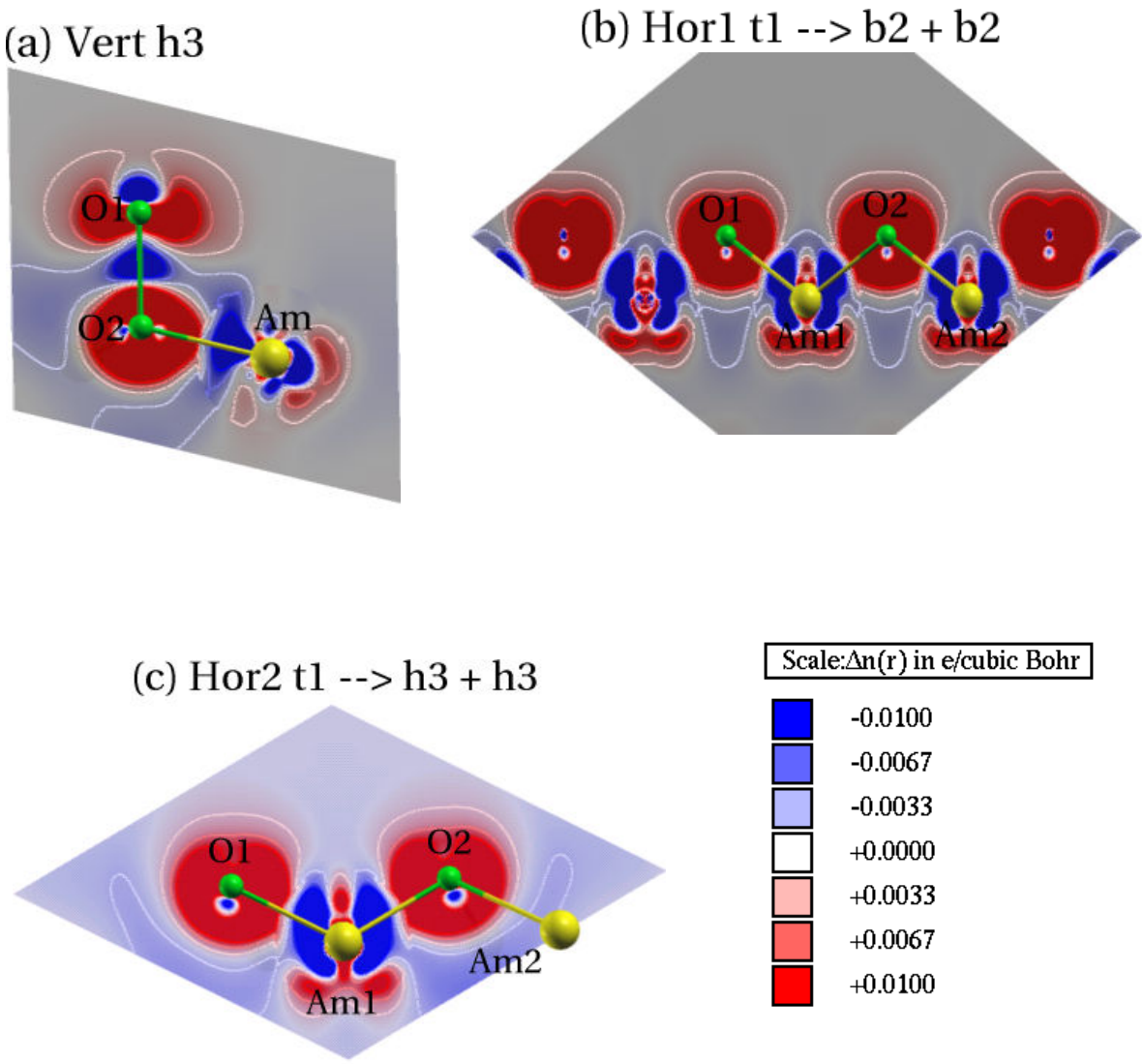

Figure 4.14 Difference charge density distributions Δn(r) for O_2 chemisorbed on the dhcp-Am(0001) surface at the most stable configurations corresponding to the Vert, Hor1 and Hor2 approaches. The scale used is shown at the bottom. Red (positive) denotes regions of charge accumulation and blue (negative) denotes regions of charge loss. Admolecule is colored green and Am atoms are colored gold.

Am. For the Hor1 approach corresponding to t1→b2+b2 in fig. 6(b) and Hor2 approach corresponding to t1→ h3+h3 in fig. 6(c), the Am-O bonds are again largely ionic in character as significant charge accumulation around the O atoms can be observed. The difference charge density plots are fairly consistent with the positive changes in the work function as well as the differential partial charges reported in tables 4-6.

We also computed the local density of states (LDOS), obtained by decomposing the total density of the single particle Kohn-Sham eigenstates into contributions from each angular momentum channel *l* of the constituent atoms inside the muffin tin spheres. Here, we have reported the LDOS for only the SOC computation, the LDOS for NSOC calculations yielding a similar qualitative description. In fig. 7, the Gaussian-broadened (with a width of 0.05 eV) *f* and *d* LDOS curves for each of the layers of the bare dhcp Am (0001) metal slab are shown. Clearly, we see well-defined peaks in the 5*f* electron LDOS in the vicinity of the Fermi level, which have also been observed for bulk dhcp-Am(0001), and tends to indicate *some* 5*f* electron localization. However, this statement should be viewed with caution because of the nature of the underlying theory, namely density functional theory and all *5f* states are treated as band states. The occupied 5*f* electron states below the Fermi level also support this conclusion, In view of our previous statement about the participation of the *5f* electrons in chemical bonding, we believe that it is possible that some *5f* electrons are localized and some are not. This question

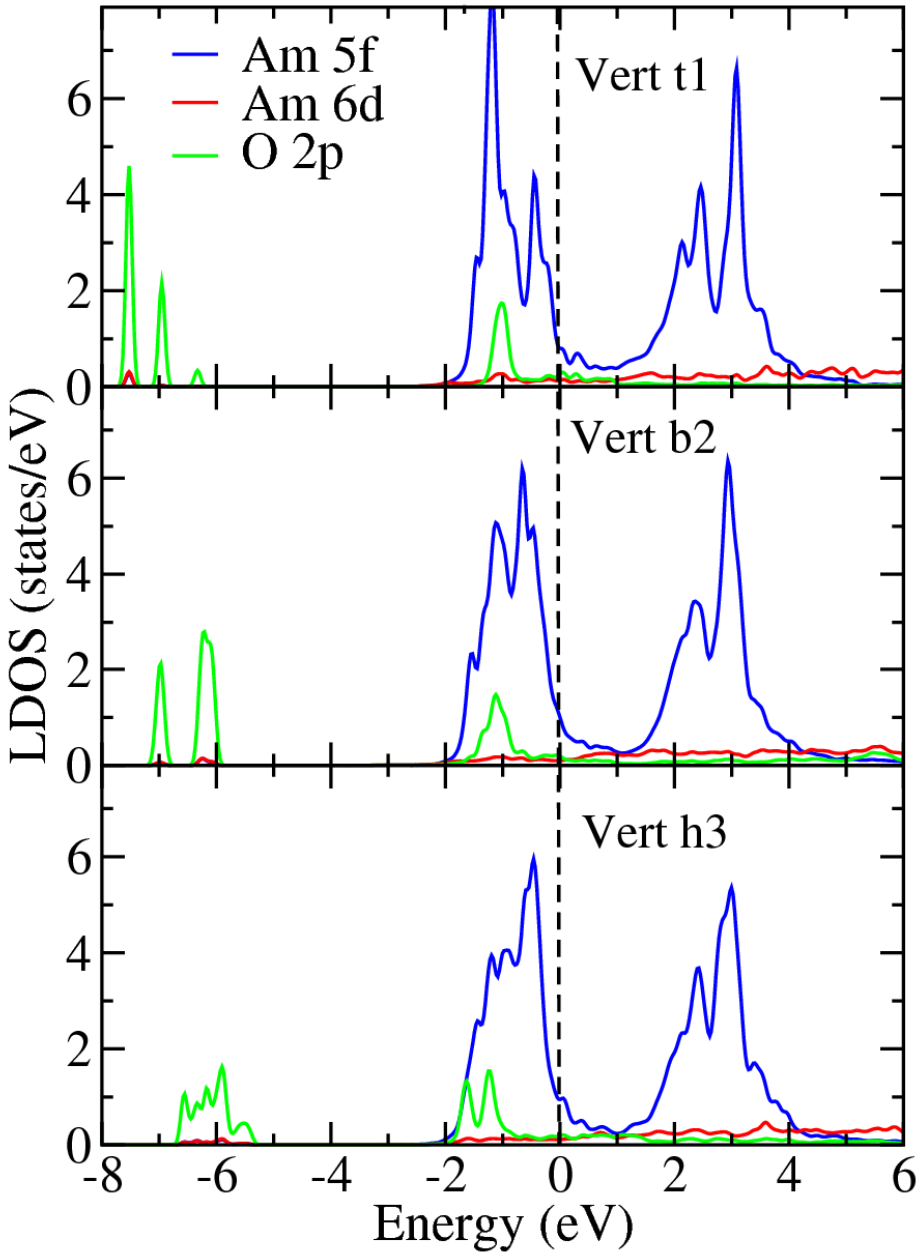

Figure 4.15 6*d* and 5*f* LDOS curves inside the muffin-tins for the Am atoms on the surface layer and 2*p* LDOS curves for O_2 admolecule for the Vert approach. Vertical line through E=0 is the Fermi level. LDOS correspond to calculations with SOC.

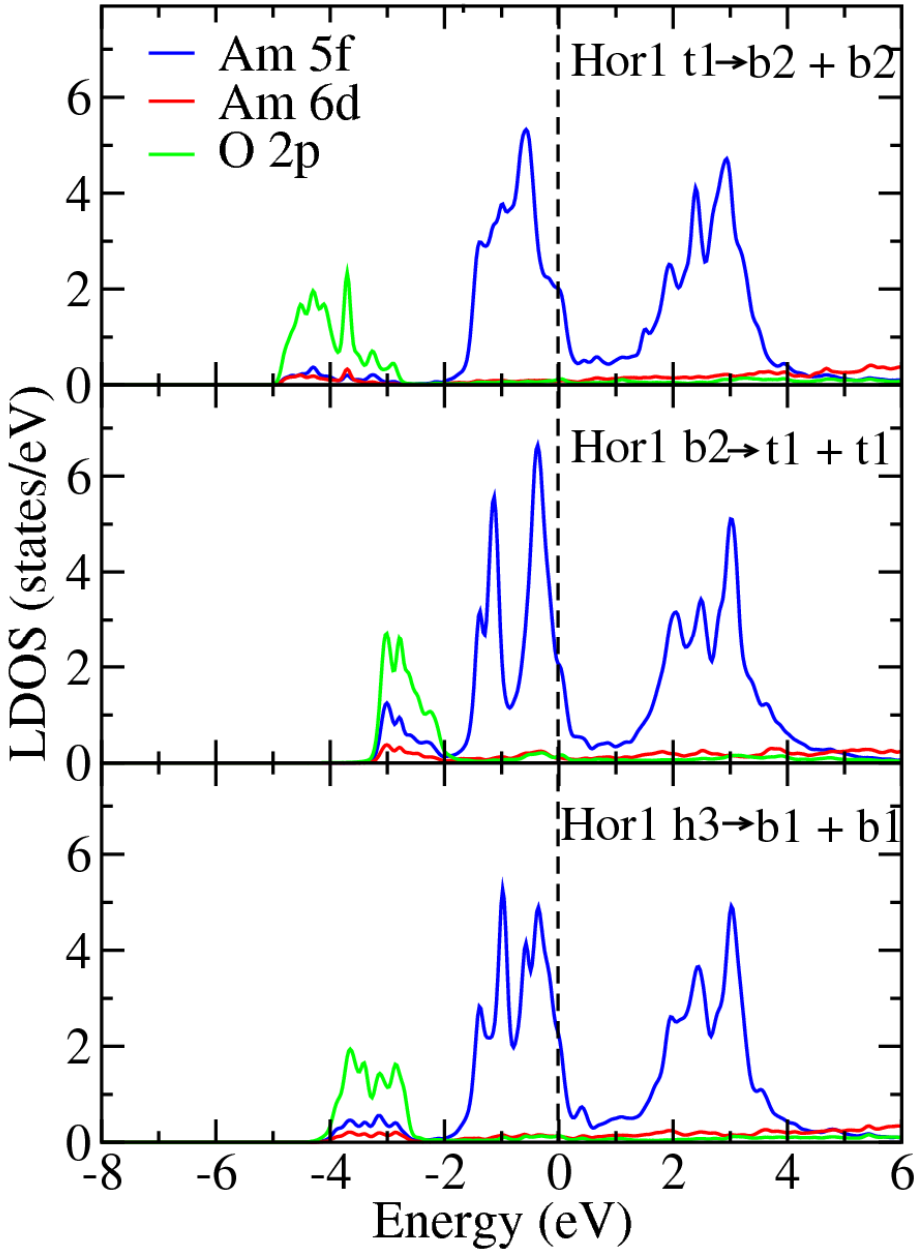

Figure 4.16 6*d* and 5*f* LDOS curves for the Am atoms on the surface layer and 2*p* LDOS curves for O atoms inside the muffin-tins for the Hor1 approach. Vertical line through E=0 is the Fermi level. LDOS correspond to calculations with SOC.

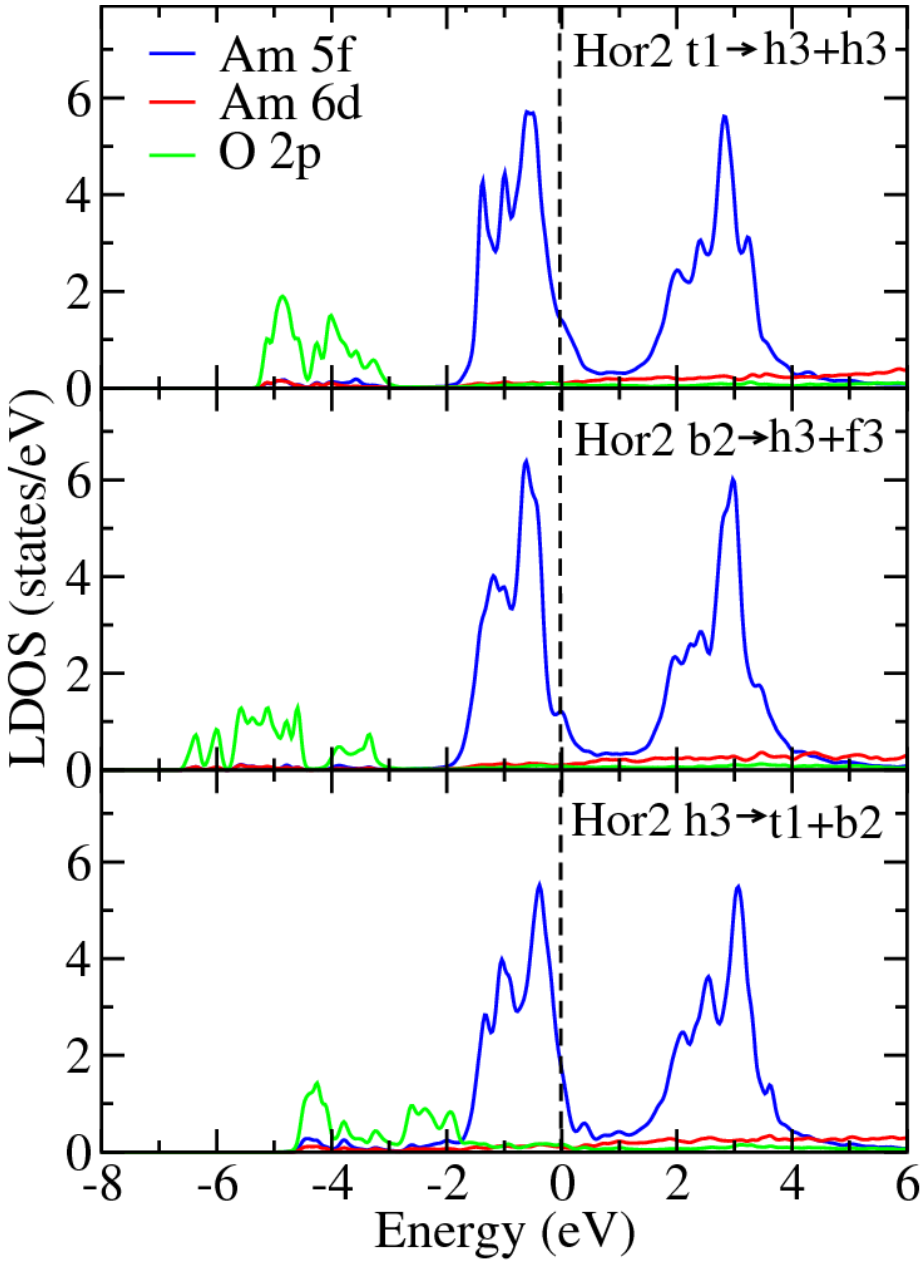

Figure 4.17 6*d* and 5*f* LDOS curves for the Am atoms on the surface layer and 2*p* LDOS curves for O atoms inside the muffin-tins for the Hor2 approach. Vertical line through E=0 is the Fermi level. LDOS correspond to calculations with SOC.

needs to be pursued in the future. We also note that the peak below the Fermi level centered on a binding energy of 1 eV below the level instead of the 2.8 eV observed in X-ray and ultraviolet photoemission spectra experiments.[20,27] In fig. 8, we show the LDOS plots for the O_2 molecule and the surface Am atoms after chemisorption for the Vert approach at the three different adsorption sites t1, b2 and h3. As there are four nonequivalent sites on the surface, we depict the LDOS for only the Am atom(s) directly bonded to the O_2 molecule (or O atoms for the cases where the molecule dissociates) in order to assess the changes in DOS upon chemisorption. At the adsorption site t1, we note some modification in the Am 5*f* DOS just below the Fermi level in comparison to the 5*f* DOS of the bare surface. More specifically, we observe a significant reduction in the 5f peak around at 0.5 eV below the Fermi level, implying the participation of *some* 5*f* electrons participate in chemical bonding. We also observe significant Am(5*f*)-Am(6*d*)-O(2*p*) hybridizations. The LDOS distributions for the b2 and h3 sites show significant modifications in the 5*f* DOS below the Fermi level in comparison to the surface layer LDOS of the bare slab. In particular the splitting of the 5*f* band (about 1 eV below the Fermi level) broadens, implying that some of the 5*f* electrons participate in bonding. Similar to the t1 site, significant Am(5f)-Am(6*d*)-O(2*p*) admixture are clearly evident in both cases.

In fig. 9, we show the LDOS plots for the O atoms and the surface Am atoms after chemisorption for the Hor1 approach corresponding each of the three dissociated configurations. For the dissociation process t1→ b2+b2, we

note a significant broadening of the Am 5*f* DOS just below the Fermi level in comparison to the bare surface layer 5*f* DOS. We also observe significant Am(5*f*)-Am(6*d*)-O(2*p*) hybridizations in the -5 eV to -3 eV range, implying that both the Am 5*f* and 6*d* orbitals contribute to bonding. The LDOS distributions for the b2→ t1+t1 and h3→ b1+ b1 dissociations show a slight reduction in the 5*f* DOS below the Fermi level, with the O 2*p* bonding state pushed to slightly higher binding energies (when compared to the DOS for t1→ b2+b2), which naturally suggests slightly weaker binding as observed in the chemisorption energies.

In fig. 10, we show the LDOS plots for the dissociated molecule and the surface Am atoms after chemisorption for the Hor2 approach corresponding to the t1→ h3+h3, b2→ h3+f3, and h3→ t1+ b2. In all cases, we observe a broadening in the 5*f* band peaks below the Fermi level when compared to the bare surface. Furthermore, a fair amount of O(2*p*) and Am(6*d*, 5*f*) hybridizations are evident. We hasten to point out that overall, the Am 5*f* states for all the Vert, Hor1, and Hor2 approaches show signatures of *slight* delocalization.

As dissociative adsorption of the oxygen molecule is clearly favored over molecular adsorption, we decided to study the dissociation pathway of oxygen molecule on the americium (0001) surface by constraint minimization of the total energy along a chosen reaction coordinate. We have thus calculated the reaction barrier for only the most favorable chemisorption site, namely for the

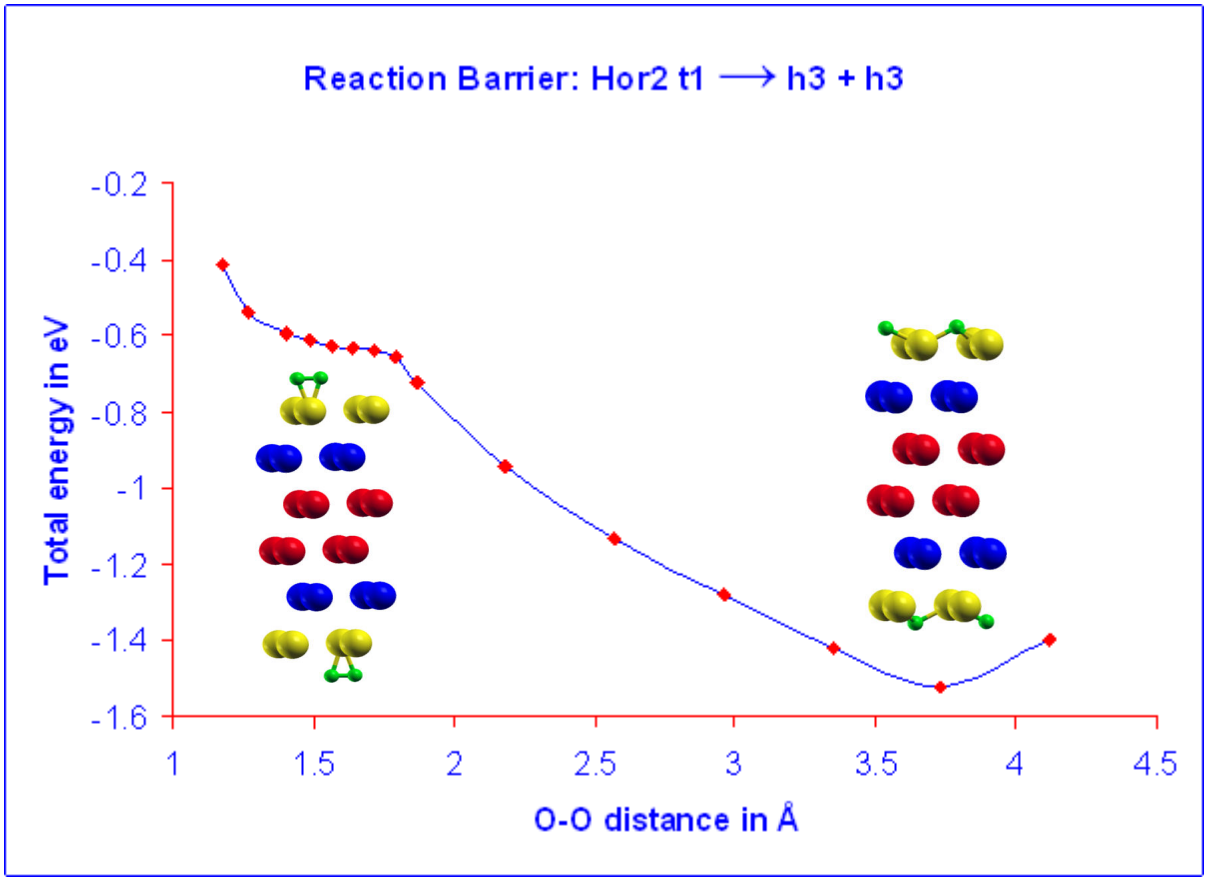

Figure 4.18 Reaction barrier for the Hor2 approach corresponding to the most favorable t1→ h3+h3 dissociation. The total energy is shifted by a constant factor.

t1→ h3+h3 dissociation corresponding to the Hor2 approach, where the initial adsorption site is t1, but upon adsorption the oxygen molecule dissociates with the two dissociated O atoms sitting on two different h3 sites. One reason behind the reaction barrier calculation for the most favorable adsorption site is that the probability of oxygen molecule adsorption at this site is higher and dissociation of the molecule is feasible provided enough energy is supplied to overcome the dissociation barrier. As for the reaction coordinate, we have chosen the O – O distances starting at the optimized bond length for the oxygen molecule. For the reaction barrier calculation O_2 was placed above the americium surface with the O – O distance held constant at a given value, and the distance between the O_2 molecule and the surface being optimized to yield the total energy of the system. Figure 9 shows the optimized energy curve with respect to different O – O distances. The energy curve shows no energy hill that the oxygen molecule needs to overcome, exhibiting the fact that no external energy is required to dissociate the oxygen molecule upon adsorption on the americium surface. However, it does indicate a possible molecular oxygen adsorption at O – O bond length of somewhere between 1.6 Å to 1.7 Å. The adsorption energy here is in the range of 3.336 eV to 3.394 eV, much lower compared to the complete dissociative oxygen adsorption energy of 9.395 eV at an O – O bond length of 3.731 Å.

In summary, we have used the generalized gradient approximation to density functional theory with the full potential LAPW+lo method to study

chemisorption of oxygen molecule on the (0001) surface of dhcp Am at two theoretical levels; one with no spin-orbit coupling (NSOC) and the other with spin-orbit coupling (SOC). The results at the two levels of theory do not vary from each other significantly. Dissociative adsorption of oxygen molecule is favored over molecular adsorption. For O_2 adsorption, the one-fold t1 site with Hor2 approach was found to be the most stable where upon adsorption of the O_2 molecule dissociated and two O atoms sit on two different three-fold h3 sites. The inclusion of spin-orbit coupling lowers the chemisorption energies by 0.089-0.493 eV. Work functions increased in all cases compared to the clean Am surface, with the lowest shift corresponding to the least coordinated t1 site and largest shifts corresponding to the maximally coordinated hollow h3 site for the Vert and Hor2 approaches, while for Hor1 approach, this was not the case. Upon adsorption, the net spin magnetic moment of the chemisorbed system decreases in each case compared to the bare surface. The partial charge analyses illustrate that *some* of the Am 5*f* electrons participate in chemical bonding. Difference charge density distributions clearly show that bonds between the surface Am atoms and the oxygen molecule at each site is largely ionic in character. A study of the local density of states showed Am (6*d*)-Am (5*f*)-O(2*p*) hybridizations after chemisorption. Overall, the Am 5*f* DOS below the Fermi Level become slightly delocalized after chemisorption.

CHAPTER 5

ADSORPTION AND DISSOCIATION OF WATER ON THE (0001) SURFACE OF DOUBLE HEXAGONAL CLOSE PACKED AMERICIUM

The DFT calculations using the Perdew-Burke-Enzerhof (PBE) formulation for the generalized gradient approximation[45] were carried out using the suite of software DMol^3,[67-70] which employs a pseudo-potential numerical basis set method, and WIEN2K,[48] which employs a full-potential linearized augmented plane wave plus local basis (FP-L/APW+lo) method. The strategy we employed was to first perform structural optimizations with the DMol^3 because of its balance between accuracy and computational efficiency and the resulting structures used for further electronic structure analysis with Wien2K because of its accuracy in predicting local electronic properties. The rationale for this hybrid approach is based on the fact that two sufficiently accurate DFT Hamiltonians, *albeit* with Hamiltonian matrix elements generated using different basis sets, should produce minimum energy structures that show little or no significant departure from each other in configuration space. We briefly outline below, the features of each code and the parameters we have employed for our calculations.

DMol3 uses numerical orbitals for the basis functions, where each

function corresponds to an atomic orbital. In DMol3, the physical wave function is expanded in accurate numerical basis set and fast convergent 3D integration is used to calculate the matrix elements occurring in the Ritz variational method. Double numerical basis sets with polarization functions (DNP) are used and a real space cut-off of 5.5 Å was used. The size of this DNP basis set is comparable to the 6-31G** basis set of Hehre et al.[66]. For americium, the outer 17 electrons ($6s^2$ $6p^6$ $5f^6$ $6d^1$ $7s^2$) are treated as valence electrons and the remaining 78 electrons are treated as core. A hardness conserving semilocal pseudopotential, density functional semicore pseudopotential (DSSP)[67-71] was used. The Density functional Semi-core PseudoPotentials were generated by fitting all-electron relativistic DFT results. Thus the DSPPs have been specifically designed to reproduce accurate DMol3 calculations. These norm conserving potentials have a nonlocal contribution for each channel up to l =2, as well as a nonlocal contribution to account for higher channels. The *k*-point sampling was done using the Monkhorst-Pack scheme.[72] The maximum number of numerical integration mesh points available in DMol3 was chosen for our computations and the threshold of density matrix convergence was set to 10^{-6} and a smearing parameter of 0.005 Ha was used. Scalar relativistic corrections are explicitly included but spin-orbit (SO) coupling is not implemented. Thus all DMol^3 calculations were performed at the scalar relativistic level.

The (FP-LAPW+lo) method as implemented in the WIEN2k code[48] makes no shape approximation to the potential or the electron density. Within the FP-LAPW+lo method, the unit cell is divided into non-overlapping muffin tins spheres and an interstitial region. Inside the muffin tin sphere of radius R_{MT}, the wave functions are expanded using radial functions (solution to the radial Schrödinger equation) times spherical harmonics with angular momenta up to $l_{\max}^{wf}$ =10. Non-spherical contributions to the electron density and potential inside the muffin tin spheres were considered up to $l_{\max}^{pot}$ =6. APW+lo basis were used to describe *s, p, d,* and *f* (*l*=0, 1, 2, 3) states and LAPW basis were used for all higher angular momentum states in the expansion of the wave function. Additional local orbitals (LO) were added to the 2*s* semi-core states of O and the 6*s*, 6*p* semi-core states of Am to improve their description. The radii of the muffin tin spheres were R_{MT}(H) = 0.70 Bohr, R_{MT}(O) = 1.1 Bohr and R_{MT}(Am) = 2.2 Bohr. The truncation of the modulus of the reciprocal lattice vector used for the expansion of the wave function in the interstitial region K_{MAX}, was set to $R_{MT}K_{MAX}$ = 8.5 for the clean slab and $R_{MT}\times K_{MAX}$ = 2.7045 for the slab-with-molecule, where R_{MT} denotes the smallest muffin tin radius, that is, R_{MT} = 2.2 Bohrs for the bare slab and R_{MT} = 0.70 Bohrs for the slab-with-molecule (this ensures that K_{MAX} is the same each case).

In the WIEN2k code, core states are treated at the fully relativistic level. Semi-core and valence states are treated at either the scalar relativistic level, i.e., no spin-orbit coupling (NSOC) or at the fully relativistic level, i.e., spin-orbit

coupling (SOC) included. Spin-orbit interactions for semi-core and valence states are incorporated via a second variational procedure using the scalar relativistic eigenstates as basis, where all eigenstates with energies below the cutoff energy of 4.5 Ry were included, with the so-called $p_{1/2}$ extension, which accounts for the finite character of the wave function at the nucleus for the $p_{1/2}$ state. We considered both the NSOC and SOC levels of theory to investigate spin-orbit coupling effects on adsorption energies. We have used the method outlined above extensively in *some* of our previous works on actinide surfaces.[38-44] We have thus performed scalar relativistic (with no spin-orbit coupling) and spin-orbit-inclusive calculations using WIEN2K at the DMOl^3 optimized geometries.

The dhcp-Am (0001) surface was modeled by a supercell consisting of a periodic 6-layer slab with a (2×2) surface unit cell and a vacuum 30 Bohr thick (Fig.1). In accordance with our previous findings, we have used an AFM configuration for the slab which consists of alternating ferromagnetic layers of up- and down-spin atoms along the *c*-axis. The spin quantization axis for the magnetic SOC calculations was along the [001] direction. The slab was initially constructed using the anti-ferromagnetic bulk optimized lattice constant of 6.702 a.u. which is in good agreement with the experimental lattice constant of 6.56 a.u..[15,21,51] Integrations in the Brillouin zone (BZ) have been performed using a (6×6×1) k-point mesh using the special k-points sampling method with a temperature broadening of the Fermi surface by the Fermi distribution, where a

broadening parameter of K_BT = 0.005 Ry has been used. The temperature broadening scheme avoids the instability from level crossings in the vicinity of the Fermi surface in metallic systems and also reduces the number of k-points necessary to calculate the total energy of metallic systems. Self-consistency is achieved when the total energy variation from iteration to iteration is 0.01 mRy or lower. Using the optimized lattice constants, that is, *a*=6.702 a.u. and c = 3.2*a*, a 2x2 hexagonal surface unit cell (2 atoms along each lateral 2D direction yielding 4 Am atoms per surface unit cell) for (0001) orientation is constructed. Then the surface unit cell is used to build the slab with 6 atomic layers and 30 a.u. vacuum. Furthermore, the slab was built to have inversion symmetry for computational efficiency. The interlayer spacing between the surface unit cells in the slab above corresponded to the bulk spacing d_0= *c/4.* As mentioned before, all structural optimizations were carried out with DMol^3 with no symmetry or geometry constraints. The optimizations were terminated when the self-consistent density, total energy, atomic forces, and atomic displacements were converged to within 5×10^{-4}, 2×10^{-5} a.u., 4×10^{-3} a.u./Å, and 5×10^{-3} Å, respectively. For the WIEN2K calculations with the DMol^3-optimized geometries as input, a charge density and total energy convergence of 10^{-3} and 10^{-5} Ry respectively were employed.

To study adsorption on the Am surface, the admolecule, corresponding to a surface coverage of Θ = 1/4 of a monolayer (ML), was allowed to approach the surface from both sides to preserve inversion symmetry. Three high

symmetry adsorption sites were considered: (i) one-fold top site t1 (admolecule is directly on top of an Am atom) (ii) two-fold bridge site b2 (admolecule is placed in the middle of two nearest neighbor Am atoms); and (iii) three-fold hollow hcp site h3 (admolecule sees a Am atom located on the layer directly below the surface layer). For molecular H_2O adsorption, we considered three initial orientations per adsorption site as shown in Fig.1: (i) upright orientation with O atom facing the adsorption site labeled Vert1 (ii) upright orientation with the two H atoms facing the adsorption site labeled Vert2 (iii) flat-lying (horizontal) orientation with O atom occupying the adsorption site labeled Hor. Thus a total 9 initial molecular adsorption configurations were considered.

For partial dissociation (fig. 2) OH1+H2, for each of the three adsorption sites, the H2 atom was placed at the h3 adsorption site as this site was found to be the most favorable site for the atomic hydrogen adsorption. For OH1 adsorption, four approaches of the OH molecule towards to the surface were considered: (a) approach vertical to the surface with O atom facing the Am surface (Vert-O approach); (b) approach vertical to the surface with H atom facing the Am surface (Vert-H approach); (c) approach parallel to a lattice vector (Hor1 approach); (d) approach perpendicular to a lattice vector (Hor2 approach). It is obvious that for both the horizontal approaches the atoms of the water molecule are at the same distance from the americium surface, whereas for the two vertical approaches either hydrogen or oxygen atom is closer to the surface than the other. For the completely dissociated H1+O+H2 configuration

we considered only one case where the adatoms were initially placed at three neighboring h3 sites as shown in fig. 3. Also the adatom separations (~5.6 a.u.) are large enough to ensure that there are no significant adatom-adatom interactions.

We will like to point out that even though the adsorptions were carried out with respect to the adatoms/admolecule placed initially at one of the high symmetry adsorption sites, the final adsorption configuration does not necessarily match the initial. After structural optimization, the adatom/admolecule moves to the preferred adsorption site which might not be same as the initial site. For the sake of brevity therefore, the label for the initial adsorption geometry was used for the corresponding optimized geometry irrespective of the final state. Nevertheless, appropriate geometric and energetic parameters were used to describe the final states to elucidate their structures.

The rumpling of a given layer i, δr_i, is defined as the maximum vertical displacement (along the z-axis) between two atoms on the layer and is given by

$$\delta r_i, = z_i^{max} - z_i^{min}.$$

The interlayer relaxation, Δ_{ij}, between layers *i* and *j* respect to the bulk interlayer spacing d_0 expressed as a percentage is defined as

$$\Delta_{ij} = 100\% \times (d_{ij} - d_0)/ d_0,$$

where $d_{ij} = |z_i - z_j|$ is the interlayer separation between layers *i* and *j*. For the case where there is rumpling of a layer, that is when $\delta r > 0$, d_{ij} is not a well-

defined quantity and we define d_{ij} as difference between the z-averaged position per layer. The adsorption energy E is computed as

E_C = E(slab)+ E(H_2O) -E(slab + adsorbate),

Where E(slab) is the total energy of the clean slab, E(H_2O) is the total energy of the free molecule, and E(slab + adsorbate) is the total energy of the slab with the adsorbates. Thus a positive value of E_C implies adsorption and a negative value implies otherwise. For the sake of consistency the H_2O and OH molecules were optimized in the same supercell as used for the slab calculation and with the same computational parameters.

In order to perform the calculations for the H_2O adsorption on the (0001) surface of dhcp-Am surface, we initially optimized the geometry of the free H_2O molecule. For the H_2O molecule, the equilibrium OH bond length and HOH bond angle were found to be 0.98 Å and 102.5° respectively, with the corresponding experimental bond length and angle being 0.96 Å and 104.5° respectively.[64] Starting with the molecular H_2O adsorption, there are three different orientations (Vert1, Vert2 and Hor) on how to place the H_2O molecule above the three adsorption sites (t1, b2 and h3) for the initial adsorption geometry. Listed in table I are the adsorption energies for the scalar and fully relativistic approximations, the average interlayer separation between layers *i* and *j* relative to the bulk in %, the rumpling of layer *i* in Å, the Am-O, Am-H, and O-H distance in Å and the HOH bond angle. For Vert1 (upright orientation with O atom facing the adsorption site) approach (fig. 1a) of the H_2O molecule at the

Table 5.1 Optimized Geometrical Parameters and Adsorption Energies for Molecular H_2O Adsorption. Δ_{ij} is the Average Interlayer Separation Between Layers *i* and *j* Relative to the Bulk in %, δr_i is the Rumpling of Layer *i* in Å, d_{XY} is the Average Bond Distance Between Atoms X and Y in Å, θ_{HOH} is the H-O-H Bond Angle in Degrees, E_{NSO} and E_{SO} are the Non Spin-Orbit and Spin-Orbit Coupling Adsorption Energies respectively.

	Site	Δ_{12}	δr_1	d_{OH}	d_{HAm}	d_{OAm}	θ_{HOH}	E_{NSO}	E_{SO}
Bare slab		1.9							
Free H_2O				0.98			102.5		
Vert1	t1	2.0	0.05	0.96		2.62	106.4	0.275	0.071
	b2	2.3	0.04	0.96		3.14	106.1	0.091	-0.121
	h3	1.2	0.10	0.97	2.89	2.62	104.5	0.359	0.214
Vert2	t1	1.1	0.08	0.96	2.95	2.65	104.6	0.347	0.195
	b2	2.8	0.22	0.96	3.06	3.23	102.8	0.144	0.009
	h3	2.4	0.09	0.96	3.18	3.28	103.6	0.162	0.032
Hor	t1	0.9	0.07	0.96	2.92	2.65	104.4	0.364	0.293
	b2	1.9	0.08	0.97	2.92	2.92	104.1	0.175	0.109
	h3	1.5	0.17	0.96	2.94	2.64	104.4	0.366	0.232

t1 adsorption site, the adsorption energies for the NSO and SO states are 0.275 eV and 0.071 eV respectively. In this case the initial geometry is same as the final geometry in that the adsorption site and the orientation of the H_2O molecule do not change after structural optimization except that the molecule sits in very close vicinity of the initial adsorption site. We wish to point out that the molecule does not sit exactly on the t1 site. It is apparent that the SO binding is less stable than the NSO. Compared to the bare interlayer separation between the surface and subsurface layers of 1.9 %, for this adsorption configuration the interlayer separation is 2.0 %. We like to mention that we have calculated the interlayer separation between the subsurface and central layers but have not quoted it in our tables due to numbers being very insignificant. For the optimized system in this case the rumpling of the surface layer is 0.05 Å. Similar to the case for interlayer separation, we have not quoted the rumpling in the subsurface and central layers throughout this work due to the fact that the rumpling in those respective layers is observed to be negligible. The OH distance decreases by 0.02 Å and the HOH bond angle increases by 3.9° compared to the free H_2O molecule.

For Vert1 approach of the H_2O molecule at the b2 adsorption site (fig. 1b), the adsorption energies for the NSO and SO states are 0.091 eV and -0.121 eV respectively. Similar to the previous case the initial geometry is same as the final geometry. Here the SO states are not bound. Compared to the bare interlayer separation between the surface and subsurface layers of 1.9 %, for

this adsorption configuration the interlayer separation is 2.3 %. In this case the rumpling of the surface layer is 0.04 Å. The OH distance decreases by 0.02 Å

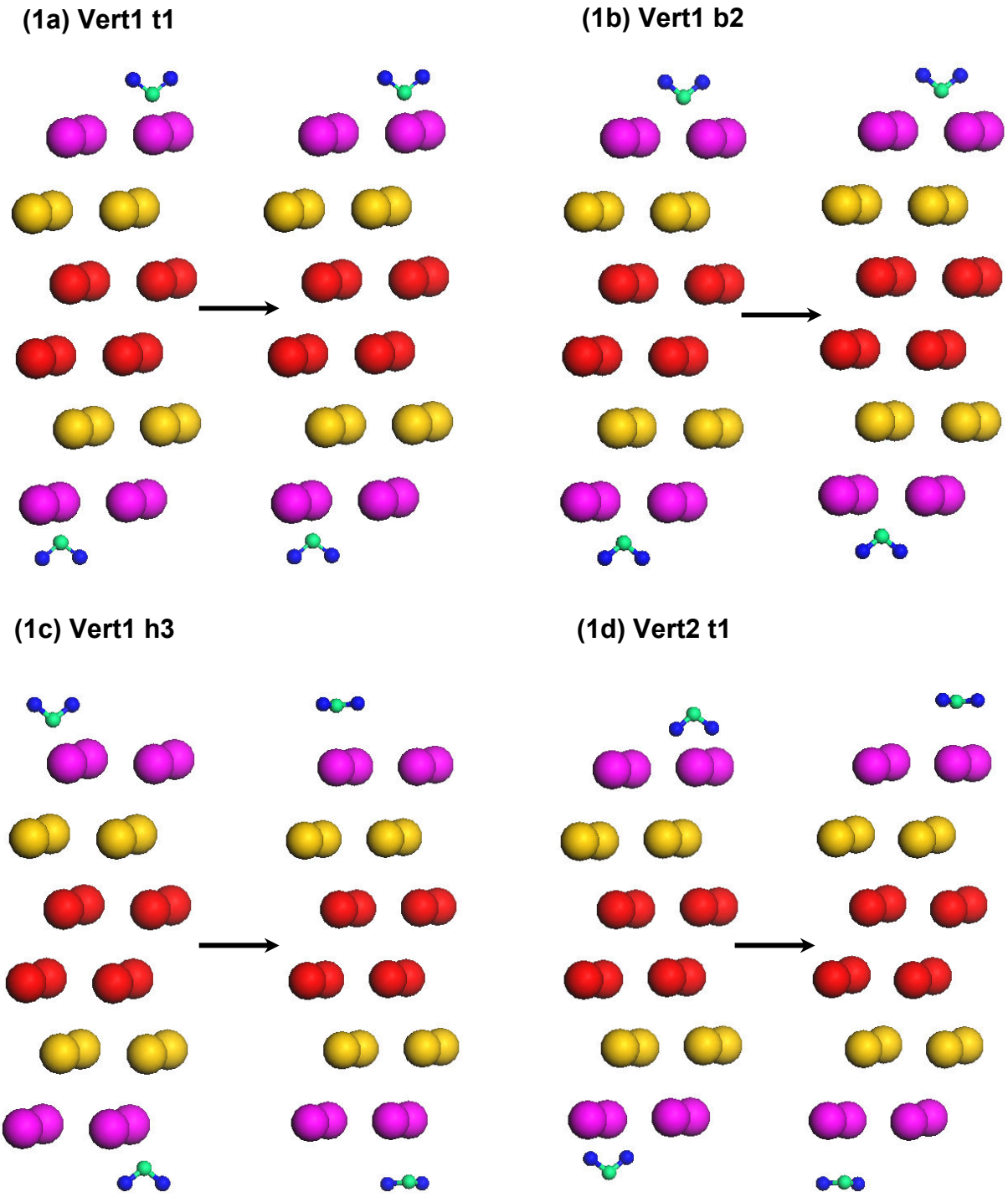

Figure 5.1 Initial and optimized molecular H_2O adsorption configurations. The initial configuration is labeled (on the left) and the arrow points to the optimized configuration. H atoms are colored blue and O atoms are colored green. Surface, subsurface, and central Am layers are colored pink, yellow, and red respectively.

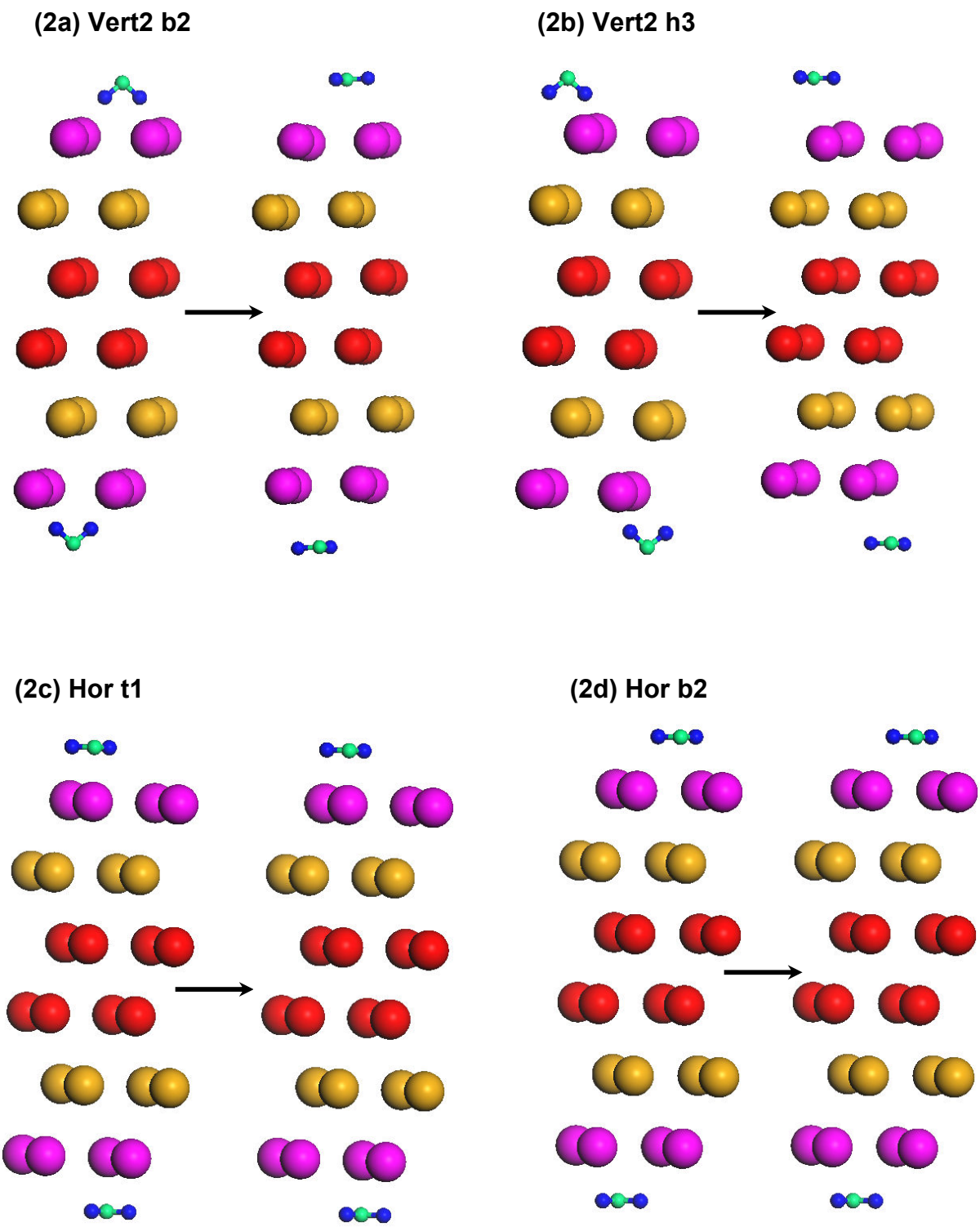

Figure 5.2 Initial and optimized molecular H_2O adsorption configurations.

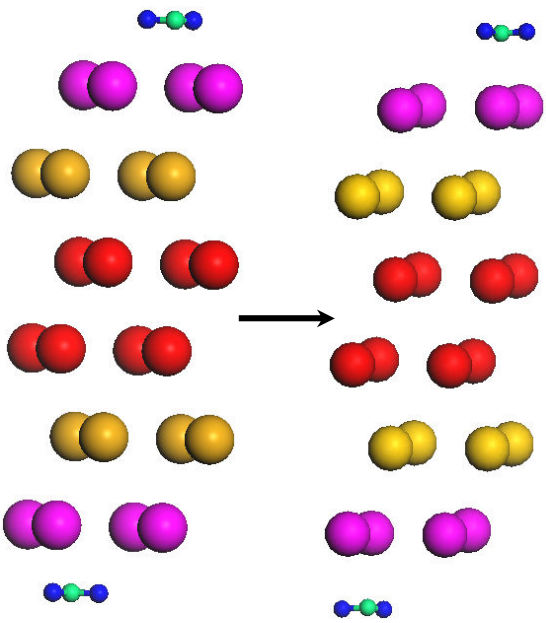

Figure 5.3 Initial and optimized molecular H_2O adsorption configurations.

and the HOH bond angle increases by 3.6˚ compared to the free H_2O molecule. For Vert1 approach of the H_2O molecule at the h3 adsorption site (fig. 1c), the adsorption energies for the NSO and SO states are 0.359 eV and 0.214 eV respectively. In this case after structural optimization, the orientation of the H_2O molecule becomes flat and it moves to the neighboring t1 site with O atom sitting close to the t1 adsorption site. Here the NSO states are strongly bound than SO states. Compared to the bare interlayer separation between the surface and subsurface layers of 1.9 %, for this adsorption configuration the interlayer separation is 1.2 %. In this case the rumpling of the surface layer is 0.10 Å. The OH molecule compresses by 0.01 Å and the HOH bond angle increases by 2.0˚ compared to the free H_2O molecule. Among all the adsorption sites for the Vert1 approach, the h3 site is found to be the most favorable and in this case the interlayer separation is the least and the rumpling of the surface layer is the most compared to the other two cases.

For Vert2 (upright orientation with the two H atom facing the adsorption site) approach (fig.1d) of the H_2O molecule at the t1 adsorption site, the adsorption energies for the NSO and SO states are 0.347 eV and 0.195 eV respectively. In this case after structural optimization, the final adsorption site t1 remains the same as the initial site but the H_2O molecule becomes flat with the O atom sitting close to t1 adsorption site. Again the NSO states are found to be more stable than the SO states. Compared to the bare interlayer separation between the surface and subsurface layers of 1.9 %, for this adsorption

configuration the interlayer separation is 1.1 %. In this case the rumpling of the surface layer is 0.08 Å. The OH distance reduces by 0.02 Å and the HOH bond angle increases by 2.1˚ compared to the free H_2O molecule. For Vert2 approach of the H_2O molecule at the b2 adsorption site (fig.1e), the adsorption energies for the NSO and SO states are 0.144 eV and 0.009 eV respectively. In this case after structural optimization, the final adsorption site b2 remains the same as the initial site but the orientation of the H_2O molecule becomes flat with the O atom sitting close to b2 adsorption site. Again the NSO states are found to be more stable than the SO states. Compared to the bare interlayer separation between the surface and subsurface layers of 1.9 %, for this adsorption configuration the interlayer separation is 2.8 %. In this case the rumpling of the surface layer is 0.22 Å showing that in this particular case the system attains stability after some considerable relaxations between the surface and subsurface layers. The OH distance reduces by 0.02 Å and the HOH bond angle increases by 0.3˚ compared to the free H_2O molecule. For Vert2 approach (fig.1f) of the H_2O molecule at the h3 adsorption site, the adsorption energies for the NSO and SO states are 0.162 eV and 0.032eV respectively. In this case after structural optimization, the final adsorption site h3 remains the same as the initial site but the orientation of the H_2O molecule becomes flat similar to the case for b2 adsorption site with the O atom sitting close to h3 adsorption site. Again the NSO states are found to be more stable than the SO states. Compared to the bare interlayer separation between the surface and

subsurface layers of 1.9 %, for this adsorption configuration the interlayer separation is 2.4 %. In this case the rumpling of the surface layer is 0.09 Å. The OH distance reduces by 0.02 Å and the HOH bond angle increases by 1.1˚ compared to the free H_2O molecule. Among all the adsorption sites for the Vert2 approach, the t1 site is found to be the most favorable and in this case the interlayer separation and rumpling of the surface layer is less compared to the other two cases.

For Hor (flat-lying (horizontal) orientation with O atom occupying the adsorption site) approach of the H_2O molecule at the t1 adsorption site (fig.1g), the adsorption energies for the NSO and SO states are 0.364 eV and 0.293 eV respectively. In this case after structural optimization, the final adsorption site t1 remains the same as the initial site with the H_2O molecule remaining flat with the O atom sitting close to t1 adsorption site. Again the NSO states are found to be more stable than the SO states. Compared to the bare interlayer separation between the surface and subsurface layers of 1.9 %, for this adsorption configuration the interlayer separation is 0.9 %. In this case the rumpling of the surface layer is 0.07 Å. The OH molecule compresses by 0.02 Å and the HOH bond angle increases by 1.9˚ compared to the free H_2O molecule. For Hor approach of the H_2O molecule at the b2 adsorption site (fig.1h), the adsorption energies for the NSO and SO states are 0.175 eV and 0.109 eV respectively. In this case after structural optimization, the final adsorption site b2 remains the same as the initial site with the H_2O molecule remaining flat with

the O atom sitting close to b2 adsorption site. Again the NSO states are found to be more stable than the SO states. Here the interlayer separation of 1.9 % is the same as that observed for the bare americium surface. In this case the rumpling of the surface layer is 0.08 Å. The OH molecule compresses by 0.01 Å and the HOH bond angle increases by 1.6˚ compared to the free H_2O molecule. For Hor approach of the H_2O molecule at the h3 adsorption site (fig.1i), the adsorption energies for the NSO and SO states are 0.366 eV and 0.232 eV respectively. In this case after structural optimization, the H_2O molecule remains flat but the preference for the adsorption site changes from h3 to t1 with the O atom sitting close to b2 adsorption site. Again the NSO states are found to be more stable than the SO states. Compared to the bare interlayer separation between the surface and subsurface layers of 1.9 %, for this adsorption configuration the interlayer separation is 1.5 %. In this case the rumpling of the surface layer is 0.15 Å. The OH molecule compresses by 0.02 Å and the HOH bond angle increases by 1.9˚ compared to the free H_2O molecule. Among all the adsorption sites for the Hor approach, the h3 site is found to be the most favorable with maximum surface layer rumpling. Also, the adsorption site t1 and h3 can be considered degenerate. For the nine cases studied for the molecular adsorption, it can be concluded that the H_2O molecule prefers the flat orientation and the transition after which the molecule sits on the t1 site is found to be the most favorable. For all the molecular adsorption cases weak physisorption is observed. For the all the approaches, the most stable

configuration is where the molecule sits on the top site, but the difference in there adsorption energies can be attributed to the fact that they are adsorbed at slightly different position with respect to the t1 site.

Moving on to the partial dissociative adsorption OH1+H2, there are four different orientations (Vert-O, Vert-H, Hor1 and Hor2) on how to place the OH1 molecule above the three adsorption sites (t1, b2 and h3) for the initial adsorption geometry. Here the hydrogen atom bonded to the oxygen atom is given as H1 and the free hydrogen atom is given as H2. Simultaneously, the H2 atom is placed at the neighboring h3 site as this was found to be the most stable site for the atomic hydrogen adsorption. Listed in table II are different parameters similar to the ones described in the previous text for table I. For Vert-O (approach vertical to the surface with O atom facing the Am surface) approach of the OH1 molecule at the t1 adsorption site (fig.2a), the adsorption energies for the NSO and SO states are 1.49 eV and 1.37 eV respectively. In this case after structural optimization, the final adsorption site t1 remains the same as the initial site for the OH1 molecule with the H2 atom sitting at the neighboring h3 site. Compared to the bare interlayer separation between the surface and subsurface layers of 1.9 %, for this adsorption configuration the interlayer separation is 1.6 %. In this case the rumpling of the surface layer is 0.09 Å. The OH molecule stretches by 0.01 Å for the chemisorbed configuration compared to the free OH molecule.

Table 5.2 Optimized Geometrical Parameters and Adsorption Energies for Partial Dissociative OH+H Adsorption. The H Atom in the OH Molecule is Labeled H1, While the Second H Atom is Labeled H2. Parameters are Defined as in Table I.

	Site	Δ_{12}	δr_1	d_{OH1}	d_{OAm}	d_{H1Am}	d_{H2Am}	E_{NSO}	E_{SO}
Free OH				0.97					
Vert-O	t1+h3	1.6	0.09	0.98	2.13		2.31	1.49	1.37
	b2+h3	1.7	0.16	0.96	2.49		2.29	2.14	2.08
	h3+h3	1.1	0.07	0.96	2.48		2.31	2.11	1.97
Vert-H	t1+h3	1.4	0.10	0.97		2.01	2.29	0.38	0.31
	b2+h3	0.9	0.18	0.96	2.37		2.25	2.04	1.97
	h3+h3	1.2	0.08	0.97		2.38	2.67	0.14	0.09
Hor1	t1+h3	1.5	0.09	0.96	2.36		2.17	1.89	1.84
	b2+h3	2.1	0.10	0.96	2.36		2.34	2.05	1.99
	h3+h3	2.2	0.19	0.96	2.44		2.27	2.23	2.14
Hor2	t1+h3	1.9	0.23	0.96	2.36		2.22	2.04	1.97
	b2+h3	1.6	0.16	0.96	2.45		2.27	2.21	2.13
	h3+h3	2.4	0.24	0.96	2.44		2.28	2.14	2.07

For Vert-O approach of the OH1 molecule at the b2 adsorption site (fig.2b), the adsorption energies for the NSO and SO states are 2.14 eV and 2.08 eV respectively. In this case after structural optimization, the OH1 molecule moves to the neighboring h3 site with the H2 atom sitting at a different neighboring h3 site. Compared to the bare interlayer separation between the surface and subsurface layers of 1.9 %, for this adsorption configuration the interlayer separation is 1.7 %. In this case the rumpling of the surface layer is 0.16 Å. The OH molecule compresses by 0.01 Å for the chemisorbed configuration compared to the free OH molecule. For Vert-O approach of the OH molecule at the h3 adsorption site (fig.2c), the adsorption energies for the NSO and SO states are 2.11 eV and 1.97 eV respectively. In this case after structural optimization, the OH1 molecule remains at the initial h3 adsorption site after optimization with the H2 atom sitting at a different neighboring h3 site. This case can be considered similar to the case of the Vert-O approach of the OH1 molecule at the b2 site as the final configuration is same as this case. The energies for both the cases are observed to be closely degenerate, with the slight difference in energy attributed to small difference in adsorption coordinates corresponding to the adsorption site. Compared to the bare interlayer separation between the surface and subsurface layers of 1.9 %, for this adsorption configuration the interlayer separation is 1.1 %. In this case the rumpling of the surface layer is 0.07 Å. The OH molecule compresses by 0.01 Å for the chemisorbed configuration compared to the free OH molecule. Among

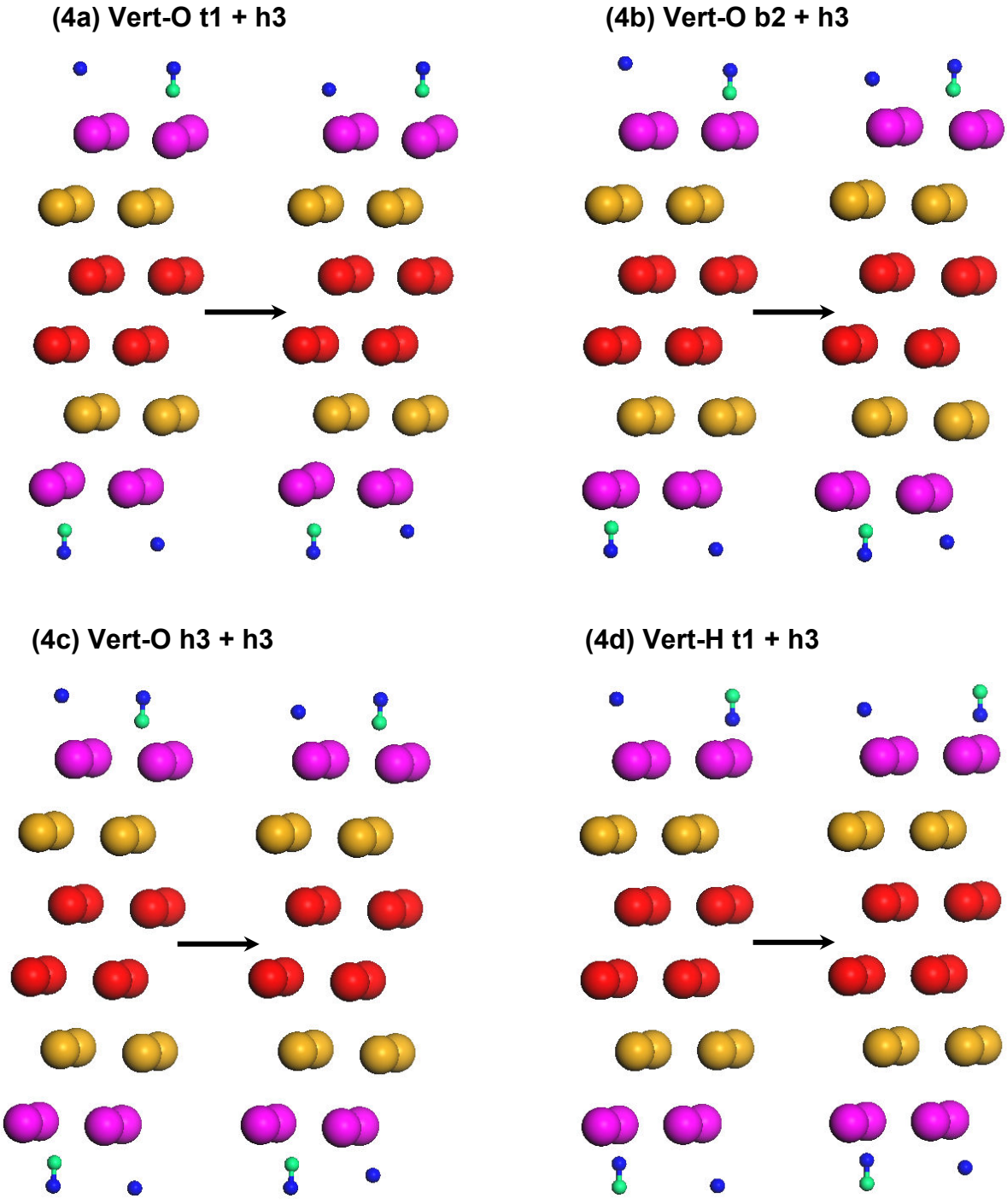

Figure 5.4 Initial and optimized partially dissociative OH+H adsorption configurations. The initial configuration is labeled (on the left) and the arrow points to the optimized configuration. H atoms are colored blue and O atoms are colored green. Surface, subsurface, and central Am layers are colored pink, yellow, and red respectively.

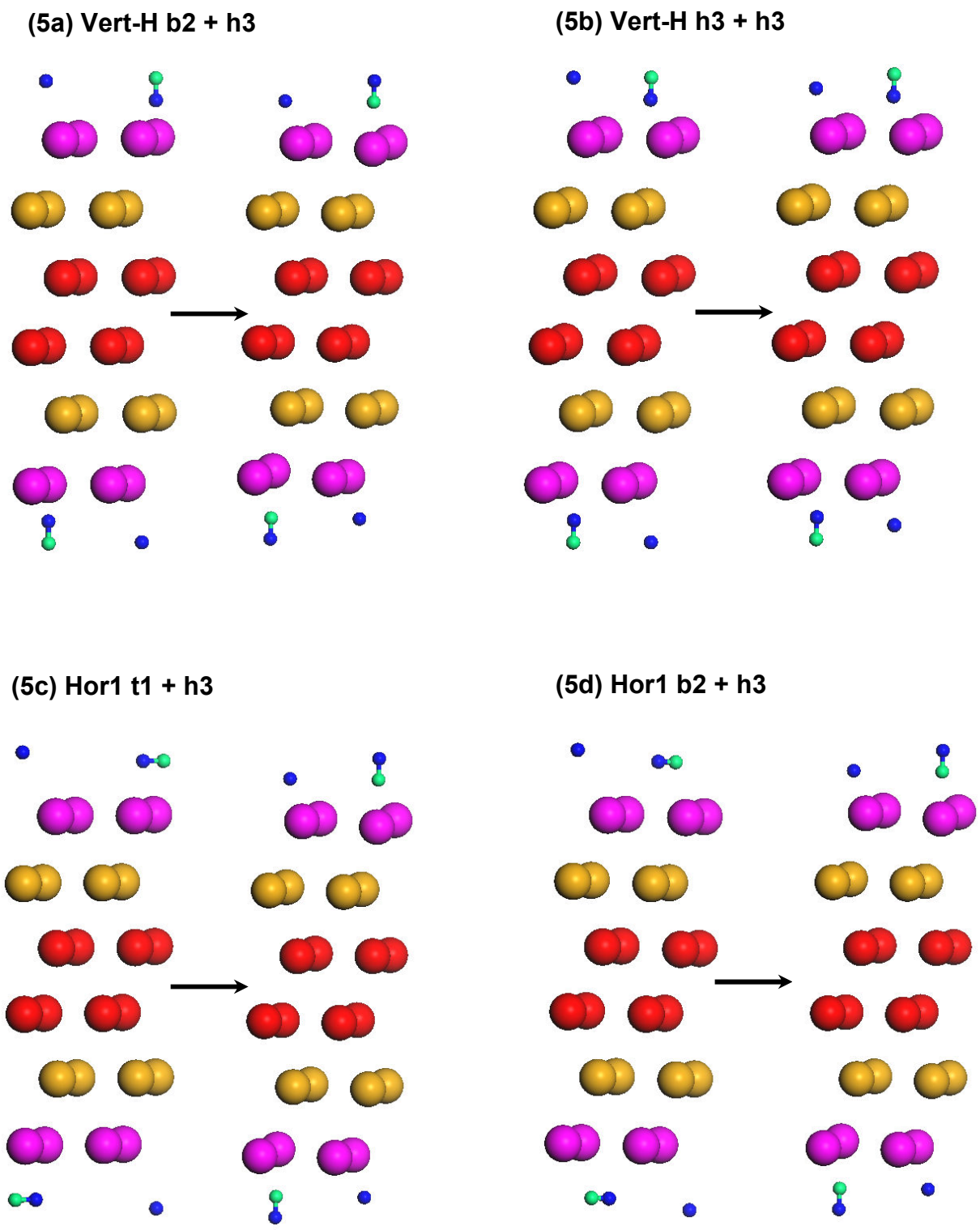

Figure 5.5 Initial and optimized partially dissociative OH+H adsorption configurations.

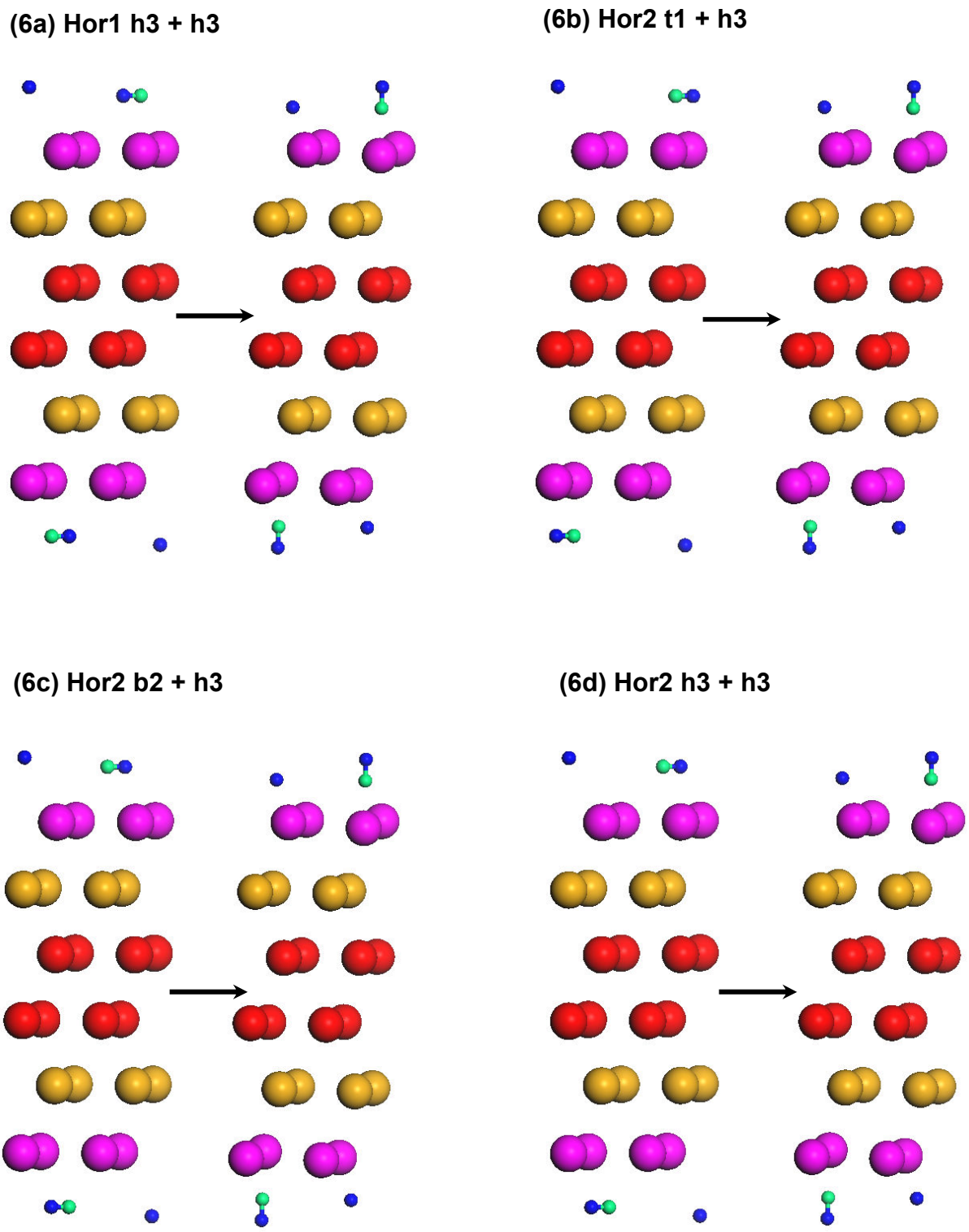

Figure 5.6 Initial and optimized partially dissociative OH+H adsorption configurations.

all the adsorption sites for the Vert-O approach of the OH molecule, the b2 site is found to be the most favorable and in this case the interlayer separation and rumpling of the surface layer is more compared to the other two cases. For the cases SO states are observed to be less stable then the NSO states.

For Vert-H (approach vertical to the surface with H atom facing the Am surface) approach of the OH1 molecule at the t1 adsorption site (fig.2d), the adsorption energies for the NSO and SO states are 0.38 eV and 0.31 eV respectively. In this case after structural optimization, the final adsorption site t1 remains the same as the initial site for the OH1 molecule with the H2 atom sitting at the neighboring h3 site. Compared to the bare interlayer separation between the surface and subsurface layers of 1.9 %, for this adsorption configuration the interlayer separation is 1.4 %. In this case the rumpling of the surface layer is 0.10 Á. The OH1 bond distance remains same as that for the free OH molecule. For Vert-H approach of the OH1 molecule at the b2 adsorption site (fig.2e), the adsorption energies for the NSO and SO states are 2.04 eV and 1.97 eV respectively. In this case after structural optimization, the final adsorption site b2 remains the same as the initial site for the OH1 molecule with the H2 atom sitting at the neighboring h3 site. But in this case the OH1 molecule flips upside down with the O atom facing surface and making it similar to the Vert-O approach. Hence the chemisorption energy range is seen to be similar to the Vert-O cases. Compared to the bare interlayer separation between the surface and subsurface layers of 1.9 %, for this adsorption

configuration the interlayer separation is 0.9 %. In this case the rumpling of the surface layer is 0.18 Å. The OH molecule compresses by 0.01 Å compared to the free OH molecule.

For Vert-H approach of the OH1 molecule at the h3 adsorption site (fig.2f), the adsorption energies for the NSO and SO states are 0.14 eV and 0.09 eV respectively. In this case after structural optimization, the final adsorption site h3 remains the same as the initial site for the OH1 molecule with the H2 atom sitting at the neighboring h3 site. Compared to the bare interlayer separation between the surface and subsurface layers of 1.9 %, for this adsorption configuration the interlayer separation is 1.2 %. In this case the rumpling of the surface layer is 0.8 Å. The OH1 bond distance remains same as that for the free OH molecule. This particular case has the least adsorption energy among all the partial dissociative adsorbed configurations. Among all the adsorption sites for the Vert-H approach of the OH molecule, the b2 site is found to be the most favorable smilar to the Vert-O approach. For all the cases SO states are observed to be less stable then the NSO states. It can be concluded that for the partial dissociative cases with vertical approaches Vert-O and Vert-H, the configurations where the H1 atom of the OH1 molecule faces the surface are found to be the least stable.

For Hor1 (approach parallel to a lattice vector) approach of the OH1 molecule the three different adsorption sites (fig.2g, 2h, 2i), the final adsorption site of the OH1 molecule is the h3 site irrespective of the where the molecule is

placed. Simultaneously the H2 atom sits at a different neighboring h3 site. The most favorable configuration is the one where the OH1 molecule was initially placed at the h3 site with the adsorption energies for the NSO and SO states being 2.23 eV and 2.14 eV. The OH1 bond distance for all the sites remain the same at 0.96 Å, compressed by 0.01 Å compared to the free OH molecule. Also the most favorable configuration has the maximum interlayer separation of 2.2 % and maximum rumpling of 0.19 Å. Even though the final adsorption configuration for all the three adsorption sites is the same, the difference in the adsorption energies is due to different positions of the OH1 molecule at the h3 site and height of the H2 atom from the h3 site.

For Hor2 (approach perpendicular to a lattice vector) approach of the OH1 molecule the three different adsorption sites (fig.2j, 2k, 2l), similar to the case for Hor1 approaches, the final adsorption site of the OH1 molecule is the h3 site irrespective of the where the molecule is placed. Simultaneously the H2 atom sits at a different neighboring h3 site. Dissimilar to the Hor1 approach, the most favorable configuration is the one where the OH1 molecule was initially placed at the b2 site with the adsorption energies for the NSO and SO states being 2.21 eV and 2.13 eV. The OH1 bond distance for all the sites remain the same at 0.96 Å, compressed by 0.01 Å compared to the free OH molecule. Also the most favorable configuration has the least interlayer separation of 1.6 % and least rumpling of 0.16 Å compared to the other two less favorable cases. Even though the final adsorption configuration for all the three adsorption sites

is the same, the difference in the adsorption energies is due to different positions of the OH1 molecule at the h3 site and vertical distance of the H2 atom from the h3 site. In general for the horizontal approaches of the OH1 molecule and H2 atom sitting at the h3 site, a common conclusion can be drawn that the OH1 molecule prefers to sit vertically at the h3 site irrespective of its initial orientation. The H2 atom prefers to sit at the h3 site. A clear picture can not be drawn regarding the interlayer separation and surface rumpling as the quantities do not have a typical trend. Among all the twelve partial dissociative OH1 + H2 cases studied, the Hor1 approach with the OH1 molecule placed initially at the h3 site is found to be the most stable. For all the cases studied, the NSO states are more stable then the SO states. The adsorption energy primarily depends on the orientation of the molecule and its adsorption position in the vicinity of the adsorption site.

Finally addressing the complete dissociation H+O+H, here the three atoms were initially placed at three different neighboring h3 adsorption sites (fig.3). The adsorption energies for this case are 3.35 eV and 3.49 eV for the NSO and SO states respectively. Similar to the molecular H_2O and partial dissociative OH+H adsorption, the NSO states are more stable then the SO states. In this case after structural optimization, the three atoms remain at there initial adsorption site. Compared to the bare interlayer separation between the surface and subsurface layers of 1.9 %, for this adsorption configuration the interlayer separation is 1.6 %. In this case the rumpling of the surface layer is

Table 5.3 Optimized Geometrical Parameters and Adsorption Energies for Complete Dissociative Adsorption H + O + H. Parameters are Defined as in Table I.

Site	Δ_{12}	δr_1	d_{OAm}	d_{H1Am}	d_{H2Am}	E_{NSO}	E_{SO}
h3+h3+h3	1.6	0.17	2.19	2.28	2.29	3.35	3.49

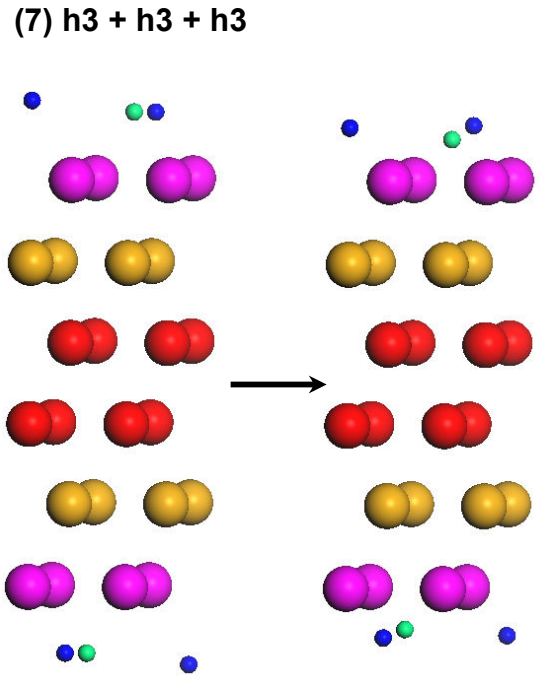

Figure 5.7 Initial and optimized fully dissociative H+O+H adsorption configuration. The initial configuration is labeled (on the left) and the arrow points to the optimized configuration. H atoms are colored blue and O atoms are colored green. Surface, subsurface, and central Am layers are colored pink, yellow, and red respectively.

0.17 Å. The distance of the three atoms are in good agreement with our previous results for atomic H and O adsorption on the same surface. [42]

The change in the work function after adsorption, ΔΦ, is listed in Table IV, V and VI for the molecular, partial dissociation and complete dissociation configurations. The adsorbate-induced work function shifts can be understood in terms of the surface dipoles arising due to the displacement of electron density from the substrate towards the adsorbates since the electronegativity of H is much larger than that of Am. The surface dipole moment μ (in Debye) and the work function shift ΔΦ (in eV) are linearly related by the Helmholtz equation $\Delta\Phi = 12\Pi\Theta\mu/A$, where A is the area in $Å^2$ per (1×1) surface unit cell and Θ is the adsorbate coverage in monolayers. The work function for the bare surface for the NSO states is Φ^{NSO} = 2.91 eV respectively. For each case of molecular adsorption ΔΦ<0; for partial dissociation ΔΦ<0 for all the cases where the O atom of the OH1 molecule faces the surface, while ΔΦ>0 for the two cases where the H atom of the OH1 molecule is facing the surface; for complete dissociation ΔΦ>0. This is a distinctive aspect for this calculation, as one expects the work function to increase upon adsorption due to charge transfer from the substrate to the adsorbate. This was the case in our previous calculations for the adsorption of atomic hydrogen, oxygen and molecular oxygen on the same americium metal slab.[42] But in the current case there is no charge transfer from the americium atoms to the H_2O molecule. To explain the decrease in work function after adsorption, we have also studied in detail the

Table 5.4 Change in work function $\Delta\Phi = \Phi^{admolecule/Am} - \Phi^{Am}$ (in eV) for both the NSOC level of theory, where Φ^{Am} is work function of the bare surface and $\Phi^{admolecule/Am}$ is the work function of the surface-with-admolecule. Φ^{Am} = 2.906 eV. Spin magnetic moments inside the muffin tin per Am atom for layer *i* S_i (in μ_B), and total (muffin-tin+interstitial) magnetic moment per Am atom S (in μ_B) for molecular H_2O adsorption.

	Site	ΔΦ	S_1	S_2	S_3	S
Bare slab			6.05	-6.02	6.14	2.46
Vert1	t1	-0.74	6.06	-6.04	6.13	2.48
	b2	-0.58	6.06	-6.04	6.14	2.48
	h3	-0.06	6.06	-6.04	6.14	2.48
Ver2	t1	-0.09	6.06	-6.04	6.14	2.48
	b2	-0.25	6.06	-6.03	6.14	2.48
	h3	-0.23	6.06	-6.03	6.14	2.48
Hor	t1	-0.08	6.06	-6.02	6.13	2.48
	b2	-0.14	6.03	-6.00	6.12	2.46
	h3	-0.11	6.06	-6.03	6.14	2.48

Table 5.5 Changes in the Work Function and Magnetic Moment for Partial Dissociative OH + O Adsorption. Parameters are Defined as in Table IV.

	Site	ΔΦ	S_1	S_2	S_3	S
Bare slab			6.05	-6.02	6.14	2.46
Vert-O	t1+h3	-0.21	6.06	-6.05	6.09	2.37
	b2+h3	-0.36	6.06	-6.05	6.08	2.39
	h3+h3	-0.33	6.06	-6.06	6.10	2.41
Vert-H	t1+h3	0.27	6.07	-6.04	6.12	2.41
	b2+h3	-0.29	6.06	-6.05	6.07	2.39
	h3+h3	0.32	6.06	-6.05	6.10	2.40
Hor1	t1+h3	-0.33	6.06	-6.04	6.08	2.38
	b2+h3	-0.37	6.07	-6.06	6.07	2.39
	h3+h3	-0.38	6.08	-6.06	6.09	2.41
Hor2	t1+h3	-0.43	6.05	-6.04	6.08	2.38
	b2+h3	-0.43	6.06	-6.04	6.09	2.41
	h3+h3	-0.34	6.06	-6.05	6.09	2.40

Table 5.6 Changes in the Work Functions and Magnetic Moments for Complete Dissociative H + O+ H Adsorption. Parameters are Defined in as Table IV.

	Site	ΔΦ	S_1	S_2	S_3	S
Bare slab			6.05	-6.02	6.14	2.46
	h3+h3+h3	0.55	6.06	-6.06	6.01	2.34

difference charge density distribution which we will discuss below. It is noteworthy that $\Delta\Phi<0$ for molecular H_2O adsorption, has also been observed in several water-metal surface interactions.[65] Changes in the work function usually arise from surface dipoles and the transfer of charge between the substrate and adsorbate. To investigate the nature of the charge transfer that occurs between the substrate and adsorbate, we computed the difference charge density $\Delta n(r)$:

$$\Delta n(\mathrm{r}) = n\ (\text{adsorbate + Am}) - n(\text{Am}) - n(\text{adsorbate}),$$

Where n(adsorbate+Am) is the total electron charge density of the Am slab-with-adsorbate, n(Am) is the total charge density of the bare Am slab, and n(adsorbate) is the total charge density of the adsorbate. In computing n(adsorbate) and n(Am), the adsorbate and Am atoms are kept fixed at exactly the same positions as they were in the physisorbed/chemisorbed systems. All charge densities reported here were computed in the plane passing through the admolecule and one or two surface Am atoms using the Xcrysden utility.[60] We have reported the difference charge density plots for the most favorable adsorption site for each of molecular, partial dissociation and complete dissociation configurations in fig 4. In fig 4a for Hor approach of H_2O molecule at the h3 site, the H_2O molecule shows strong polarization, with charge accumulation between O and H. Due to the two dimensionality of the difference charge plots, it is tough to show the all the three atoms of H_2O in one picture, but the same picture is derived for the other H atom bonded with O atom. Also there is no charge sharing between the surface Am atoms and the water

(4a) Molecular H_2Oadsorption

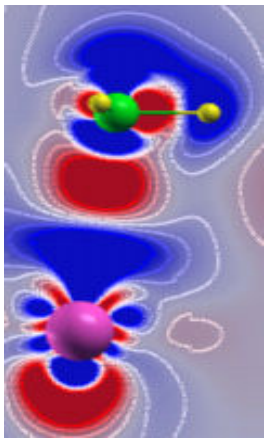

(4b) Partial OH + H dissociation

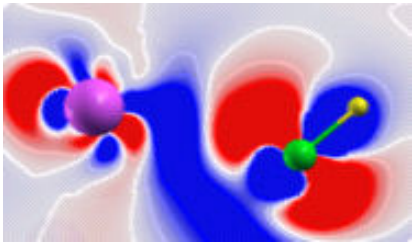

(4c) Complete H + O H+ H dissociation

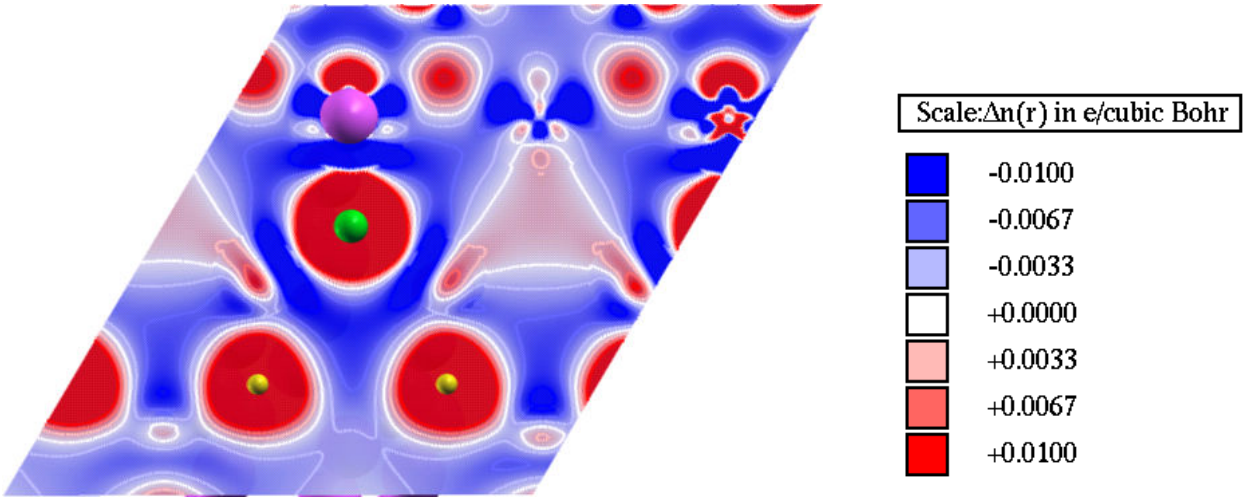

Figure 5.8 Difference charge density distributions Δn(r) for H_2O chemisorbed on the dhcp-Am(0001) surface at the most stable configurations corresponding to the molecular H2O adsorption, partial dissociative OH+H adsorption and complete dissociation H+O+H adsorption respectively. The scale used is shown at the bottom. Red (positive) denotes regions of charge accumulation and blue (negative) denotes regions of charge loss. H_2 molecule is colored blue and Am atoms are colored gold.

molecule. This in turn makes the interaction very weak which results in physisorption of H_2O molecule. In a way the H_2O molecule adheres to the surface through Van der Waals (weak intermolecular) interactions. From our previous results, after the adsorption of atomic hydrogen and oxygen we observed significant charge transfer from the surface Am atoms to the hydrogen atom which resulted in an increase in the adsorption energy and ionic bonding. But due to the fact that in the current case the adsorbate is a covalently bonded H_2O molecule, it does not require any external charge to stabilize the system and achieves a configuration which is stable on its own.

Water molecule has a non-zero dipole moment which is not the case for atomic adsorbate. The sign and magnitude of $\Delta\Phi$ is greatly affected by the net orientation preference of the molecule.[65] In Fig. 4(b) for the Hor1 approach with OH1 and H sitting on two neighboring h3 sites, again the OH molecule becomes strongly polarized. However there is some charge transfer from the substrate to the adsorbate; $\Delta\Phi<0$. Moreover for the case of Vert-H approach for the t1 adsorption site, where the OH1 molecule is vertical to the surface with the H1 atom facing the surface, $\Delta\Phi>0$. This therefore implies that charge transfer alone is not sufficient to explain the origins of the reduction in the work function. We thus characterize the origin of negative $\Delta\Phi$ to a combination of molecular polarization, charge transfer, the orientation of the molecule. For the fully dissociated cases, $\Delta\Phi$ is greater than zero, which clearly agrees with previous calculations on atomic H and O adsorption on (0001) surface of dhcp-Am. In

this case substrate to adsorbate charge transfer, which is evident from Fig. 4(c), can be used to explain the fact that $\Delta\Phi>0$. The strong ionic bonds formed as result of chemisorption corresponding to fully dissociated configurations.

In table IV, V and VI the spin magnetic moments inside the muffin tin per Am atom for layer *i* S_i (in μ_B), and total (muffin-tin+interstitial) magnetic moment per Am atom S (in μ_B) are reported for the clean and adsorbate-covered surfaces. Minor changes in the moments after adsorptions occurred on only the surface layer; no significant changes were observed on the subsurface and central layers. Also, the spin moments reported correspond to the NSO calculations. The initial anti-ferromagnetic order was preserved in all cases after adsorption. The spin moment for bare slab was S=2.46 μ_B/Am. The average change in the spin moment upon adsorption, ΔS is approximately zero for molecular adsorption, which again asserts the fact that the interaction between the molecule and the surface is very weak. For the partially dissociated configurations, ΔS for the surface layer ranges between -0.7 to -0.4μ_B/Am, indicating some interaction between the adsorbates and the surface layer. In particular, the fully dissociated adsorbates leads to the largest quench in the moments with $\Delta S = -0.13$ for the surface layer implying that a fair amount of charge is transferred from Am to the adsorbates as can clearly be seen from the difference charge density plots for complete dissociation in Fig. 4(c)

To further probe the substrate-adsorbate interaction, we also computed the local density of states (LDOS), obtained by decomposing the total density of

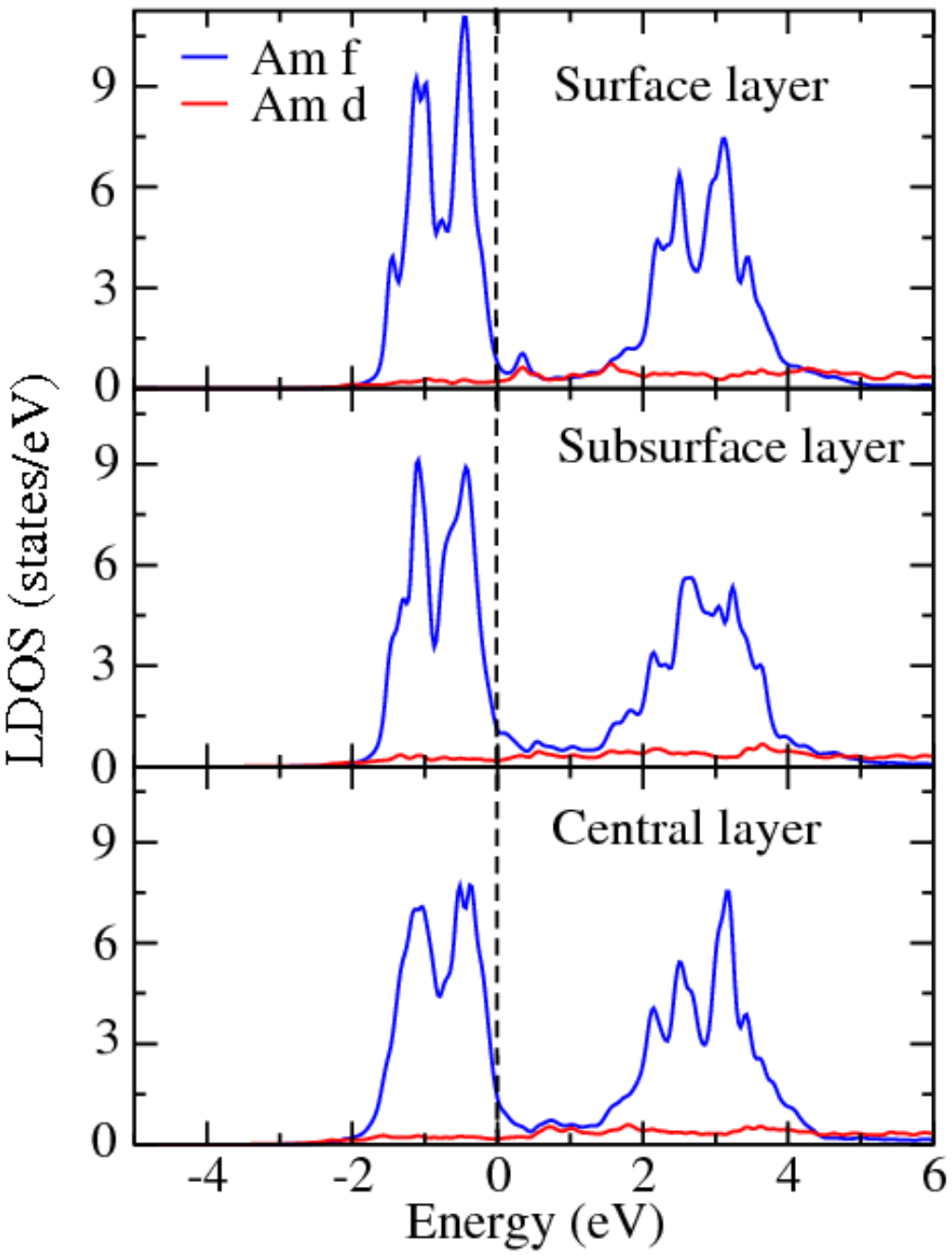

Figure 5.9 6*d* and 5*f* LDOS curves inside the muffin-tins for each layer of the bare dhcp-Am(0001) slab. Vertical line through E=0 is the Fermi level.

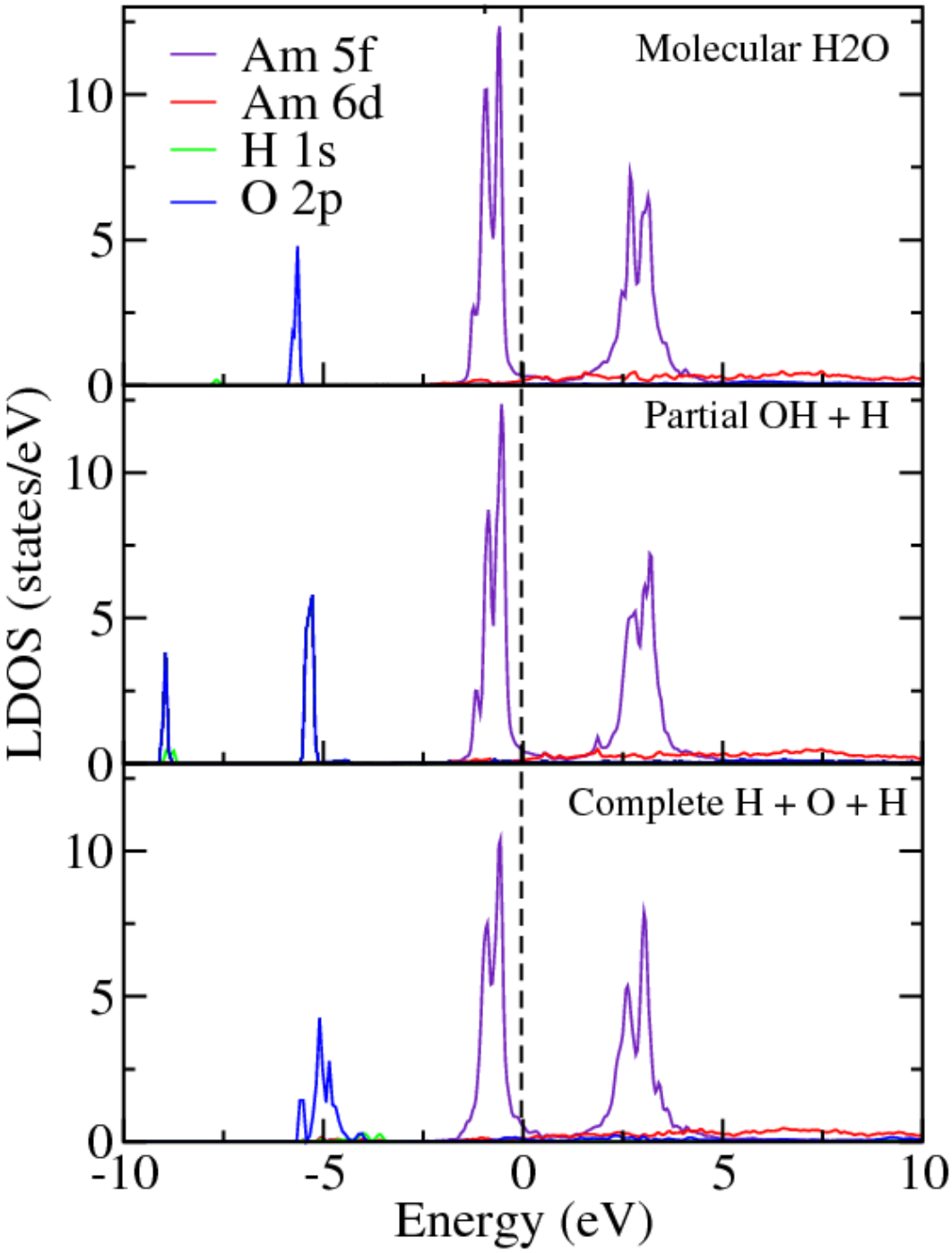

Figure 5.10 6*d* and 5*f* LDOS curves inside the muffin-tins for the Am atoms on the surface layer, 1*s* LDOS curves for H atom and 2*p* LDOS for the most favorable cases for molecular H2O adsorption, partial dissociative OH+H adsorption and complete dissociative H+O+H. Vertical line through E=0 is the Fermi level.

the single particle Kohn-Sham eigenstates into contributions from each angular momentum channel *l* of the constituent atoms inside the muffin tin spheres. Here, we have reported the LDOS for only the NSO states, the LDOS for SO states yielding a similar qualitative description. In fig. 5, the Gaussian-broadened (with a width of 0.05 eV) *f* and *d* LDOS curves for each of the layers of the bare dhcp Am (0001) metal slab are shown. Clearly, we see well-defined peaks in the 5*f* electron LDOS in the vicinity of the Fermi level, which have also been observed for bulk dhcp-Am(0001), and tends to indicate *some* 5*f* electron localization. However, this statement should be viewed with caution because of the nature of the underlying theory, namely density functional theory and all *5f* states are treated as band states. The occupied 5*f* electron states below the Fermi level also support this conclusion. In view of our previous statement about the participation of the *5f* electrons in chemical bonding, we believe that it is possible that some *5f* electrons are localized and some are not. This question needs to be pursued in the future. However, the $5f_{5/2}$ peak centered on a binding energy of 1 eV below the Fermi level instead of the 2.8 eV observed in X-ray and ultraviolet photoemission spectra experiments .[20,27] In fig. 6, we show the LDOS plots for the H_2O molecule and the surface Am atoms after adsorption for the most favorable case for each of the three adsorption cases, namely molecular H_2O, partial dissociative OH+H, and complete dissociative H+O+H adsorptions. The LDOS for the all other adsorption sites among different approaches show the same qualitative and quantitative pictures and

hence are not shown here. As there are four nonequivalent sites on the surface, we depict the LDOS for only the Am atom(s) which are direct nearest neighbors to the H_2O molecule in order to assess the changes in DOS upon adsorption. In the top panel of fig. 7, the LDOS for the most favorable molecular H_2O adsorption at h3 site with Hor approach can be seen. Overall, very little adsorbate-Am interaction can be observed as predicted earlier by the low adsorption energies. The Am 5*f* bands retain their shape and character when compared to the bare slab. In the center panel of fig. 7, the LDOS for the most favorable partial dissociative OH+H adsorption is shown. Am 6*d* states contribute fairly to the H 1*s* and O 2*p* states, while the Am 5*f* states remain effectively unchanged. It is therefore reasonable to say that adsorbate-Am bonding is primarily governed by H(1*s*)-O(2*p*)-Am(6*d*) hybridizations. In the bottom panel of fig. 7, the LDOS for the complete dissociative H+O+H adsorption is shown. Here, noteworthy H(1*s*)-O(2*p*)-Am(6*d*) hybridizations can be observed at around E = -5 eV. However, there is a *slight* reduction in the Am-5*f* DOS at around E = -1.2 eV indicating signatures of *slight* delocalization of *some* 5*f* electrons, which is supported by the quench in the magnetic moments and the significant charge transfer which is clearly visible in the difference charge density plots in Fig. 4(c). The overlap of O 2*p* bands with the Am 5*f* bands decreases and O 2*p* bands are pushed to lower energies which is reflected in the strong binding energy for this particular configuration. Finally,

the sharp and peaky nature of the 5*f* bands are retained in general after chemisorption as no significant broadening of the bands is observed.

In summary, we have used the generalized gradient approximation to density functional theory with the full potential LAPW+lo method to study adsorption of water in its molecular, partial, and completely dissociated configurations on the (0001) surface of dhcp Am at two theoretical states; one with no spin-orbit coupling (NSO) and the other with spin-orbit coupling (SO). Weak physisorptions were observed for all molecular cases studied, whereas partial and completely dissociated configurations chemisorbed. Complete dissociation is most stable, followed by partial dissociation, then molecular adsorption. The SO states were found to be less stable then NSO states for all the molecular and partial dissociation cases considered, while for complete dissociation it was the exact opposite. Work functions decreased in all cases compared to the clean Am surface for the molecular adsorption and majority of the partial dissociation cases. For the complete dissociation configuration work function increased after chemisorption owing to significant substrate to adsorbate charge transfer. Upon adsorption, the net spin magnetic moment of the chemisorbed system decreased slightly in each case compared to the bare surface. Difference charge density distributions clearly show that the interaction between the surface Am atoms and the water molecule for all molecular configurations is governed by weak Van der Waals interactions and the water molecule becomes polarized. A study of the local density of states showed that

adsorbate-Am bonding is primarily governed by H(1*s*)-O(2*p*)-Am(6*d*) hybridizations. Overall, the localized behavior of Am 5*f* below the Fermi Level is primarily retained after adsorption.

CHAPTER 6

CONCLUSIONS

In summary, we have used the generalized gradient approximation to density functional theory with the full potential LAPW+lo method to study atomic hydrogen and oxygen, molecular hydrogen and oxygen and water in its molecular, partial, and completely dissociated configurations on the (0001) surface of dhcp Am at two theoretical states; one with no spin-orbit coupling (NSO) and the other with spin-orbit coupling (SO). Starting with the atomic adsorptions, for H adsorption, the hollow hcp site was the most preferred site, while the bridge adsorption was the most preferred site in O adsorption. The inclusion of spin-orbit coupling lowers the chemisorption energies in all cases considered. Work functions increased in all cases compared to the clean Am surface, with the largest shift corresponding to the least coordinated top site and lowest shifts corresponding to the maximally coordinated hollow hcp sites. Upon adsorption, the net spin magnetic moment of the chemisorbed system decreases in each case compared to the bare surface. Difference charge density distributions clearly show that bonds between the surface Am atoms and the adatoms at each site is largely ionic in character. A study of the local density of states for O showed Am (6*d*)-Am (5*f*)-adatom(2*p*) hybridizations at the top site electrons upon chemisorption, while at the bridge and hollow hcp

sites the interactions are dominated by Am(6*d*)- adatom(2*p*). In the general, the 5*f* electron localization behavior of the Am atoms is primarily retained after chemisorption.

Moving on to the molecular adsorptions, for hydrogen molecule, weak molecular adsorptions were observed for all the cases studied. For H_2 adsorption, the one-fold t1 site with Hor2 approach was found to be the most favorable. The inclusion of spin-orbit coupling did not lower the adsorption energies for all the cases. Work functions decreased in all cases compared to the clean Am surface. Upon adsorption, the net spin magnetic moment of the chemisorbed system decreased slightly in each case compared to the bare surface. The partial charge analyses illustrate that none of the Am 5*f* electrons participate in chemical bonding. The hydrogen molecule tends to stay far away from the americium surface giving rise to physisorption. Difference charge density distributions clearly show that the interaction between the surface Am atoms and the hydrogen molecule at each site is governed by weak Van der Waals interactions and the hydrogen molecule becomes polarized. A study of the local density of states showed no Am (6*d*)-Am (5*f*)-H(1*s*) hybridizations after adsorption. Overall, the localized behavior of Am 5*f* below the Fermi Level is primarily retained after adsorption. Reaction barrier calculations for the dissociation of hydrogen molecule at the t1 adsorption site for the Hor2 approach show the presence of an energy barrier, indicating that activation

energy is required to dissociate the hydrogen molecule upon adsorption on (0001) surface of dhcp-Am.

For oxygen molecule adsorption, the results at the two levels of theory do not vary from each other significantly. Dissociative adsorption of oxygen molecule is favored over molecular adsorption. For O_2 adsorption, the one-fold t1 site with Hor2 approach was found to be the most stable where upon adsorption of the O_2 molecule dissociated and two O atoms sit on two different three-fold h3 sites. The inclusion of spin-orbit coupling lowers the chemisorption energies for all the cases considered. Work functions increased in all cases compared to the clean Am surface, with the lowest shift corresponding to the least coordinated t1 site and largest shifts corresponding to the maximally coordinated hollow h3 site for the Vert and Hor2 approaches, while for Hor1 approach, this was not the case. Upon adsorption, the net spin magnetic moment of the chemisorbed system decreases in each case compared to the bare surface. The partial charge analyses illustrate that *some* of the Am 5*f* electrons participate in chemical bonding. Difference charge density distributions clearly show that bonds between the surface Am atoms and the oxygen molecule at each site is largely ionic in character. A study of the local density of states showed Am (6*d*)-Am (5*f*)-O(2*p*) hybridizations after chemisorption. Overall, the Am 5*f* DOS below the Fermi Level become slightly delocalized after chemisorption.

Finally for water adsorption, weak physisorptions were observed for all molecular cases studied, whereas partial and completely dissociated configurations chemisorbed. Complete dissociation is most stable, followed by partial dissociation, then molecular adsorption. The SO states were found to be less stable then NSO states for all the molecular and partial dissociation cases considered, while for complete dissociation it was the exact opposite. Work functions decreased in all cases compared to the clean Am surface for the molecular adsorption and majority of the partial dissociation cases. For the complete dissociation configuration work function increased after chemisorption owing to significant substrate to adsorbate charge transfer. Upon adsorption, the net spin magnetic moment of the chemisorbed system decreased slightly in each case compared to the bare surface. Difference charge density distributions clearly show that the interaction between the surface Am atoms and the water molecule for all molecular configurations is governed by weak Van der Waals interactions and the water molecule becomes polarized. A study of the local density of states showed that adsorbate-Am bonding is primarily governed by H(1*s*)-O(2*p*)-Am(6*d*) hybridizations. Overall, the localized behavior of Am 5*f* below the Fermi Level is primarily retained after adsorption.

APPENDIX A

FRACTIONAL INPUT COORDINATES FOR BARE AMERICIUM, ATOMIC HYDROGEN AND OXYGEN, MOLECULAR HYDROGEN AND OXYGEN, AND WATER ADSORBED AMERICIUM SURFACES

H atom adsorbed on dhcp-Am surface at the t1 site.

Am -1: X=0.66666660 Y=0.33333333 Z=0.54718979
-1: X=0.33333330 Y=0.66666666 Z=0.45281021
Am -2: X=0.66666666 Y=0.83333333 Z=0.54718979
-2: X=0.33333333 Y=0.16666666 Z=0.45281021
Am -3: X=0.16666666 Y=0.83333333 Z=0.54718979
-3: X=0.83333333 Y=0.16666666 Z=0.45281021
Am -4: X=0.16666666 Y=0.33333333 Z=0.54718979
-4: X=0.83333333 Y=0.66666666 Z=0.45281021
Am -5: X=0.83333333 Y=0.16666666 Z=0.64156938
-5: X=0.16666666 Y=0.83333333 Z=0.35843062
Am -6: X=0.83333333 Y=0.66666666 Z=0.64156938
-6: X=0.16666666 Y=0.33333333 Z=0.35843062
Am -7: X=0.33333333 Y=0.66666666 Z=0.64156938
-7: X=0.66666666 Y=0.33333333 Z=0.35843062
Am -8: X=0.33333333 Y=0.16666666 Z=0.64156938
-8: X=0.66666666 Y=0.83333333 Z=0.35843062
Am -9: X=0.66666666 Y=0.33333333 Z=0.73783655
-9: X=0.33333333 Y=0.66666666 Z=0.26216345
Am -10: X=0.66666666 Y=0.83333333 Z=0.73783655
-10: X=0.33333333 Y=0.16666666 Z=0.26216345
Am -11: X=0.16666666 Y=0.83333333 Z=0.73783655
-11: X=0.83333333 Y=0.16666666 Z=0.26216345
Am -12: X=0.16666666 Y=0.33333333 Z=0.73783655
-12: X=0.83333333 Y=0.66666666 Z=0.26216345
H -13: X=0.66666666 Y=0.83333333 Z=0.80842619
-13: X=0.33333334 Y=0.16666667 Z=0.19157381

H atom adsorbed on dhcp-Am surface at the b2 site.

Am -1: X=0.66666660 Y=0.33333333 Z=0.54718979
-1: X=0.33333330 Y=0.66666666 Z=0.45281021
Am -2: X=0.66666666 Y=0.83333333 Z=0.54718979
-2: X=0.33333333 Y=0.16666666 Z=0.45281021
Am -3: X=0.16666666 Y=0.83333333 Z=0.54718979
-3: X=0.83333333 Y=0.16666666 Z=0.45281021
Am -4: X=0.16666666 Y=0.33333333 Z=0.54718979
-4: X=0.83333333 Y=0.66666666 Z=0.45281021
Am -5: X=0.83333333 Y=0.16666666 Z=0.64156938
-5: X=0.16666666 Y=0.83333333 Z=0.35843062
Am -6: X=0.83333333 Y=0.66666666 Z=0.64156938
-6: X=0.16666666 Y=0.33333333 Z=0.35843062
Am -7: X=0.33333333 Y=0.66666666 Z=0.64156938
-7: X=0.66666666 Y=0.33333333 Z=0.35843062
Am -8: X=0.33333333 Y=0.16666666 Z=0.64156938
-8: X=0.66666666 Y=0.83333333 Z=0.35843062
Am -9: X=0.66666666 Y=0.33333333 Z=0.73783655
-9: X=0.33333333 Y=0.66666666 Z=0.26216345
Am -10: X=0.66666666 Y=0.83333333 Z=0.73783655
-10: X=0.33333333 Y=0.16666666 Z=0.26216345
Am -11: X=0.16666666 Y=0.83333333 Z=0.73783655
-11: X=0.83333333 Y=0.16666666 Z=0.26216345
Am -12: X=0.16666666 Y=0.33333333 Z=0.73783655
-12: X=0.83333333 Y=0.66666666 Z=0.26216345
H -13: X=0.16666667 Y=0.58333333 Z=0.78712608
-13: X=0.83333333 Y=0.41666667 Z=0.21287392

H atom adsorbed on dhcp-Am surface at the h3 site.

Am -1: X=0.66666660 Y=0.33333333 Z=0.54718979
-1: X=0.33333330 Y=0.66666666 Z=0.45281021
Am -2: X=0.66666666 Y=0.83333333 Z=0.54718979
-2: X=0.33333333 Y=0.16666666 Z=0.45281021
Am -3: X=0.16666666 Y=0.83333333 Z=0.54718979
-3: X=0.83333333 Y=0.16666666 Z=0.45281021
Am -4: X=0.16666666 Y=0.33333333 Z=0.54718979
-4: X=0.83333333 Y=0.66666666 Z=0.45281021
Am -5: X=0.83333333 Y=0.16666666 Z=0.64156938
-5: X=0.16666666 Y=0.83333333 Z=0.35843062
Am -6: X=0.83333333 Y=0.66666666 Z=0.64156938
-6: X=0.16666666 Y=0.33333333 Z=0.35843062
Am -7: X=0.33333333 Y=0.66666666 Z=0.64156938
-7: X=0.66666666 Y=0.33333333 Z=0.35843062
Am -8: X=0.33333333 Y=0.16666666 Z=0.64156938
-8: X=0.66666666 Y=0.83333333 Z=0.35843062
Am -9: X=0.66666666 Y=0.33333333 Z=0.73783655
-9: X=0.33333333 Y=0.66666666 Z=0.26216345
Am -10: X=0.66666666 Y=0.83333333 Z=0.73783655
-10: X=0.33333333 Y=0.16666666 Z=0.26216345
Am -11: X=0.16666666 Y=0.83333333 Z=0.73783655
-11: X=0.83333333 Y=0.16666666 Z=0.26216345
Am -12: X=0.16666666 Y=0.33333333 Z=0.73783655
-12: X=0.83333333 Y=0.66666666 Z=0.26216345
H -13: X=0.33333333 Y=0.16666666 Z=0.77656404
-13: X=0.66666666 Y=0.83333333 Z=0.22343596

O atom adsorbed on dhcp-Am surface at the t1 site.

Am -1: X=0.66666660 Y=0.33333333 Z=0.54718979
-1: X=0.33333330 Y=0.66666666 Z=0.45281021
Am -2: X=0.66666666 Y=0.83333333 Z=0.54718979
-2: X=0.33333333 Y=0.16666666 Z=0.45281021
Am -3: X=0.16666666 Y=0.83333333 Z=0.54718979
-3: X=0.83333333 Y=0.16666666 Z=0.45281021
Am -4: X=0.16666666 Y=0.33333333 Z=0.54718979
-4: X=0.83333333 Y=0.66666666 Z=0.45281021
Am -5: X=0.83333333 Y=0.16666666 Z=0.64156938
-5: X=0.16666666 Y=0.83333333 Z=0.35843062
Am -6: X=0.83333333 Y=0.66666666 Z=0.64156938
-6: X=0.16666666 Y=0.33333333 Z=0.35843062
Am -7: X=0.33333333 Y=0.66666666 Z=0.64156938
-7: X=0.66666666 Y=0.33333333 Z=0.35843062
Am -8: X=0.33333333 Y=0.16666666 Z=0.64156938
-8: X=0.66666666 Y=0.83333333 Z=0.35843062
Am -9: X=0.66666666 Y=0.33333333 Z=0.73783655
-9: X=0.33333333 Y=0.66666666 Z=0.26216345
Am -10: X=0.66666666 Y=0.83333333 Z=0.73783655
-10: X=0.33333333 Y=0.16666666 Z=0.26216345
Am -11: X=0.16666666 Y=0.83333333 Z=0.73783655
-11: X=0.83333333 Y=0.16666666 Z=0.26216345
Am -12: X=0.16666666 Y=0.33333333 Z=0.73783655
-12: X=0.83333333 Y=0.66666666 Z=0.26216345
O -13: X=0.66666666 Y=0.83333333 Z=0.80314517
-13: X=0.33333334 Y=0.16666667 Z=0.19685483

O atom adsorbed on dhcp-Am surface at the b2 site.

Am -1: X=0.66666660 Y=0.33333333 Z=0.54718979
-1: X=0.33333330 Y=0.66666666 Z=0.45281021
Am -2: X=0.66666666 Y=0.83333333 Z=0.54718979
-2: X=0.33333333 Y=0.16666666 Z=0.45281021
Am -3: X=0.16666666 Y=0.83333333 Z=0.54718979
-3: X=0.83333333 Y=0.16666666 Z=0.45281021
Am -4: X=0.16666666 Y=0.33333333 Z=0.54718979
-4: X=0.83333333 Y=0.66666666 Z=0.45281021
Am -5: X=0.83333333 Y=0.16666666 Z=0.64156938
-5: X=0.16666666 Y=0.83333333 Z=0.35843062
Am -6: X=0.83333333 Y=0.66666666 Z=0.64156938
-6: X=0.16666666 Y=0.33333333 Z=0.35843062
Am -7: X=0.33333333 Y=0.66666666 Z=0.64156938
-7: X=0.66666666 Y=0.33333333 Z=0.35843062
Am -8: X=0.33333333 Y=0.16666666 Z=0.64156938
-8: X=0.66666666 Y=0.83333333 Z=0.35843062
Am -9: X=0.66666666 Y=0.33333333 Z=0.73783655
-9: X=0.33333333 Y=0.66666666 Z=0.26216345
Am -10: X=0.66666666 Y=0.83333333 Z=0.73783655
-10: X=0.33333333 Y=0.16666666 Z=0.26216345
Am -11: X=0.16666666 Y=0.83333333 Z=0.73783655
-11: X=0.83333333 Y=0.16666666 Z=0.26216345
Am -12: X=0.16666666 Y=0.33333333 Z=0.73783655
-12: X=0.83333333 Y=0.66666666 Z=0.26216345
O -13: X=0.16666667 Y=0.58333333 Z=0.77832437
-13: X=0.83333333 Y=0.41666667 Z=0.22167563

O atom adsorbed on dhcp-Am surface at the h3 site.

Am -1: X=0.66666660 Y=0.33333333 Z=0.54718979
-1: X=0.33333330 Y=0.66666666 Z=0.45281021
Am -2: X=0.66666666 Y=0.83333333 Z=0.54718979
-2: X=0.33333333 Y=0.16666666 Z=0.45281021
Am -3: X=0.16666666 Y=0.83333333 Z=0.54718979
-3: X=0.83333333 Y=0.16666666 Z=0.45281021
Am -4: X=0.16666666 Y=0.33333333 Z=0.54718979
-4: X=0.83333333 Y=0.66666666 Z=0.45281021
Am -5: X=0.83333333 Y=0.16666666 Z=0.64156938
-5: X=0.16666666 Y=0.83333333 Z=0.35843062
Am -6: X=0.83333333 Y=0.66666666 Z=0.64156938
-6: X=0.16666666 Y=0.33333333 Z=0.35843062
Am -7: X=0.33333333 Y=0.66666666 Z=0.64156938
-7: X=0.66666666 Y=0.33333333 Z=0.35843062
Am -8: X=0.33333333 Y=0.16666666 Z=0.64156938
-8: X=0.66666666 Y=0.83333333 Z=0.35843062
Am -9: X=0.66666666 Y=0.33333333 Z=0.73783655
-9: X=0.33333333 Y=0.66666666 Z=0.26216345
Am -10: X=0.66666666 Y=0.83333333 Z=0.73783655
-10: X=0.33333333 Y=0.16666666 Z=0.26216345
Am -11: X=0.16666666 Y=0.83333333 Z=0.73783655
-11: X=0.83333333 Y=0.16666666 Z=0.26216345
Am -12: X=0.16666666 Y=0.33333333 Z=0.73783655
-12: X=0.83333333 Y=0.66666666 Z=0.26216345
O -13: X=0.33333333 Y=0.16666666 Z=0.76705820
-13: X=0.66666666 Y=0.83333333 Z=0.23294180

H_2 molecule with a Vert approach adsorbed on dhcp-Am surface at the t1 site.

Am -1: X=0.66666660 Y=0.33333333 Z=0.54718979
-1: X=0.33333330 Y=0.66666666 Z=0.45281021
Am -2: X=0.66666666 Y=0.83333333 Z=0.54718979
-2: X=0.33333333 Y=0.16666666 Z=0.45281021
Am -3: X=0.16666666 Y=0.83333333 Z=0.54718979
-3: X=0.83333333 Y=0.16666666 Z=0.45281021
Am -4: X=0.16666666 Y=0.33333333 Z=0.54718979
-4: X=0.83333333 Y=0.66666666 Z=0.45281021
Am -5: X=0.83333333 Y=0.16666666 Z=0.64156938
-5: X=0.16666666 Y=0.83333333 Z=0.35843062
Am -6: X=0.83333333 Y=0.66666666 Z=0.64156938
-6: X=0.16666666 Y=0.33333333 Z=0.35843062
Am -7: X=0.33333333 Y=0.66666666 Z=0.64156938
-7: X=0.66666666 Y=0.33333333 Z=0.35843062
Am -8: X=0.33333333 Y=0.16666666 Z=0.64156938
-8: X=0.66666666 Y=0.83333333 Z=0.35843062
Am -9: X=0.66666666 Y=0.33333333 Z=0.73783655
-9: X=0.33333333 Y=0.66666666 Z=0.26216345
Am -10: X=0.66666666 Y=0.83333333 Z=0.73783655
-10: X=0.33333333 Y=0.16666666 Z=0.26216345
Am -11: X=0.16666666 Y=0.83333333 Z=0.73783655
-11: X=0.83333333 Y=0.16666666 Z=0.26216345
Am -12: X=0.16666666 Y=0.33333333 Z=0.73783655
-12: X=0.83333333 Y=0.66666666 Z=0.26216345
H -13: X=0.66666670 Y=0.83333330 Z=0.84345696
-13: X=0.33333330 Y=0.16666670 Z=0.15654304
H -14: X=0.66666670 Y=0.83333330 Z=0.86966729
-14: X=0.33333330 Y=0.16666670 Z=0.13033271

H_2 molecule with a Hor1 approach adsorbed on dhcp-Am surface at the b2 site.

Am -1: X=0.66666660 Y=0.33333333 Z=0.54718979
-1: X=0.33333330 Y=0.66666666 Z=0.45281021
Am -2: X=0.66666666 Y=0.83333333 Z=0.54718979
-2: X=0.33333333 Y=0.16666666 Z=0.45281021
Am -3: X=0.16666666 Y=0.83333333 Z=0.54718979
-3: X=0.83333333 Y=0.16666666 Z=0.45281021
Am -4: X=0.16666666 Y=0.33333333 Z=0.54718979
-4: X=0.83333333 Y=0.66666666 Z=0.45281021
Am -5: X=0.83333333 Y=0.16666666 Z=0.64156938
-5: X=0.16666666 Y=0.83333333 Z=0.35843062
Am -6: X=0.83333333 Y=0.66666666 Z=0.64156938
-6: X=0.16666666 Y=0.33333333 Z=0.35843062
Am -7: X=0.33333333 Y=0.66666666 Z=0.64156938
-7: X=0.66666666 Y=0.33333333 Z=0.35843062
Am -8: X=0.33333333 Y=0.16666666 Z=0.64156938
-8: X=0.66666666 Y=0.83333333 Z=0.35843062
Am -9: X=0.66666666 Y=0.33333333 Z=0.73783655
-9: X=0.33333333 Y=0.66666666 Z=0.26216345
Am -10: X=0.66666666 Y=0.83333333 Z=0.73783655
-10: X=0.33333333 Y=0.16666666 Z=0.26216345
Am -11: X=0.16666666 Y=0.83333333 Z=0.73783655
-11: X=0.83333333 Y=0.16666666 Z=0.26216345
Am -12: X=0.16666666 Y=0.33333333 Z=0.73783655
-12: X=0.83333333 Y=0.66666666 Z=0.26216345
H -13: X=0.16666667 Y=0.63887570 Z=0.84345696
-13: X=0.83333333 Y=0.36112430 Z=0.15654304
H -14: X=0.16666667 Y=0.52779096 Z=0.84345696
-14: X=0.83333333 Y=0.47220904 Z=0.15654304

H_2 molecule with a Hor2 approach adsorbed on dhcp-Am surface at the h3 site.

Am -1: X=0.66666660 Y=0.33333333 Z=0.54718979
-1: X=0.33333330 Y=0.66666666 Z=0.45281021
Am -2: X=0.66666666 Y=0.83333333 Z=0.54718979
-2: X=0.33333333 Y=0.16666666 Z=0.45281021
Am -3: X=0.16666666 Y=0.83333333 Z=0.54718979
-3: X=0.83333333 Y=0.16666666 Z=0.45281021
Am -4: X=0.16666666 Y=0.33333333 Z=0.54718979
-4: X=0.83333333 Y=0.66666666 Z=0.45281021
Am -5: X=0.83333333 Y=0.16666666 Z=0.64156938
-5: X=0.16666666 Y=0.83333333 Z=0.35843062
Am -6: X=0.83333333 Y=0.66666666 Z=0.64156938
-6: X=0.16666666 Y=0.33333333 Z=0.35843062
Am -7: X=0.33333333 Y=0.66666666 Z=0.64156938
-7: X=0.66666666 Y=0.33333333 Z=0.35843062
Am -8: X=0.33333333 Y=0.16666666 Z=0.64156938
-8: X=0.66666666 Y=0.83333333 Z=0.35843062
Am -9: X=0.66666666 Y=0.33333333 Z=0.73783655
-9: X=0.33333333 Y=0.66666666 Z=0.26216345
Am -10: X=0.66666666 Y=0.83333333 Z=0.73783655
-10: X=0.33333333 Y=0.16666666 Z=0.26216345
Am -11: X=0.16666666 Y=0.83333333 Z=0.73783655
-11: X=0.83333333 Y=0.16666666 Z=0.26216345
Am -12: X=0.16666666 Y=0.33333333 Z=0.73783655
-12: X=0.83333333 Y=0.66666666 Z=0.26216345
H -13: X=0.39746344 Y=0.19873172 Z=0.83641560
-13: X=0.60253656 Y=0.80126828 Z=0.16358440
H -14: X=0.26920322 Y=0.13460162 Z=0.83641560
-14: X=0.73079678 Y=0.86539838 Z=0.16358440

O_2 molecule with a Vert approach adsorbed on dhcp-Am surface at the t1 site.

Am -1: X=0.66666660 Y=0.33333333 Z=0.54718979
-1: X=0.33333330 Y=0.66666666 Z=0.45281021
Am -2: X=0.66666666 Y=0.83333333 Z=0.54718979
-2: X=0.33333333 Y=0.16666666 Z=0.45281021
Am -3: X=0.16666666 Y=0.83333333 Z=0.54718979
-3: X=0.83333333 Y=0.16666666 Z=0.45281021
Am -4: X=0.16666666 Y=0.33333333 Z=0.54718979
-4: X=0.83333333 Y=0.66666666 Z=0.45281021
Am -5: X=0.83333333 Y=0.16666666 Z=0.64156938
-5: X=0.16666666 Y=0.83333333 Z=0.35843062
Am -6: X=0.83333333 Y=0.66666666 Z=0.64156938
-6: X=0.16666666 Y=0.33333333 Z=0.35843062
Am -7: X=0.33333333 Y=0.66666666 Z=0.64156938
-7: X=0.66666666 Y=0.33333333 Z=0.35843062
Am -8: X=0.33333333 Y=0.16666666 Z=0.64156938
-8: X=0.66666666 Y=0.83333333 Z=0.35843062
Am -9: X=0.66666666 Y=0.33333333 Z=0.73783655
-9: X=0.33333333 Y=0.66666666 Z=0.26216345
Am -10: X=0.66666666 Y=0.83333333 Z=0.73783655
-10: X=0.33333333 Y=0.16666666 Z=0.26216345
Am -11: X=0.16666666 Y=0.83333333 Z=0.73783655
-11: X=0.83333333 Y=0.16666666 Z=0.26216345
Am -12: X=0.16666666 Y=0.33333333 Z=0.73783655
-12: X=0.83333333 Y=0.66666666 Z=0.26216345
O -13: X=0.66666670 Y=0.83333330 Z=0.80825021
-13: X=0.33333330 Y=0.16666670 Z=0.19174979
O -14: X=0.66666670 Y=0.83333330 Z=0.85040164
-14: X=0.33333330 Y=0.16666670 Z=0.14959836

O_2 molecule with a Hor1 approach adsorbed on dhcp-Am surface at the b2 site.

Am -1: X=0.66666660 Y=0.33333333 Z=0.54718979
-1: X=0.33333330 Y=0.66666666 Z=0.45281021
Am -2: X=0.66666666 Y=0.83333333 Z=0.54718979
-2: X=0.33333333 Y=0.16666666 Z=0.45281021
Am -3: X=0.16666666 Y=0.83333333 Z=0.54718979
-3: X=0.83333333 Y=0.16666666 Z=0.45281021
Am -4: X=0.16666666 Y=0.33333333 Z=0.54718979
-4: X=0.83333333 Y=0.66666666 Z=0.45281021
Am -5: X=0.83333333 Y=0.16666666 Z=0.64156938
-5: X=0.16666666 Y=0.83333333 Z=0.35843062
Am -6: X=0.83333333 Y=0.66666666 Z=0.64156938
-6: X=0.16666666 Y=0.33333333 Z=0.35843062
Am -7: X=0.33333333 Y=0.66666666 Z=0.64156938
-7: X=0.66666666 Y=0.33333333 Z=0.35843062
Am -8: X=0.33333333 Y=0.16666666 Z=0.64156938
-8: X=0.66666666 Y=0.83333333 Z=0.35843062
Am -9: X=0.66666666 Y=0.33333333 Z=0.73783655
-9: X=0.33333333 Y=0.66666666 Z=0.26216345
Am -10: X=0.66666666 Y=0.83333333 Z=0.73783655
-10: X=0.33333333 Y=0.16666666 Z=0.26216345
Am -11: X=0.16666666 Y=0.83333333 Z=0.73783655
-11: X=0.83333333 Y=0.16666666 Z=0.26216345
Am -12: X=0.16666666 Y=0.33333333 Z=0.73783655
-12: X=0.83333333 Y=0.66666666 Z=0.26216345
O -13: X=0.16666667 Y=0.78897193 Z=0.80120880
-13: X=0.83333333 Y=0.21102807 Z=0.19879120
O -14: X=0.16666667 Y=0.37769473 Z=0.80120880
-14: X=0.83333333 Y=0.62230527 Z=0.19879120

O_2 molecule with a Hor2 approach adsorbed on dhcp-Am surface at the h3 site.

Am -1: X=0.66666660 Y=0.33333333 Z=0.54718979
-1: X=0.33333330 Y=0.66666666 Z=0.45281021
Am -2: X=0.66666666 Y=0.83333333 Z=0.54718979
-2: X=0.33333333 Y=0.16666666 Z=0.45281021
Am -3: X=0.16666666 Y=0.83333333 Z=0.54718979
-3: X=0.83333333 Y=0.16666666 Z=0.45281021
Am -4: X=0.16666666 Y=0.33333333 Z=0.54718979
-4: X=0.83333333 Y=0.66666666 Z=0.45281021
Am -5: X=0.83333333 Y=0.16666666 Z=0.64156938
-5: X=0.16666666 Y=0.83333333 Z=0.35843062
Am -6: X=0.83333333 Y=0.66666666 Z=0.64156938
-6: X=0.16666666 Y=0.33333333 Z=0.35843062
Am -7: X=0.33333333 Y=0.66666666 Z=0.64156938
-7: X=0.66666666 Y=0.33333333 Z=0.35843062
Am -8: X=0.33333333 Y=0.16666666 Z=0.64156938
-8: X=0.66666666 Y=0.83333333 Z=0.35843062
Am -9: X=0.66666666 Y=0.33333333 Z=0.73783655
-9: X=0.33333333 Y=0.66666666 Z=0.26216345
Am -10: X=0.66666666 Y=0.83333333 Z=0.73783655
-10: X=0.33333333 Y=0.16666666 Z=0.26216345
Am -11: X=0.16666666 Y=0.83333333 Z=0.73783655
-11: X=0.83333333 Y=0.16666666 Z=0.26216345
Am -12: X=0.16666666 Y=0.33333333 Z=0.73783655
-12: X=0.83333333 Y=0.66666666 Z=0.26216345
O -13: X=0.54248286 Y=0.27124143 Z=0.79416744
-13: X=0.45751714 Y=0.72875857 Z=0.20583256
O -14: X=0.12418380 Y=0.06209191 Z=0.79416744
-14: X=0.87581620 Y=0.93790809 Z=0.20583256

H_2O molecule with a Vert1 approach adsorbed on dhcp-Am surface at the t1 site

Am -1: X=0.66910453 Y=0.33455226 Z=0.54979737
-1: X=0.33089547 Y=0.66544774 Z=0.45020263
Am -2: X=0.16883120 Y=0.33415245 Z=0.54896024
-2: X=0.83116880 Y=0.66584755 Z=0.45103976
Am -3: X=0.66931266 Y=0.83465633 Z=0.54902159
-3: X=0.33068734 Y=0.16534367 Z=0.45097841
Am -4: X=0.16883120 Y=0.83467875 Z=0.54896024
-4: X=0.83116880 Y=0.16532125 Z=0.45103976
Am -5: X=0.83238105 Y=0.16481539 Z=0.64787430
-5: X=0.16761895 Y=0.83518461 Z=0.35212570
Am -6: X=0.33031188 Y=0.16515594 Z=0.64774500
-6: X=0.66968812 Y=0.83484406 Z=0.35225500
Am -7: X=0.83238105 Y=0.66756566 Z=0.64787430
-7: X=0.16761895 Y=0.33243434 Z=0.35212570
Am -8: X=0.33035276 Y=0.66517638 Z=0.64787550
-8: X=0.66964724 Y=0.33482362 Z=0.35212450
Am -9: X=0.66870599 Y=0.33435299 Z=0.74497958
-9: X=0.33129401 Y=0.66564701 Z=0.25502042
Am -10: X=0.16814215 Y=0.33393829 Z=0.74757186
-10: X=0.83185785 Y=0.66606171 Z=0.25242814
Am -11: X=0.66785776 Y=0.83392888 Z=0.75105201
-11: X=0.33214224 Y=0.16607112 Z=0.24894799
Am -12: X=0.16814215 Y=0.83420386 Z=0.74757186
-12: X=0.83185785 Y=0.16579614 Z=0.25242814
H -13: X=0.67278195 Y=0.72689791 Z=0.85655474
-13: X=0.32721805 Y=0.27310209 Z=0.14344526
O -14: X=0.67112594 Y=0.83556297 Z=0.83793476

-14: X=0.32887406 Y=0.16443703 Z=0.16206524

H -15: X=0.67278195 Y=0.94588404 Z=0.85655474

-15: X=0.32721805 Y=0.05411596 Z=0.14344526

H_2O molecule with a Vert2 approach adsorbed on dhcp-Am surface at the b2 site

Am -1: X=0.16345041 Y=0.33225837 Z=0.54950522

-1: X=0.83654959 Y=0.66774163 Z=0.45049478

Am -2: X=0.16345041 Y=0.83119204 Z=0.54950522

-2: X=0.83654959 Y=0.16880796 Z=0.45049478

Am -3: X=0.66135843 Y=0.33067922 Z=0.54911472

-3: X=0.33864157 Y=0.66932078 Z=0.45088528

Am -4: X=0.66575327 Y=0.83287663 Z=0.54946844

-4: X=0.33424673 Y=0.16712337 Z=0.45053156

Am -5: X=0.32085744 Y=0.16042872 Z=0.64850510

-5: X=0.67914256 Y=0.83957128 Z=0.35149490

Am -6: X=0.32679220 Y=0.66339610 Z=0.64832042

-6: X=0.67320780 Y=0.33660390 Z=0.35167958

Am -7: X=0.82452143 Y=0.16346033 Z=0.64778873

-7: X=0.17547857 Y=0.83653967 Z=0.35221127

Am -8: X=0.82452143 Y=0.66106109 Z=0.64778873

-8: X=0.17547857 Y=0.33893891 Z=0.35221127

Am -9: X=0.15289506 Y=0.32806834 Z=0.74748100

-9: X=0.84710494 Y=0.67193166 Z=0.25251900

Am -10: X=0.15289506 Y=0.82482672 Z=0.74748100

-10: X=0.84710494 Y=0.17517328 Z=0.25251900

Am -11: X=0.64967716 Y=0.32483858 Z=0.74953922

-11: X=0.35032284 Y=0.67516142 Z=0.25046078

Am -12: X=0.65565376 Y=0.82782688 Z=0.74540444

-12: X=0.34434624 Y=0.17217312 Z=0.25459556

H -13: X=0.32807282 Y=0.55783950 Z=0.83696864

-13: X=0.67192718 Y=0.44216050 Z=0.16303136

O -14: X=0.23011306 Y=0.61505653 Z=0.83633478

-14: X=0.76988694 Y=0.38494347 Z=0.16366522

H -15: X=0.32807282 Y=0.77023331 Z=0.83696864

-15: X=0.67192718 Y=0.22976669 Z=0.16303136

H_2O molecule with a Hor approach adsorbed on dhcp-Am surface at the h3 site

Am -1: X=0.16824093 Y=0.33577551 Z=0.54892951

-1: X=0.83175907 Y=0.66422449 Z=0.45107049

Am -2: X=0.16814382 Y=0.83647291 Z=0.54901381

-2: X=0.83185618 Y=0.16352709 Z=0.45098619

Am -3: X=0.66837170 Y=0.33613880 Z=0.54959503

-3: X=0.33162830 Y=0.66386120 Z=0.45040497

Am -4: X=0.66884841 Y=0.83635937 Z=0.54908462

-4: X=0.33115159 Y=0.16364063 Z=0.45091538

Am -5: X=0.33086976 Y=0.16356913 Z=0.64796315

-5: X=0.66913024 Y=0.83643087 Z=0.35203685

Am -6: X=0.33288755 Y=0.66428734 Z=0.64742708

-6: X=0.66711245 Y=0.33571266 Z=0.35257292

Am -7: X=0.83289469 Y=0.16482724 Z=0.64754550

-7: X=0.16710531 Y=0.83517276 Z=0.35245450

Am -8: X=0.83313002 Y=0.66581836 Z=0.64789182

-8: X=0.16686998 Y=0.33418164 Z=0.35210818

Am -9: X=0.16809715 Y=0.33698727 Z=0.74674469

-9: X=0.83190285 Y=0.66301273 Z=0.25325531

Am -10: X=0.16790386 Y=0.83577703 Z=0.75092598

-10: X=0.83209614 Y=0.16422297 Z=0.24907402

Am -11: X=0.66671539 Y=0.33545845 Z=0.74620788

-11: X=0.33328461 Y=0.66454155 Z=0.25379212

Am -12: X=0.66881068 Y=0.83612509 Z=0.74622128

-12: X=0.33118932 Y=0.16387491 Z=0.25377872

H -13: X=0.04220076 Y=0.66390785 Z=0.84165832

-13: X=0.95779924 Y=0.33609215 Z=0.15834168

O -14: X=0.17294266 Y=0.80310327 Z=0.83832682

-14: X=0.82705734 Y=0.19689673 Z=0.16167318

H -15: X=0.28943505 Y=0.77063980 Z=0.84038657

-15: X=0.71056495 Y=0.22936020 Z=0.15961343

OH+H with a Vert-O approach adsorbed on dhcp-Am surface at the b2 site

Am -1: X=0.66438319 Y=0.33455738 Z=0.55055378

-1: X=0.33561681 Y=0.66544262 Z=0.44944622

Am -2: X=0.16675485 Y=0.33715225 Z=0.54869988

-2: X=0.83324515 Y=0.66284775 Z=0.45130012

Am -3: X=0.66772345 Y=0.83620328 Z=0.54926355

-3: X=0.33227655 Y=0.16379672 Z=0.45073645

Am -4: X=0.16656932 Y=0.83385996 Z=0.54881320

-4: X=0.83343068 Y=0.16614004 Z=0.45118680

Am -5: X=0.83524633 Y=0.16427790 Z=0.64844055

-5: X=0.16475367 Y=0.83572210 Z=0.35155945

Am -6: X=0.34028787 Y=0.16817252 Z=0.64585414

-6: X=0.65971213 Y=0.83182748 Z=0.35414586

Am -7: X=0.83544327 Y=0.66748394 Z=0.64835254

-7: X=0.16455673 Y=0.33251606 Z=0.35164746

Am -8: X=0.33435779 Y=0.66482889 Z=0.64805199

-8: X=0.66564221 Y=0.33517111 Z=0.35194801

Am -9: X=0.65060337 Y=0.32484055 Z=0.74772006

-9: X=0.34939663 Y=0.67515945 Z=0.25227994

Am -10: X=0.16747922 Y=0.33000475 Z=0.75267817

-10: X=0.83252078 Y=0.66999525 Z=0.24732183

Am -11: X=0.65228025 Y=0.82516679 Z=0.75194019

-11: X=0.34771975 Y=0.17483321 Z=0.24805981

Am -12: X=0.16778289 Y=0.83319156 Z=0.75255641

-12: X=0.83221711 Y=0.16680844 Z=0.24744359

H -13: X=0.33112823 Y=0.16315546 Z=0.78844747

-13: X=0.66887177 Y=0.83684454 Z=0.21155253

O -14: X=0.32847464 Y=0.66205414 Z=0.79984668

-14: X=0.67152536 Y=0.33794586 Z=0.20015332

H -15: X=0.32602465 Y=0.66052363 Z=0.83166803

-15: X=0.67397535 Y=0.33947637 Z=0.16833197

OH+H with a Hor1 approach adsorbed on dhcp-Am surface at the h3+h3 sites

Am -1: X=0.16701976 Y=0.33444657 Z=0.54931325

-1: X=0.83298024 Y=0.66555343 Z=0.45068675

Am -2: X=0.16884160 Y=0.83637180 Z=0.54927219

-2: X=0.83115840 Y=0.16362820 Z=0.45072781

Am -3: X=0.66905843 Y=0.33753431 Z=0.54894486

-3: X=0.33094157 Y=0.66246569 Z=0.45105514

Am -4: X=0.66759288 Y=0.83645988 Z=0.54932291

-4: X=0.33240712 Y=0.16354012 Z=0.45067709

Am -5: X=0.33224247 Y=0.16249419 Z=0.64807332

-5: X=0.66775753 Y=0.83750581 Z=0.35192668

Am -6: X=0.33139466 Y=0.65985453 Z=0.64776957

-6: X=0.66860534 Y=0.34014547 Z=0.35223043

Am -7: X=0.83109674 Y=0.16292908 Z=0.64778924

-7: X=0.16890326 Y=0.83707092 Z=0.35221076

Am -8: X=0.83243528 Y=0.66464696 Z=0.64748099

-8: X=0.16756472 Y=0.33535304 Z=0.35251901

Am -9: X=0.17287338 Y=0.33194402 Z=0.74930170

-9: X=0.82712662 Y=0.66805598 Z=0.25069830

Am -10: X=0.16595032 Y=0.83781853 Z=0.75156386

-10: X=0.83404968 Y=0.16218147 Z=0.24843614

Am -11: X=0.66875380 Y=0.34208336 Z=0.75535654

-11: X=0.33124620 Y=0.65791664 Z=0.24464346

Am -12: X=0.67623720 Y=0.82927013 Z=0.74652270

-12: X=0.32376280 Y=0.17072987 Z=0.25347730

H -13: X=0.83747864 Y=0.67422999 Z=0.78856986

-13: X=0.16252136 Y=0.32577001 Z=0.21143014

O -14: X=0.33358879 Y=0.16622702 Z=0.79927480

-14: X=0.66641121 Y=0.83377298 Z=0.20072520

H -15: X=0.32335229 Y=0.16155984 Z=0.83102902

-15: X=0.67664771 Y=0.83844016 Z=0.16897098

OH+H with a Vert-O approach adsorbed on dhcp-Am surface at the h3 site

Am -1: X=0.16345041 Y=0.33225837 Z=0.54950522

-1: X=0.83654959 Y=0.66774163 Z=0.45049478

Am -2: X=0.16345041 Y=0.83119204 Z=0.54950522

-2: X=0.83654959 Y=0.16880796 Z=0.45049478

Am -3: X=0.66135843 Y=0.33067922 Z=0.54911472

-3: X=0.33864157 Y=0.66932078 Z=0.45088528

Am -4: X=0.66575327 Y=0.83287663 Z=0.54946844

-4: X=0.33424673 Y=0.16712337 Z=0.45053156

Am -5: X=0.32085744 Y=0.16042872 Z=0.64850510

-5: X=0.67914256 Y=0.83957128 Z=0.35149490

Am -6: X=0.32679220 Y=0.66339610 Z=0.64832042

-6: X=0.67320780 Y=0.33660390 Z=0.35167958

Am -7: X=0.82452143 Y=0.16346033 Z=0.64778873

-7: X=0.17547857 Y=0.83653967 Z=0.35221127

Am -8: X=0.82452143 Y=0.66106109 Z=0.64778873

-8: X=0.17547857 Y=0.33893891 Z=0.35221127

Am -9: X=0.15289506 Y=0.32806834 Z=0.74748100

-9: X=0.84710494 Y=0.67193166 Z=0.25251900

Am -10: X=0.15289506 Y=0.82482672 Z=0.74748100

-10: X=0.84710494 Y=0.17517328 Z=0.25251900

Am -11: X=0.64967716 Y=0.32483858 Z=0.74953922

-11: X=0.35032284 Y=0.67516142 Z=0.25046078

Am -12: X=0.65565376 Y=0.82782688 Z=0.74540444

-12: X=0.34434624 Y=0.17217312 Z=0.25459556

H -13: X=0.32807282 Y=0.55783950 Z=0.83696864

-13: X=0.67192718 Y=0.44216050 Z=0.16303136

O -14: X=0.23011306 Y=0.61505653 Z=0.83633478

-14: X=0.76988694 Y=0.38494347 Z=0.16366522

H -15: X=0.32807282 Y=0.77023331 Z=0.83696864

-15: X=0.67192718 Y=0.22976669 Z=0.16303136

OH+H with a Vert-H approach adsorbed on dhcp-Am surface at the b2 site

Am -1: X=0.16824093 Y=0.33577551 Z=0.54892951

-1: X=0.83175907 Y=0.66422449 Z=0.45107049

Am -2: X=0.16814382 Y=0.83647291 Z=0.54901381

-2: X=0.83185618 Y=0.16352709 Z=0.45098619

Am -3: X=0.66837170 Y=0.33613880 Z=0.54959503

-3: X=0.33162830 Y=0.66386120 Z=0.45040497

Am -4: X=0.66884841 Y=0.83635937 Z=0.54908462

-4: X=0.33115159 Y=0.16364063 Z=0.45091538

Am -5: X=0.33086976 Y=0.16356913 Z=0.64796315

-5: X=0.66913024 Y=0.83643087 Z=0.35203685

Am -6: X=0.33288755 Y=0.66428734 Z=0.64742708

-6: X=0.66711245 Y=0.33571266 Z=0.35257292

Am -7: X=0.83289469 Y=0.16482724 Z=0.64754550

-7: X=0.16710531 Y=0.83517276 Z=0.35245450

Am -8: X=0.83313002 Y=0.66581836 Z=0.64789182

-8: X=0.16686998 Y=0.33418164 Z=0.35210818

Am -9: X=0.16809715 Y=0.33698727 Z=0.74674469

-9: X=0.83190285 Y=0.66301273 Z=0.25325531

Am -10: X=0.16790386 Y=0.83577703 Z=0.75092598

-10: X=0.83209614 Y=0.16422297 Z=0.24907402

Am -11: X=0.66671539 Y=0.33545845 Z=0.74620788

-11: X=0.33328461 Y=0.66454155 Z=0.25379212

Am -12: X=0.66881068 Y=0.83612509 Z=0.74622128

-12: X=0.33118932 Y=0.16387491 Z=0.25377872

H -13: X=0.04220076 Y=0.66390785 Z=0.84165832

-13: X=0.95779924 Y=0.33609215 Z=0.15834168

O -14: X=0.17294266 Y=0.80310327 Z=0.83832682

-14: X=0.82705734 Y=0.19689673 Z=0.16167318

H -15: X=0.28943505 Y=0.77063980 Z=0.84038657

-15: X=0.71056495 Y=0.22936020 Z=0.15961343

H+O+H adsorbed on dhcp-Am surface at the h3+h3+h3 sites

Am -1: X=0.16817202 Y=0.33615046 Z=0.54974716

-1: X=0.83182798 Y=0.66384954 Z=0.45025284

Am -2: X=0.16808670 Y=0.83600215 Z=0.54974497

-2: X=0.83191330 Y=0.16399785 Z=0.45025503

Am -3: X=0.66848409 Y=0.33601676 Z=0.54836889

-3: X=0.33151591 Y=0.66398324 Z=0.45163111

Am -4: X=0.66806354 Y=0.83591745 Z=0.54946728

-4: X=0.33193646 Y=0.16408255 Z=0.45053272

Am -5: X=0.33357328 Y=0.16652810 Z=0.64788453

-5: X=0.66642672 Y=0.83347190 Z=0.35211547

Am -6: X=0.33042427 Y=0.66475371 Z=0.65156227

-6: X=0.66957573 Y=0.33524629 Z=0.34843773

Am -7: X=0.83134464 Y=0.16513278 Z=0.64756187

-7: X=0.16865536 Y=0.83486722 Z=0.35243813

Am -8: X=0.83050092 Y=0.66348637 Z=0.64727733

-8: X=0.16949908 Y=0.33651363 Z=0.35272267

Am -9: X=0.17660944 Y=0.31658316 Z=0.75555524

-9: X=0.82339056 Y=0.68341684 Z=0.24444476

Am -10: X=0.16678267 Y=0.82891035 Z=0.75950942

-10: X=0.83321733 Y=0.17108965 Z=0.24049058

Am -11: X=0.66964888 Y=0.32768292 Z=0.75408546

-11: X=0.33035112 Y=0.67231708 Z=0.24591454

Am -12: X=0.67914853 Y=0.82100712 Z=0.75242180

-12: X=0.32085147 Y=0.17899288 Z=0.24757820

H -13: X=0.34129396 Y=0.15661196 Z=0.79283656

-13: X=0.65870604 Y=0.84338804 Z=0.20716344

O -14: X=0.34085299 Y=0.65893401 Z=0.77786018

-14: X=0.65914701 Y=0.34106599 Z=0.22213982

H -15: X=0.83676641 Y=0.65911888 Z=0.79173667

-15: X=0.16323359 Y=0.34088112 Z=0.20826333

APPENDIX B

PROGRAM FOR CALCULATING DIFFERENCE CHARGE DENSITY

Program to calculate difference charge density[73]

```
      implicit none

      integer ii,jj,kk,npxup,npyup,npxdn,
      real  chargeup(5000,5000), chargedn(5000,5000),xlup
      real  ylup,xldn,yldn, xl,yl
      real  charge(5000,5000),charge1(5000,5000)

      open(14,file='rho.1',status='old')
      open(15,file='rho.2',status='old')
      open(17,file='rho.3',status='old')
      open(16,file='*.rho',status='unknown')
      open(18,file='gnu_dat',status='unknown')


      read(14,*)npxup, npyup, xlup, ylup
      read(15,*)npxdn, npydn, xldn, yldn
      read(17,*)npx, npy, xl, yl

      read(14,11) ((chargeup(ii,jj),jj=1,npyup),
      read(15,11) ((chargedn(ii,jj),jj=1,npydn),
      read(17,11) ((charge1(ii,jj),jj=1,npy),ii=1,npx)


      close(14)
      close(15)
      close(17)

      do ii=1,npxup
        do jj=1,npyup
          charge(ii,jj)=chargeup(ii,jj)-chargedn(ii,jj)
          write(18,*)charge(ii,jj)
        end do
          write(18,*)
      end do
```

APPENDIX C

PROGRAM TO CALCULATE DENSITY OF STATES

Program to calculate density of states[73]

```
implicit none
      integer ii, jj, kk, nat
      real*8 dup(2000,7), ddn(2000,7), xx, yy

      read(11,*)nat
      read(12,*)nat
      do ii=1,nat
        read(11,*)dup(ii,1),dup(ii,2),dup(ii,3),dup(ii,4),dup(ii,5)
        ,dup(ii,6)
        read(12,*)ddn(ii,1),ddn(ii,2),ddn(ii,3),ddn(ii,4),ddn(ii,5)
        ,ddn(ii,6)
      end do
      close(11)
      close(12)

      open(14, file='*dat',status='unknown')
      open(15, file='*.dat',status='unknown')

      do ii=1, nat
           xx = dup(ii,2)+ddn(ii,2)+dup(ii,3)+ddn(ii,3)
           xx = xx+dup(ii,4)+ddn(ii,4)
           yy = dup(ii,5)+ddn(ii,5)+dup(ii,6)+ddn(ii,6)
           yy = yy+dup(ii,7)+ddn(ii,7)

      end do

      close(14)
      close(15)

      stop
      end
```

REFERENCES

[1] http://nobelprize.org/nobel_prizes/chemistry/laureates/2007/chemadv07.pdf

[2] J. J. Katz, G. T. Seaborg, and L. R. Morss, *The Chemistry of the Actinide Elements* (Chapman and Hall, 1986);

[3] L. R. Morss and J. Fuger, Eds. *Transuranium Elements: A Half Century* (American Chemical Society, Washington, D. C. 1992);

[4] L. R. Morss, N. M. Edelstein, J. Fuger, Eds. and J. J. Katz, Hon. Ed. *The Chemistry of the Actinide and Transactinide Elements, Vols. 1-5* (Springer, New York, 2006).

[5] L. Soderholm, J. J. Joyce, M. F. Nicol, D. K. Shuh, and J. G. Tobin, Eds., *Actinides 2005-Basic Science, Applications, and Technology,*Proceedings of the Materials Research Society, 802 (2004).

[6] J. L. Sarrao, A. J. Schwartz, M. R. Antonio, P. C. Burns, R. G. Haire, and H. Nitsche, Eds. *Actinides 2005-Basic Science, Applications, and Technology,* Proceedings of the Materials Research Society, 893 (2005);

[7] K. J. M. Blobaum, E.A. Chandler, L. Havela, M. B. Maple, M. P. Neu, Eds. *Actinides 2006-Basic Science, Applications, and Technology,* Proceedings of the Materials Research Society, 986 (2006).

[8] K. K. S. Pillay and K. C. Kim, Eds. *Plutonium Futures˜ The Science,* American Institute of Physics Conference Proceedings, 532 (2000);

[9] G. D. Jarvinen, Ed. *Plutonium Futures˜ The Science*, American Institute of Physics Conference Proceedings, 673 (2003).

[10] A. M. Boring and J. L. Smith, "*Plutonium Condensed-Matter Physics: A Survey of Theory and Experiment,*" in *Challenges in Plutonium Science*, Los Alamos Science, 1, No. 26, 90 (2000).

[11] D. Hoffman, Ed. *Advances in Plutonium Chemistry 1967-2000* (American Nuclear Society, La Grange, Illinois and University Research Alliance, Amarillo, Texas, 2002).

[12] M. J. Fluss, D. E. Hobart, P. G. Allen, and J. D. Jarvinen, *Proceedings of the Plutonium Futures – The Science 2006 Conference*, Journal of Alloys and Compounds, 444-445 (2007)..

[13] G. T. Seaborg and W. D. Loveland, p. 17, in *The Elements beyond Uranium,* (John Wiley & Sons, Inc. 1990).

[14] S. Y. Savrasov, K. Haule, and G. Kotliar, Phys. Rev. Lett. 96, 036404 (2006).

[15] S. Heathman, R. G. Haire, T. Le Bihan, A. Lindbaum, K. Litfin, Y. Méresse, and H. Libotte, Phys. Rev. Lett. 85, 2961 (2000).

[16] G. H. Lander and J. Fuger, Endeavour, 13, 8, (1989).

[17] A. J. Freeman and D. D. Koelling, in The *Actinides: Electronic Structure and Related Properties,* edited by A. J. Freeman and J. B. Darby, Jr. (Academic, New York, 1974).

[18] B. Johansson, Phys. Rev. B. 11, 2740 (1975).

[19] H. L. Skriver, O. K. Andersen, and B. Johansson, Phys. Rev. Lett. 41, 42 (1978).

[20] J. R. Naegele, L. Manes, J. C. Spirlet, and W. Müller, Phys. Rev. Lett. 52, 1834 (1984).

[21] A. Lindbaum, S. Heathman, K. Litfin and Y. Méresse, Phys. Rev. B. 63, 214101 (2001).

[22] M. Pénicaud, J. Phys. Cond. Matt. 14, 3575 (2002).

[23] M. Pénicaud, J. Phys. Cond. Matt. 17, 257 (2005).

[24] P. Sõderlind, R. Ahuja, O. Eriksson, B. Johansson, and J. M. Wills, Phys. Rev. B. 61, 8119 (2000);

[25] P. Sõderlind and A. Landa, 72, 024109 (2005).

[26] P. G. Huray, S. E. Nave, and R. G. Haire, J. Less-Com. Met. 93, 293 (1983).

[27] T. Gouder, P. M. Oppeneer, F. Huber, F. Wastin, and J. Rebizant, Phys. Rev. B 72, 115122 (2005).

[28] L. E. Cox, J. W. Ward, and R. G. Haire, Phys. Rev. B 45, 13239 (1992).

[29] O. Eriksson and J. M. Wills, Phys. Rev. B 45, 3198 (1992).

[30] A. L. Kutepov, and S. G. Kutepova, J. Magn. Magn. Mat. 272-276, e329 (2004).

[31] A. Shick, L. Havela, J. Kolorenc, V. Drchal, T. Gouder, and P. M. Oppeneer, Phys. Rev. B 73, 104415 (2006).

[32] S. Y. Savrasov, G. Kotliar, and E. Abrahams, Nature 410, 793 (2001);

[33] G. Kotliar and D. Vollhardt, Phys. Today 57, 53 (2004);

[34] X. Dai, S. Y. Savrasov, G. Kotliar, A. Migliori, H. Ledbetter, and E. Abrahams, Science 300, 953 (2003).

[35] B. Johansson and A. Rosengren, Phys. Rev. B 11, 2836 (1975).

[36] J. L. Smith and R. G. Haire, Science 200, 535 (1978).

[37] J. C. Griveau, J. Rebizant, G. H. Lander, and G. Kotliar, Phys. Rev. Lett. 94, 097002 (2005).

[38] D. Gao and A. K. Ray, Eur. Phys. J. B, 50, 497 (2006).

[39] D. Gao and A. K. Ray, Surf. Sci., 600, 4941 (2006);

[40] D. Gao and A. K. Ray, Eur. Phys. J. B 55, 13 (2007);

[41] D. Gao and A. K. Ray, Phys. Rev. B, 77, 035123 (2008).

[42] P. P. Dholabhai, R. Atta-Fynn and A. K. Ray, Eur. Phys. J. B, 61, 261-270 (2008); P. P. Dholabhai and A. K. Ray, submitted for publication

[43] R. Atta-Fynn and A. K. Ray, Physica B, 392, 112 (2007);

[44] P. P. Dholabhai, R. Atta-Fynn and A. K. Ray (Submitted for publication).

[45] J. P. Perdew, K. Burke, and M. Ernzerhof, Phys. Rev. Lett. 77, 3865 (1996).

[46] P. Hohenberg and W. Kohn, Phys. Rev. 136, B864 (1964);

[47] W. Kohn and L. J. Sham, Phys. Rev. 140, A1133 (1965).

[48] P. Blaha, K. Schwarz, G. K. H. Madsen, D. Kvasnicka, and J. Luitz, *WIEN2k*, *An Augmented Plane Wave Plus Local Orbitals Program for Calculating Crystal properties* (Vienna University of Technology, Austria, 2001).

[49] D. D. Koelling and B. N. Harmon, J. Phys. C 10, 3107 (1977).

[50] J. Kunes, P. Novak, R. Schmid, P. Blaha, and K. Schwarz, Phys. Rev. B 64 153102 (2001).

[51] R. W. G. Wyckoff, *Crystal Structure*s Volume 1 (Wiley, New York, 1963).

[52] F. D. Murnaghan, Proc. Natl. Acad. Sci. USA 30, 244 (1944).

[53] S. Heathman, R. G. Haire, T. Le Bihan, A. Lindbaum, K. Litfin, Y. Méresse, and H. Libotte, Phy. Rev. Lett. 85, 2961 (2000).

[54] A. Lindbaum, S. Heathman, K. Litfin, Y. Méresse, R. G. Haire, T. Le Bihan, and H. Libotte, Phy. Rev. B 63, 214101 (2001).

[55] F. Wagner, Th. Laloyaux, and M. Scheffler, Phys. Rev. B 57, 2102 (1998).

[56] R. Atta-Fynn and A. K. Ray, Phys. Rev. B, 75 ,195112 (2007).

[57] B. G. Briner, M. Doering, H.-P. Rust, and A. M. Bradshaw, Phys. Rev. Lett. 78, 1516 (1997).

[58] S. Y. Liem, J. H. R. Clarke, and G. Kresse, Comp. Mat. Sci. 17, 133 (2000).

[59] G. Katz, R. Kosloff, and Y. Zeiri, J. Chem. Phys 120, 3931 (2004).

[60] A. Kokalj, J. Mol. Graphics Modeling 17, 176 (1999); code available from http://www.xcrysden.org

[61] M. N. Huda and A. K. Ray. Int. J. Quant. Chem., 105, 280 (2005).

[62] T. C. Leung, C. L. Kao, W. S. Su, T. C. Leung, C. L. Kao, and W. S. Su Phys. Rev. B 68, 195408 (2003).

[63] A. Nojima and K. Yamashita. Surf. Sci. 601, 3003–3011(2007).

[64] P. A. Thiel and T. E. Madey, Surf. Sci. Rep. 7, 211 (1978).

[65] M. A. Henderson, Surf. Sci. Rep. 46, 1 (2002).

[66] W. J. Hehre, L. Radom, P. v. R. Schlyer, and J. A. Pople. Ab Initio Molecular Orbital Theory; John Wiley: New York, 1986.

[67] B. Delley. J. Chem. Phys 92, 508 (1990).

[68] B. Delley. Int. J. Quan. Chem 69, 423 (1998).

[69] B. Delley. J. Chem. Phys 113, 7756 (2000).

[70] B. Delley. Phys. Rev. B 65, 085403 (2002).

[71] A. Kessi and B. Delley. Int. J. Quan. Chem 68, 135 (1998).

[72] H. J. Monkhorst and J. D. Pack. Phys. Rev. B 13, 5188 (1976).

[73] R. Atta-Fynn, Private communications

BIOGRAPHICAL INFORMATION

The author has received his Bachelors of Science in Physics in 2000 from the Maharaja Sayajirao University of Baroda in India. In 2002 he earned a Master of Science degree in Physics specializing in Nuclear physics from the Maharaja Sayajirao University of Baroda in India. In 2005 he earned a Master of Science degree in Physics from The University of Texas at Arlington, Arlington.